

The Role of Subsurface Oxygen in Silver-Catalyzed Partial Oxidation Reactions

PROEFSCHRIFT

ter verkrijging van de graad van doctor aan de Technische
Universiteit Eindhoven, op gezag van de Rector Manificus,
prof. dr. M. Rem, voor een commissie aangewezen door het
College voor Promoties in het openbaar te verdedigen op
maandag 11 januari 1999 om 16.00 uur

door

Anton Nagy

geboren te Chicago

Dit proefschrift is goedgekeurd door de promotoren:

prof. dr. R.A. van Santen (TUE)

en

prof. dr. R. Schlögl, (Fritz-Haber Max Planck Inst. Berlijn,
Duitsland)

Copromotoren:

prof. dr. J.A. Lercher (UT)

dr. J.W. Niemantsverdriet

Samenstelling promotiecommissie:

Rector Magnificus, prof. dr. M. Rem, voorzitter

Prof. dr. R.A. van Santen, Technische Universiteit Eindhoven,
1e promotor

Prof. dr. R. Schlögl, Fritz-Haber-Inst. Der Max Planck Institut,
Berlijn, Duitsland, 2e promotor

Prof. J.A. Lercher, Technische Universiteit Twente

Dr. J.W. Niemantsverdriet, Technische Universiteit Eindhoven

Prof. Dr. H.H. Brongersma, Technische Universiteit
Eindhoven

Prof. A.G. De With, Technische Universiteit Eindhoven

Dr. M.H.J.M de Crom, Technische Universiteit Eindhoven

The Role of Subsurface Oxygen in Silver-Catalyzed Partial Oxidation Reactions

PhD Thesis

Drs. Anton J. Nagy
The Technical University of Eindhoven
Department of Technical Chemistry
P.O. Box 513
5600 MB Eindhoven
The Netherlands

Abstract

Silver is used industrially as a catalyst for both the epoxidation of ethylene to ethylene epoxide as well as the oxi-dehydrogenation of methanol to formaldehyde. The remarkable activity of silver for these reactions lies its ability to activate molecular oxygen into a number of different, catalytically active, forms.

Atomic oxygen is formed above 160K *via* dissociative chemisorption of gas-phase, molecular oxygen. This atomic-surface oxygen is referred to as O_α and is a strong nucleophile which preferentially reacts with organic molecules to complete oxidation products. It is formed preferentially on high-Miller indices terminating silver crystal surfaces. This species desorbs from the silver surface at approximately 523K. O_α may diffuse into the silver bulk above 573K when a partial pressure of oxygen is present, occupying octahedral holes in the silver lattice. This bulk-dissolved oxygen is termed O_β . The dominant diffusion mechanism is grain-boundary diffusion or octahedral hole jumping for temperatures below 923K. The hole jumping mechanism is strongly anisotropic and results in preferential channeling of oxygen in the [110] direction in the silver crystallites.

Above 923K, the interstitialcy diffusion of oxygen in the silver bulk becomes activated and results in the incorporation of oxygen into the silver lattice. Under steady-state reaction conditions at temperatures in excess of 923K, both oxygen in interstitial and lattice positions is present. Oxygen will undergo equimolar counter-diffusion where it dissolves into the bulk and segregate to the surface under steady-state reaction conditions. At the same time, the silver surface undergoes massive restructuring. This restructuring arises from the thermodynamic drive of the silver surface to obtain a minimum surface energy configuration. This process results in the formation of surface facets. These are believed to consist of (111) terraces and (110)-terminating steps. The (111) terraces exhibit extremely low sticking coefficients for oxygen adsorption ($\theta < 10^{-6}$) and does not form significant amounts of O_α . The (110) steps exhibit a high sticking coefficient for oxygen ($\theta \sim 10^{-3}$) and provide channels for the above-mentioned diffusion of oxygen along the [110] direction into the silver bulk. This oxygen may either diffuse back to the (110) surface or may diffuse to the (111) planes *via* interstitialcy diffusion. This lattice oxygen may react with gas-phase organic species in that moment when it has segregated into the uppermost silver layer. This species is referred to as

O_γ and is responsible for the direct dehydrogenation of organic molecules. The diffusion of oxygen through silver is a strong function of silver morphology as bulk oxygen will always seek out the path of least resistance. It is the coincidence of the morphological restructuring of the silver into a thermodynamically favorable (111) terminating structure and the activation of the interstitialcy diffusion mechanism at temperatures greater than 923K which culminate in the diffusion of oxygen in a direction other than [110] and ultimately in the formation of O_γ .

Studies on the methanol oxidation reaction show an excellent correlation between the various diffusion mechanisms and the catalytic activity. The dominant diffusion mechanism may be estimated from the location of holes which act as morphological fingerprint which sub-surface oxygen leaves after reacting with bulk-dissolved hydrogen resulting from the dehydrogenation of methanol to formaldehyde. The absence of holes for reaction temperatures lower than 573K indicates that the reaction takes place entirely at the silver surface. The presence of holes at silver grain boundaries for temperatures between 623K and 823K shows that grain-boundary diffusion of oxygen acts as the primary diffusion path for the formation of O_β . Reaction temperatures above 823K results in the proliferation of holes across the silver surface, indicating the participation of oxygen which is transported by volume diffusion. The morphological restructuring of silver results in grain boundary sintering above 623K. Catalyst sintering therefore explains the deactivation of fresh silver catalysts for reaction between 573K and 823K.

The measured activation energy of diffusion for the oxidative coupling of methane to C_2 hydrocarbons of 138 kJ/mol corresponds excellently with the activation energy of oxygen diffusion in the silver bulk of 140 kJ/mol. This provides a quantitative correlation between the kinetics of bulk-oxygen diffusion and the rate of catalytic reaction. This is, therefore, quantitative evidence for the proposed mechanism of O_β and O_γ formation. The activity and selectivity of reaction also act as excellent qualitative indicators for the formation of O_γ which is correlated with the formation of (111) facet terraces.

Contents

Abstract		i-ii
Stellingen		viii-xi
Chapter 1	Introduction	1
1.1	The Industrial Relevance of Silver-Catalyzed Partial Oxidation Reactions	1
1.2	The Formaldehyde Synthesis Reaction	2
	The BASF Process	2
	Figure of Flow Scheme for the BASF Process	3
1.3	Fundamental Research on Silver-Catalyzed Partial Oxidation Reactions.	5
1.3.1	The Silver-Oxygen Interaction	5
	Single-Crystal Studies	5
	Adsorption on Polycrystalline Ag	8
	Addition of Modifiers and Impurities	9
1.4	The Methanol Oxidation Reaction	11
1.4.1	The Role of Gas-Phase, Homogeneous Reaction	12
1.5	Thesis Motivation	14
Chapter 2	Experimental Methods	18
2.1	Introduction	18
2.2	Reactor Characteristics	20
2.3	Thermodynamics of the Reactions Studied	21
2.4	Reactor Design	22
	2.4.1 Mass and Heat Transfer Limitations	24
2.5	Characterization Techniques	26
	2.5.1 X-Ray Photoelectron Spectroscopy	26
	2.5.2 Temperature Desorption Spectroscopy	29
	2.5.3 Ion Scattering Spectroscopy	31
	2.5.4 X-Ray Diffraction	33

2.5.5	Scanning Electron Microscopy and Energy-Dispersive X-Ray Analysis	35
2.5.6	Scanning Tunneling Microscopy	36
2.6	Summary	37
Chapter 3	The Correlation of Sub-Surface Oxygen Diffusion With Variations of Silver Morphology in the Silver Oxygen System	39
3.1	Introduction	40
3.2	Experimental	43
3.3	Results and Discussion	46
3.3.1	SEM Analysis of Pretreated Foil	46
3.3.2	TDS as a Tool for Studying Structural Changes	48
3.3.3	Pretreatment at 573K	49
3.3.4	Pretreatment at 773K	51
3.3.5	Pretreatment at 973K	52
3.3.6	Interpretation	53
3.3.7	Activation Energies of Diffusion/Desorption	54
3.3.8	In-situ XRD-Temperature Dependence	56
3.3.9	STM Results	62
3.3.10	TDS vs. XPS Evidence for Surface Diffusion Inhibition	63
3.3.11	ISS Evidence for the Reconstruction/Diffusion Relationship	66
3.4	Discussion	67
3.5	Conclusions	69
Chapter 4	The Dynamic Restructuring of Electrolytic Silver During the Formaldehyde Synthesis Reaction	73
4.1	Introduction	74
4.2	Experimental	75
4.3	Results	77
4.3.1	The Conversion Obtained Over	77

	An Aged Catalyst	
4.3.2	Catalytic Activity of a Fresh Catalyst	79
4.3.3	The Hysteresis of Reaction	81
	Cycle 1 (423-573-423K)	81
	Cycle 2 (423-773-423K)	82
	Cycle 3 (423-948-423K)	84
4.3.4	Diffusion Control of Reaction	85
4.3.5	Contributions from Homogeneous, Gas-Phase Reactions	86
4.3.6	Evidence for the Temperature-Dependent Shift of the Reaction Mechanism	89
4.3.7	Reaction-Induced Changes in Catalyst Morphology	91
4.4	Discussion	94
4.5	Conclusions	105
Chapter 5	The Oxidative Coupling of Methane as a Test Reaction To Clarify the Role of Sub-Surface Oxygen in Silver- Catalyzed, Partial-Oxidation Reactions	109
5.1	Introduction	109
	The Model	110
5.2	Experimental	113
5.3	Results and Discussion	114
	5.3.1 Comparison of OCM Reaction Kinetics and the Oxygen Diffusion Kinetics in Silver	114
	Plug Flow and Absence of Radial Temperature Gradients	114
	Presence of Local Temperature Gradients	115
	Reaction in Series or Parallel	118
	The Arrhenius Temperature Dependence of Reaction	119
	The Irreversibility of Reaction	120
	The Correlation of Reaction Rate with Bulk-Oxygen Diffusion	120
	Estimating the Depth of O_p Penetration into	121

Silver During Reaction	
5.3.2 Results Obtained Under Unsteady State	123
Conditions	
Isothermal Run Without SiO ₂	124
Changes in Reaction Rate	124
Changes in Product Selectivity	125
The Absence of Ag ₂ O	128
Isothermal Run with SiO ₂ Diluted	129
Ag Catalyst	
Changes in Reaction Rate	130
Changes in Selectivity	131
The Effect of Sintering	132
The Effect of Surface Pinning	133
Evidence for Surface-Controlled	134
Facet Growth	
The Contribution of Sublimation	135
To Facet Growth	
5.4 Conclusions	137
Summary	141
Samenvatting	144
Acknowledgements	147
Curriculum Vitae	149

The work in this thesis is based, in part, on the following publications.

1. Herein, D., A. Nagy, H. Schubert, G. Weinberg, E. Kitzelmann and R. Schlögl: 'The Reaction of molecular oxygen with silver at technical catalytic conditions: Bulk structural consequences of a gas-solid interface reaction.', *Z. Phys. Chem.* **197**, 67 (1996)
2. Herein, D., H. Werner, Th. Schedel-Niedrig, Th. Neisius, A. Nagy, S. Bernd, and R. Schlögl: The selective oxidation of methanol: A comparison of the mode of action of metal and oxide catalysts. In: Proc. 3rd World Congress on Oxidation Catalysts, San Diego, CA, 21-26.9.97. Eds. S.T. Oyama et al., Elsevier Science B.V. Amsterdam, Accepted
3. A.J. Nagy, R. Schlögl, The Interaction of NO with Electrolytic Silver and it's Effect on the Partial Oxidation of Methanol to Formaldehyde. XXX. Jahrestreffen deutscher Katalytiker, Eisenach, Germany
4. D. Zemlyanov, A. Nagy, Th. Schedel Niedrig, R. Schlögl, 'The Reaction of the NO/O₂ Mixture with Silver', *Applied Surface Science* **133**, 171 (1998)
5. A. Nagy, G. Weinberg, Th. Rühle, G. Mestl, 'The Dynamic Restructuring of Electrolytic Silver During the Partial Oxidation of Methanol to Formaldehyde', *J. Catal* **179**, 548 (1998)
6. A. Nagy, G. Mestl, D. Herein, G. Weinberg, E. Kitzelmann, R. Schlögl, "The Correlation of Sub-Surface Oxygen Diffusion with Variations of Silver Morphology in the Silver-Oxygen System", Accepted in the Journal of Catalysis for Publication.
7. A. Nagy, G. Mestl, R. Schlögl, "Using the Oxidative Coupling of Methane as a Test Reaction for Understanding the Role of Sub-Surface Oxygen in Silver-Catalyzed Partial Oxidation Reactions", Submitted to the Journal of Catalysis for Publication.
8. A. Nagy, R. Schlögl, "The Possibility of Using Electrolytic Silver for the Selective Catalytic Decomposition of NO_x", Chapter 6 in "Criterion for a technically relevant and clean running diesel ship motor; Techniques for removal of NO_x from flue gas emissions". *Fortschritt-Berichte VDI* Vol 15, Nr. 198,

Stellingen

1. In hun studie van zuurstoftransport door Ag (110), polykristallijn Ag en Zr-gedoteerd Ag hebben Outlaw et al. zich onvoldoende rekenschap gegeven van de mogelijkheid van structurele transformaties in de bestudeerde materialen. De omstandigheden waaraan deze zijn blootgesteld zijn zeker afdoende geweest om zowel textuurvorming in het inwendige als facettering te bewerkstelligen. De implicatie is, dat het (110) éénkristal waarschijnlijk niet meer als een ideaal éénkristal beschouwd had mogen worden.

Outlaw R.A., Wu D., Davidson M.R., Hoflund G.B., *J. Vac. Sci. Technol.*, A **10**(4) 1497 (1992).

2. Een veel voorkomend probleem in de surface science literatuur is het gebrek aan aandacht voor morfologische veranderingen die kunnen plaatsvinden tijdens de monstervoorbereiding. Cycli van oxidatie, flashing en annealing leiden onherroepelijk tot een oppervlak dat morfologisch verschilt van dat van het oorspronkelijke kristal. De verschijning van een TLK structuur of van facetten is niet altijd zichtbaar met LEED, de meest gebruikelijke techniek ter bestudering van de homogeniteit van éénkristaloppervlakken. Onderstaande auteurs gebruikten voorbehandelingscondities die waarschijnlijk tot zulke transformaties geleid hebben.

Campbell C., Paffet M., *Surf. Sci.*, **143**, 517 (1984).

Wachs I., Madix R., *Surf. Sci.*, **76**, 531 (1978).

Bowker M., Barteau M., Madix R., *Surf. Sci.*, **92**, 528 (1980).

3. Lefferts et al. hebben in hun studie van temperatuurgeprogrammeerde oxidatie en -reductie van zilver een aantal verschillende zuurstofspecies geïdentificeerd. Ter detectie van desorberende gassen hadden zij slechts de beschikking over een thermal conductivity detector (TCD), met als evidente nadeel het ontbreken van de mogelijkheid tot nadere identificatie. Hun toekenning van een brede desorptiepiek bij 623 K aan moleculaire zuurstof is dan ook onnauwkeurig; waarschijnlijker is dat het signaal toegeschreven had moeten worden aan desorptie van koolmonoxide dat immers vrijwel altijd gevormd wordt uit koolstofverontreinigingen in het monster.

Lefferts L., Ommen J., Ross J., *Appl. Catal.*, **31** 291 (1987).

4. De bewering van Backx *et al.* dat subsurface zuurstof zelfs gevormd kan worden bij een temperatuur van 373 K maar niet kan desorberen bij temperaturen lager dan 723 K lijkt inwendig tegenstrijdig. Waarom het oplossen van zuurstof in het inwendige bij veel lagere temperatuur zou kunnen optreden dan segregatie in het inwendige is ook niet duidelijk. In het werk beschreven in dit proefschrift is opname van zuurstof bij temperaturen lager dan 473 K niet waargenomen.

Backx C., de Groot C., Biloen P., *Surf. Sci.*, **104**, 300 (1981).

5. Er is een overvloed aan publicaties beschikbaar waarin het gebruik van temperatuur-geprogrammeerde oxidatie en -reductie (TPO/TPR) ter bestudering van katalysatormaterialen en katalytische reacties wordt beschreven. Een aantal van zulke studies is gericht op beter begrip van de epoxidatie van etheen en de synthese van formaldehyde, beide zilvergekatalyseerde reacties. Gebruik van TPO/TPR verschaft wel degelijk waardevol inzicht, maar men dient terdege te beseffen dat de situatie waarin het katalysatorsysteem van de ene uiterste oxidatietoestand in de andere gebracht wordt sterk afwijkt van die in een katalytische reactie. Vorming en participatie van suboxides, die kunnen bestaan in de steady-state van een katalytische reactie, te weten onder constante partiële spanning van een reductor en een oxidator, zijn met een dergelijke techniek waarschijnlijk niet waarneembaar.

Henriques C., Portela M., Mazzochia C., "*New Developments in Selective Oxidation II*", Elsevier Science, 499-506 (1994).

Schubert H., Tegtmeier U., Herein D., Bao X., Muhler M., Schlögl R., *Catal. Lett.*, **33**, 305 (1995).

6. Een aantal publicaties is gewijd aan morfologische veranderingen van zilver na blootstelling aan de condities van de methanoloxidatiereactie. In geen van die publicaties is rekening gehouden met de extreme exothermiciteit van de reactie die aanleiding geeft tot grote temperatuurgradiënten in de nabijheid van het zilveroppervlak (zie Hoofdstuk 2 en 5 van dit proefschrift) en tot lokale oververhitting van het monster. De vorming van holten en het afwezig zijn van facettering aan het oppervlak kan veroorzaakt zijn door smelten van het oppervlak, en niet noodzakelijkerwijs door recombinitie van hydroxylgroepen in het inwendige onder vorming van water.

Rehren C., Muhler M., Bao X., Schlögl R., Ertl G., *Z. Phys. Chem.*, **174**, 11 (1991).

Millar G., Nelson M., Uwins P., *Catal. Lett.*, **43**, 97, (1997).

Lefferts L., van Ommen J., Ross J., *Appl. Catal.*, **34**, 329 (1987).

7. In het laboratorium is in een aantal gevallen de vorming van mierzuur als een bijproduct van de methanoloxidatiereactie waargenomen, naar bleek in hoeveelheden die toenamen met toenemende monsterlusteratuur in de gaschromatograaf. Verlaging van die temperatuur tot 423 K bleek afdoende om de hoeveelheid mierzuur tot beneden de detectielimiet terug te brengen. De vorming ervan werd kennelijk door het staa van de monsterlus gekatalyseerd.
8. Het gebruik van éénkristallen in modelstudies is alleen zinvol bij condities die zo mild zijn dat facetvorming en textuurvorming in het inwendige niet optreden. Polykristallijne folies zijn in veel gevallen ideale studieobjecten juist vanwege het statistisch voorkomen van verschillende ordeningen. Een éénkristal daarentegen kan men beschouwen als een thermodynamisch uiterste. Een (111) oppervlak is theoretisch het meest stabiele, een (110) oppervlak in vergelijking minder stabiel. Het probleem in elk van beide gevallen is dat bij bestudering van het éénkristallijne materiaal voorbehandeling en reactie irreversibele modificaties veroorzaken, en dat elke volgende meting de geaccumuleerde effecten van alle vorige omvat.
9. De rol van homogene gasfase-reacties in verschillende "heterogeen" gekatalyseerde processen is onderwerp van debat. Het feit dat desalniettemin slechts weinig publicaties aan dit onderwerp zijn gewijd is te wijten aan de moeilijkheid van de detectie van gasfaseradicalen onder reactiecondities, een experimenteel probleem dat in de toekomst meer aandacht verdient. Het is waarschijnlijk niet louter toevallig dat de meeste oxidatiereacties bij voorkeur bedreven worden bij gassamenstellingen die dichtbij de explosiegrenzen liggen, omstandigheden waarbij makkelijk radicalen gevormd worden.
10. Het bestaan en voorkomen van zg. sub-surface zuurstof is door verscheidene auteurs verondersteld. De precieze locatie ervan en relevante diffusieprocessen zijn daarbij nauwelijks besproken. Liever dan alles onder het oppervlak als een black box te beschouwen, zou men bij wijze van verstandig vervolg op de veronderstelling pogingen kunnen ondernemen verschillende soorten sub-surface zuurstof te onderscheiden.
11. Om tot definitieve uitspraken te komen over de rol van verschillende zuurstofspecies in verschillende reactiepaden zijn ^{18}O labelingsexperimenten en identificatie met snelle

(seconden) *in situ* spectroscopische technieken noodzakelijk. Een duidelijke correlatie van variaties in de katalyse met variaties van spectroscopische vingerafdrukken van verschillende species, gevormd met mengsels van ^{16}O en ^{18}O in verschillende verhoudingen als een functie van de tijd, zou een sprong voorwaarts betekenen van ons begrip van heterogeen gekatalyseerde oxidatiereacties. Er zou van meerduidigheid als gevolg van het “pressure gap” niet langer sprake zijn.

12. In het werk beschreven in dit proefschrift is vastgesteld dat zuurstof opgelost in het inwendige van zilver in feite opgesloten raakt wanneer het oppervlak bij hogere temperaturen ondoorlaatbaar wordt. Dit fenomeen leidt tot een hoge-temperatuur zuurstofdesorptiepiek doorgaans aangeduid als O_2 . De voornaamste methode om de oplosbaarheid van zuurstof in zilver te bepalen is temperatuurgeprogrammeerde desorptie (TPD). Het is dus waarschijnlijk dat met TPD bepaalde oplosbaarheidsconstanten een verhoudingsgewijs grote foutmarge bezitten. In beginsel zou men, om door middel van desorptie de hoeveelheid zuurstof te bepalen die bij een gegeven temperatuur in zilver is opgelost, het monster moeten verhitten tot het smeltpunt.

An Introduction to the Problem of Silver-Catalyzed, Partial-Oxidation Reactions

1.1 The Industrial Relevance of Silver-Catalyzed Partial-Oxidation Reactions

Silver is used in industry as a catalyst for a number of partial-oxidation reactions. Those which have received by far the most attention are the ethylene epoxidation reaction and the formaldehyde synthesis reaction. The importance of these reactions is not to be understated. Both ethylene epoxide and formaldehyde serve as the chemical building blocks for a wide variety of materials which find use in an enormous number of products. There is, therefore, a great scientific and economic motivation for understanding the niceties of these reactions and, in particular, for unlocking the secret to the exceptional catalytic activity of silver.

The focus of this thesis deals with an intensive study of the electrolytic silver catalyst used for the partial oxidation of methanol to formaldehyde. Much of the theory presented here is based on earlier work performed at the Fritz-Haber Institute. The majority of the previous work involved the use of a variety of spectroscopic characterization techniques to determine the nature of the active silver catalyst. The goal of the work presented here is to bridge the gap between UHV studies and measurements made under more realistic reaction conditions. Chapter 3 deals the silver-oxygen interaction. Understanding the ability of silver to activate gas-phase, molecular oxygen is crucial to gaining an in-depth understanding of silver-catalyzed, partial-oxidation reactions. Chapter 4 tackles the methanol oxidation problem directly. The interpretations made in Chapter 4 are, to a large extent, based on the understanding obtained from Chapter 3. It will be shown, however, that a number of problems appear for the methanol oxidation reaction. The decision was made therefore to use the oxidative coupling of methane to C_2 hydrocarbons (OCM) as a test reaction. Use of this reaction made it possible to study the oxidative nature of the silver-oxygen system in much greater detail. The result of the OCM runs proved to be extremely fruitful. In this chapter a number of conclusions are reached which confirm the model proposed for the methanol oxidation reaction. The result is a novel, but very global model for understanding the behavior of partial oxidation reactions in general.

The present chapter provides a brief outline of the state-of-the-art knowledge on the formaldehyde synthesis reaction as well as studies concerning the oxygen-silver interaction. No review of literature regarding the ethylene oxidation reaction is presented here. This is due, primarily, to space constraints. Articles concerning the ethylene oxide reaction are cited in subsequent chapters where appropriate.

1.2 The Formaldehyde Synthesis Reaction

The importance of the partial oxidation of methanol to formaldehyde is rooted in the fact that formaldehyde acts as an invaluable feedstock for a broad spectrum of organic synthesis reactions. The products of these reactions end up as adhesive resins for the woodworking industry, curable molding for plastics, paper and textile additives, binders and foamed resins.¹ Hydrocyanic acid reacts with formaldehyde to form glycolonitrile.² α -Hydroxymethylated adducts may be formed by the acid-catalyzed reaction of formaldehyde with olefins.³ Sugars may be formed by reacting formaldehyde with strong alkalis or calcium hydroxide.⁴ Formaldehyde may react with amines to produce methylamines.⁵ Resins may also be produced *via* reaction with urea, melamine, urethanes, cyanamide, aromatic sulfonamides and amines and phenols.¹ These are just a few of the many reactions which use formaldehyde as a feedstock.

A number of synthesis processes have been developed over the course of the last 100 years. These have all been heterogeneously catalyzed reactions not very much different from the first recorded synthesis of formaldehyde by Hoffman in 1867 who synthesized formaldehyde by passing methanol over a heated platinum spiral. One of the most important of these, the BASF Process, is outlined in greater detail below.

1.2.1 The BASF Process

The silver-catalyzed partial oxidation of methanol to formaldehyde was first employed on an industrial scale by BASF AG in 1905. This process remains largely unchanged and is still in use today. Advances in process design have made yields as high as 91-92 mol% possible. Figure 1 shows a flow chart of the process. A packed-bed reactor is used with a heat exchanger located directly downstream of the reactor for rapid cooling of the extremely unstable gas-phase formaldehyde. The reactor bed consists of a thin layer of electrolytic silver grains 2-3mm thick sandwiched between silver gauze. The reactant throughput is limited by the diameter of the catalyst bed. The reaction is carried run adiabatically. The overall reaction is believed to consist of two primary reaction pathways. The first is the oxidation of methanol to formaldehyde where water is produced as the primary side

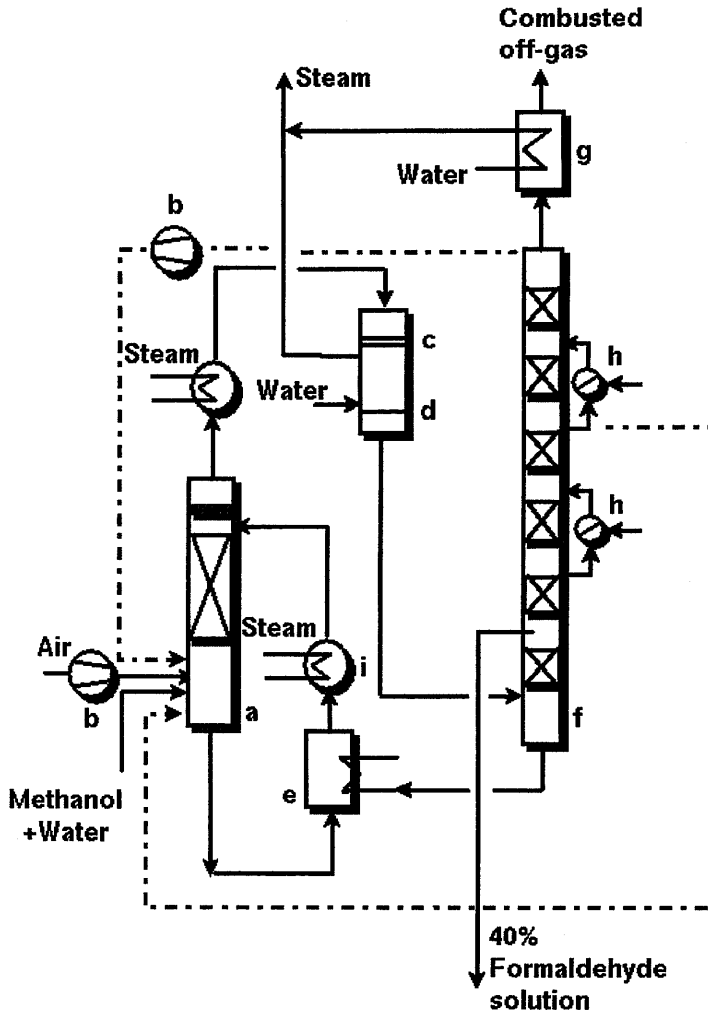


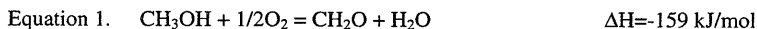
Figure 1. Flowchart of formaldehyde production by the BASF process.

a) Evaporator, b) Blower, c) Reactor, d) Boiler, e) Heat exchanger, f) Absorption Column, g) Steam Generator, h) Cooler, i) Superheater

Upper dashed line represents the off-gas scheme

Lower dashed line represents the formaldehyde solution scheme

product. The second is the direct dehydrogenation of methanol to formaldehyde. These are shown below.



The net ΔH value of -75 kJ/mol shows that the reaction is highly exothermic. The reactor temperature is controlled by varying the $\text{CH}_3\text{OH}/\text{O}_2$ ratio as well as the amount of water which is mixed in the feed. Water is an excellent heat conductor and acts to carry away unwanted heat which might lead to the formation of local hotspots and eventually to reaction runaway. The question as to whether or not water directly participates in reaction is hotly debated and is still not 100% clear⁶. The product stream (point a in Figure 1) consists of a mixture of H_2O , CH_3OH and CH_2O . The exact composition is determined to a large extent by the recycle schemes in operation. The first scheme is referred to as the off-gas recycling scheme. Light-components are removed from the overhead of the adsorption column and are fed back into the reactor with the methanol/air mixture. This is shown by the dotted line in the upper half of Figure 1.

1.2.2 Figure of Flow Scheme for the BASF process

The second scheme is known as the formaldehyde recycle scheme. This is shown by the dotted line in the lower half of Figure 1. Here, a portion of the heavier fraction of the adsorption column is removed and is recycled into the feed. The choice of recycle scheme depends mostly on the desired composition of the final formaline solution. Formaldehyde is not available in a pure form using the oxidative dehydrogenation synthesis method. Gas-phase formaldehyde is unstable at room temperature and polymerizes quickly below 373 K . For this reason, formaldehyde is usually available in an aqueous solution with methanol as a stabilizing agent to prevent polymerization. 40 wt% formaldehyde represents the upper limit for formaldehyde concentrations obtainable with the silver-based technology. Elaborate separation techniques including vacuum distillation have been developed in order to produce gas-phase formaldehyde of high purity¹. These separation procedures are complicated and require a number of separation steps. The economic feasibility of carrying out such elaborate separation steps is therefore questionable. As a result, there exists a great economic incentive for developing an industrial process for the direct production of anhydrous formaldehyde.

The extent to which equations (1) and (2) play a role in reaction is determined primarily by the temperature and the $\text{CH}_3\text{OH}/\text{O}_2$ ratio. Selectivity to dehydrogenation products (equation 2)

increases with increasing temperature and $\text{CH}_3\text{OH}/\text{O}_2$ ratio. It is generally accepted that different oxygen species formed on and in silver function as the active species for both of these reactions^{7,8,9,10,11,12}. The nature of these species is, however, widely debated.

Alternative processes have been developed for the formaldehyde synthesis reaction. These are based primarily on Mo-Fe systems containing a variety of promoters. These processes fall out of the scope of interest of this work and are therefore not dealt with. A number of publications dealing with these technologies have been published and are summarized in Ullman's Encyclopedia of Industrial Chemistry¹.

1.3 Fundamental Research on Silver-Catalyzed Partial Oxidation Reactions

The main body of work presented in this thesis was carried out with the goal of better understanding the partial oxidation of methanol to formaldehyde over unsupported, electrolytic silver. A short summary of literature regarding the formaldehyde synthesis reaction and the silver-oxygen interaction is presented in this chapter. The establishment of a clear understanding of this is necessary before moving on to the more complicated problem of understanding silver-catalyzed partial oxidation reactions.

1.3.1 The Silver-Oxygen Interaction

Research over the last 50 years has seen the development of a number of schools of thought regarding the mechanism of the formaldehyde synthesis reaction. The combined knowledge of model studies made on single crystals under UHV conditions and the testing of industrial catalysts under realistic reaction conditions have provided valuable information explaining the exceptional catalytic activity of silver for partial-oxidation reactions. Despite their many differences in interpretation, one topic these studies have in common is the general acceptance of the importance of understanding the silver-oxygen interaction. Determination of the types of oxygen formed on and in silver as well as an elucidation of the mechanism leading to their formation is viewed by many as a necessary prerequisite to understanding silver-catalyzed partial-oxidation reactions in greater detail.

Single-crystal studies: Research on single-crystal surfaces under UHV conditions forms the largest body of information regarding the silver-oxygen interaction. The majority of single-crystal work has focused on the (110) surface as its relatively high sticking coefficient for oxygen (10^{-3}) significantly simplifies the interpretation of data. Work on the Ag (110) surface has led to the general consensus that oxygen adsorption results in the formation of 3 different oxygen species. Their existence has been confirmed using an arsenal of surface

science techniques such as TDS, HREELS, LEED, XPS, UPS and ISS^{13,14,15,16,17,18,19}. A peroxy-like molecularly adsorbed state partially desorbs as O₂ at 190K and partially decomposes forming surface atomic oxygen. This surface-atomic oxygen recombines and desorbs as O₂ at 600K. Surface-atomic oxygen may also dissolve into the silver bulk forming sub-surface oxygen which begins to become mobile around 540K. This problem will be dealt with in more detail in Chapter 3. A number of silver-oxygen studies are summarized below.

Bowker et. al²⁰ investigated the adsorption and reaction of H₂, H₂O, CO and CO₂ on Ag (110). Isotope labelled studies showed molecular oxygen to be present below 160K. Molecular oxygen dissociated into surface-bound atomic oxygen above this temperature. This oxygen reacted with water to form highly mobile surface OH groups and with CO to form stable surface carbonates which decompose at 485K. LEED results showed ordered oxygen adsorption under these conditions which decomposed with an activation energy of 170kJ/mol. The presence of subsurface oxygen which desorbs around 773K was also suggested. Pre-adsorption of oxygen was found to significantly increase the interaction of silver with organic and water molecules.

Backx et. al²¹ performed what has become one of the classic silver surface-science studies. An investigation of oxygen adsorption on Ag(110) was made in the hope of learning more about the mechanism of ethylene epoxidation. Using electron-energy loss spectroscopy and temperature-programmed desorption, the authors determined that diatomic oxygen desorbs and/or forms atomic oxygen at 173K. A charge transfer model showing electron donation to the π^* antibonding orbital of molecular oxygen which leads to a weakening of the bond with eventual rupture was proposed. This has come to be the more or less accepted model for oxygen activation over silver. The presence of adsorbed atomic oxygen was proposed and it was suggested that this oxygen can diffuse into the sub-surface region above 423K. Bulk-dissolved oxygen was formed above 723K. Both surface and sub-surface species were suggested to be essential for the efficient epoxidation of ethylene to ethylene epoxide over silver.

Less work has been done on the Ag (111) surface. This is due to the fact that the very low sticking coefficient for oxygen adsorption ($\theta < 10^{-6}$) makes studying in anything but the most immaculate UHV conditions impossible. It was suggested that an atomically-adsorbed oxygen species is formed which desorbs at approximately 550K. Grant et. al²² suggested that molecularly-bound surface oxygen desorbs at 380K. The presence of sub-surface oxygen was also suggested.

Cambell et. al. studied the adsorption of oxygen on an Ag (111) single crystal²³. They suggested the presence of 3 states of adsorbed oxygen on the (111) surface. The first was attributed to molecularly-bound oxygen and desorbed at about 215K. This is 50K lower than desorption from the (110) surface. The second species was assigned to surface-bound atomic oxygen and desorbed at 580K. A sub-surface species was proposed as well and exhibited a desorption temperature of 780K. The desorption temperature shifted slightly to higher desorption temperature with increasing dosing pressures. High pressure doses for longer times led to the formation of thermal desorption peaks at 540 and 565K. These peaks were not studied in greater detail. Surface-bound atomic oxygen was found to form ordered overlayers for adsorption on both the (111) and (110) surface. The (111) surface tended to form a $p(4 \times 4)$ surface structure which desorbed at 580K and the (110) surface a $c(6 \times 2)$ structure which desorbed at 617K. The ordered overlayers could be observed at sub-monolayer coverages indicating the formation of islands under these conditions. The XPS O(1s) binding energy assigned to surface atomic oxygen was centered at 528.1eV. Physisorbed oxygen exhibited an O(1s) binding energy of 536eV.

Campbell et al.²⁴ also studied the interaction of oxygen with the Ag (110) surface. The formation of surface-bound atomic oxygen (maximum coverage=0.86) which formed two distinct overlayer coverages was found. Dosing 50 Torr O₂ at 485K led to the formation of a $c(6 \times 2)$ -O overlayer which reacted readily with CO until a coverage of 0.5 was achieved at which point reactivity decreased. This decrease in activity correlated with the formation of a $p(2 \times 1)$ overlayer. The formation of three oxygen species was supposed: O_a (528.1eV), O_{2,a} (529.3eV) and CO_{3,a} (529.9eV). These species exhibit thermal desorption peaks at 170K, 600K and 475K respectively. The presence of sub-surface oxygen was also supposed and was suggested to be inactive for CO titration.

Work on the (111) surface was first conducted by Engelhard and Menzel²⁵ who carried out a thorough study of the (100), (111) and (110) silver surfaces. It is worth mentioning that this is one of the few early studies where the authors took the care to study the influence of standard UHV cleaning techniques (oxidizing, annealing, sputtering) on the morphology of the single-crystalline silver surfaces. LEED and work function measurements showed the (110) face to adsorb oxygen most strongly. It typically formed $(n \times 1)$ superstructures with n varying from 2 to 7. The oxygen saturated surface exhibited a work function increase of 0.87eV relative to the Fermi level. The sticking coefficient on (110) was estimated to be 3×10^{-3} at room temperature. This article is also ahead of its time in that the authors investigated the solid-state chemistry literature in order to take the dissolution of oxygen of the bulk into account. Adsorption measurements were, therefore, made under conditions where oxygen dissolution in the bulk was unlikely. Relatively little information is provided on the (100) and (111)

surfaces as their relatively low sticking coefficients complicate analysis. It was shown, however, that adsorption on the (100) surface was disordered. The presence of both a surface and subsurface (possibly molecular species) was proposed. Adsorption on the (111) surface was believed to occur primarily at defect sites.

Campbell et al.²⁶ investigated the silver (111) surface. This is one of the first studies where a quantitative determination of the oxygen sticking coefficient of 5×10^{-6} for the silver (111) surface was performed. Time has shown this value to be rather large, probably as a result of the high oxygen dosing temperatures ($T < 650\text{K}$) used and the rather aggressive cleaning methods used which likely resulted in a faceted or stepped (111) surface. Molecular oxygen desorbs at 217K and forms atomically-adsorbed oxygen with an O(1s)BE of 528.2eV at 490K. Oxygen was also found to form islands displaying a $p(4 \times 4)$ -O LEED pattern. Saturation was observed for a coverage of 0.41. Subsurface oxygen was observed for oxygen adsorption performed at temperatures in excess of 600K. The titration of oxygen with CO was also presented.

Bao et. al.²⁷ detected the formation of a number of oxygen species on and in Ag(111) using a variety of surface-science methods. Oxygen was found to be incorporated in the interstitial sites of silver at temperatures above 573K. This species exhibited a broad XPS signal at 530 eV. A second oxygen species which is intercalated in the uppermost silver layers was shown to be formed at temperatures in excess of 773K. This species showed a binding energy of 529eV. UPS and Auger spectroscopy combined with ISS showed this species to be confined to the uppermost silver layer. It's formation resulted in a 1eV increase in the silver work function relative to the fermi level. This species was suggested to be the oxygen species responsible for the selective dehydrogenation of methanol to formaldehyde. Further work in this group²⁸ showed the (111) surface to reconstruct during this pretreatment. This reconstruction resulted in the formation of facets with a slight expansion of the (111) surface due to the incorporation of oxygen into the silver lattice.

Adsorption on polycrystalline Ag: A number of studies have been dedicated to the investigation of oxygen adsorption on polycrystalline samples. Studying a polycrystalline sample as opposed to a single crystal was one of the first steps to understanding the interaction of oxygen with a real silver catalyst. The necessity of studying gradually more complex systems stems from the fact that chemistry has very seldom proven be the sum of its parts. Oversimplification of a heterogeneously catalyzed system is a danger which surface-science studies have made all too obvious. The contribution of single-crystal studies forms the foundation for the interpretation of the data obtained for these more realistic catalysts.

Wang et al. have studied the adsorption of oxygen on polycrystalline ribbons using reflection-adsorption infrared spectroscopy.^{29,30,31} These studies were performed in-situ with a polycrystalline catalyst. This is an excellent series of studies using isotope-labeling experiments in conjunction with TDS and RAIRS experiments to characterize the nature of oxygen species formed over a broad range of conditions. The thermodynamics of the adsorption processes involved in their formation was also presented. Results show the formation of two forms of molecularly adsorbed oxygen. The first (622cm^{-1}) was found to adsorb parallel to the surface and desorbs at 183K. The second (983cm^{-1} , probably a peroxide) is bound perpendicular or tilted to the surface and desorbs at 263K. Both adsorption processes are activated and the adsorption enthalpies are linear functions of the coverages. The atomic-bound state desorbs at 604K and shows a coverage-independent adsorption enthalpy. All adsorption processes appeared to be activated.

Rehren et al.³² studied the adsorption of oxygen as well as its subsequent reaction with H_2 over silver foils. This study is truly pioneering in the sense that it is one of the first studies dedicated to the study of a silver system under conditions approaching that of the actual formaldehyde synthesis conditions. It was determined that a great deal of oxygen dissolves in the silver lattice. This oxygen was supposed to preferentially occupy octahedral holes in the silver lattice. Changes of morphology after treatment in O_2 and H_2 were studied. In particular, the formation of holes resulting from the recombination of sub-surface oxygen and hydrogen resulting in sub-surface water formation with subsequent mechanical failure of the silver leading to rupture and hole formation was suggested. A thorough XPS study was also performed. The role of impurities in the interpretation of the XPS, UPS and Auger spectra was particularly well described. This work forms more or less the foundation of the theory presented in this thesis. It was also shown that one of the greatest difficulties encountered by those studying oxygen adsorption on silver is the formation of surface carbonates *via* reaction of oxygen with both bulk carbon impurities and background gases in the UHV chamber. These impurities typically desorb in two peaks at 350 and 450K.⁶ The O (1s) binding energy of surface carbonate is 529.9 eV. It is critical to determine the amount of carbon bound to the surface before interpreting the O (1s) data. Failure to do this will result in the false assignment of surface species.

Addition of surface modifiers & impurities: Many catalysts contain promoters (K, Cl, Cs, C, Na) which are used to improve catalyst performance in one way or another. The exact reason why promoters lead to improved performance is not known. Detailed studies often culminate in a rather vague explanation based on a "synergetic effect" between pure-component catalysts and those mixed with promoters. The presence of even trace amounts of impurities may dramatically affect catalytic performance. A number of studies have been

carried out with the goal of better understanding the role of promoters and impurities for silver-catalyzed, partial oxidation reactions.

It was discovered some time ago that addition of trace amounts of alkali metals to the ethylene epoxidation feed stream results in significant improvement in yields to ethylene epoxide.^{33,34} This discovery stimulated a great deal of research into the elucidation of the mechanism leading to this enhanced catalytic performance. The majority of this work was dedicated to studying the influence of pre- or co- adsorbed alkali metals on the types of oxygen species formed. This was typically done ex-situ, using a variety of surface- science tools under UHV conditions. Au et. al³⁵ studied the interaction of oxygen and water pretreated Ag (110) surfaces with HCl vapor. They concluded that the role of HCl was to displace weakly-bound surface atomic oxygen, O_2^- which was believed to be responsible for the total oxidation of ethylene. Analysis of a catalytically active, industrial E.O. catalyst showed a broad XPS signal at approximately 532eV. This was assigned to molecularly adsorbed oxygen, O_2^- . The conclusion was made, therefore, that molecularly adsorbed oxygen was critical to reaction. This is a rather weak argument in light of the fact that hydroxyl groups also show an XPS binding energy of 532eV. The presence of both hydrogen and oxygen in the reactant streams would likely lead to the formation of hydroxyls. The assignment to molecular oxygen at temperatures up to 473K is in contradiction to the findings of the majority of other authors that molecular oxygen desorbs above 190K^{6,7,8,9,10,11,12}.

Ayyoob et. al³⁶ studied the adsorption of oxygen on silver foils which were treated with either potassium or cesium. Addition of either of the alkali metals prior to oxygen dosing at room temperature was found to significantly enhance oxygen adsorption. In particular, potassium pre-adsorption was believed to lead to the formation of O_2^- (533.2eV), OX^- (530.2eV) and O_2^-- (528.2eV). Cesium treatment led to the formation of OX^- (530.2eV) and O_2^-- (528.2eV). with O_2^- (533.2eV) only being formed at higher cesium coverages. Despite the suggestion that the work was motivated by a desire to better understand the ethylene epoxidation reaction, no suggestion was made as to how these changes induced by metal adsorption might affect catalytic activity.

Carbon is present as a bulk impurity in all silver samples^{37,38} and is a major problem for those wishing to study clean metal systems. Significant amounts of carbon may be formed during both the ethylene epoxidation reaction and the formaldehyde synthesis as the reactants in both cases are hydrocarbons. It is, therefore, important to answer the question as to whether or not this carbon has any effect on catalytic activity.

Boronin et al.³⁹ impregnated silver films and foils with carbon and studied the effect on oxygen adsorption. It was found that only atomic (528.5 eV) and sub-surface atomic oxygen (530 eV) could be prepared on these silver foils. This surface atomic oxygen reacts readily with carbon forming surface carbonates which subsequently decompose at about 420K. Increasing the amount of carbon led to a significant rise in the amount of sub-surface oxygen. The formation of a molecular state of oxygen was proposed for carbon-treated samples treated in excess of 10Pa O₂ (530.3eV). The fact that the oxygen species formed show a strong dependence on the carbon content present led the authors to conclude that elemental carbon likely affects the catalytic activity and selectivity for the ethylene epoxidation reaction.

As seen above, the majority of literature regarding the silver-oxygen system is based on studies made using standard UHV techniques. Most of these studies suffer from the common flaw that they are performed under conditions which are far removed from those encountered in the industrial process. This is the so-called "Pressure Gap" problem. The validity of this work comes into question when considering whether the relevant reaction parameters are sufficiently represented under UHV conditions.

This is one problem which is tackled in this thesis. Thermal desorption spectroscopy and XPS results presented in subsequent chapters were taken after pretreatment under conditions approaching, as closely as possible, those of the catalyst under reaction conditions. One can always argue that this post-mortem analysis may not be representative of the actual state of the catalyst under reaction conditions. This is an inherent weakness to these types of measurements. The error introduced by such methods can be minimized, however, by carefully choosing the optimal conditions for pretreatment and analysis. A closer analysis of the conditions under which such problems can be eliminated is presented in chapter 2 which focuses on the experimental set-ups used to obtain the data presented in this thesis.

1.4 The Methanol Oxidation Reaction

Uwins et al.⁴⁰ have provided great insight into the variation of the silver morphology under reaction conditions by using environmental scanning microscopy for the *in-situ* characterization of the silver catalyst during reaction. A major problem with these studies is that no gas-phase analysis was performed during reaction. In addition, the in-situ cell used, is far removed from an actual catalytic reactor. Design of an in-situ reactor should not only be made with the goal in mind of optimizing the resolution of the spectroscopic or microscopic method in question. The reactor design characteristics should also be taken into consideration when deriving results for a catalytically-relevant system.

Wachs and Madix carried out a detailed study of methanol oxidation over a (110) silver single crystal.⁴¹ Both the isotopes O^{18} and CH_3OD were used to determine the transfer processes occurring in the various reaction pathways. Surface methoxy was found to be the dominant species and was suggested to be the longest-lived intermediate in the partial oxidation of methanol to formaldehyde. The formation of surface oxygen was necessary for methanol adsorption, which occurred, for the most part, dissociatively. The interaction of methanol with pre-adsorbed oxygen occurred entirely *via* dehydrogenation of the hydroxyl D forming CH_3O and $D_2^{18}O$ as products. Further dehydrogenation of the methoxy intermediate leads to formaldehyde formation with subsequent desorption into the gas phase. This article is one of the pioneering articles dealing with the silver-catalyzed, partial oxidation of methanol to formaldehyde. The value of the information must, however, be weighed with the fact that the conditions used are incredibly far removed from the actual conditions of catalysis. TPR measurements were made with a maximum temperature of 330K. This is 643K lower than the 973K temperature used in the industrial reaction. The difference between the dosing pressure and partial pressure of reactants in the reactor as well as the lack of steady-state measurements lend even more ambiguity as to the actual value of the results presented.

Schubert et al.⁴² showed that silver undergoes massive restructuring after being used in the methanol-oxidation reaction. Atomic force microscopy (AFM) analysis of samples which had undergone reaction for various times showed that the system was in a dynamic equilibrium with its reactive surroundings. The participation of the previously mentioned (see Bao et al.) O_a , O_b and O_c was also proposed here. Further work in the group by Herein et al.⁴³ showed that the silver bulk and surface undergo massive morphological restructuring after treatment in oxygen or methanol. The facet formation is driven by the oxygen-induced anisotropy of the surface-free energy. The incorporation of oxygen into the silver bulk results in a texturing of the bulk which exhibits a strong dependence on pretreatment pressure and temperature.

1.4.1 The role of gas-phase, homogeneous reaction

A number of authors have suggested that homogenous, gas-phase reactions, play an important role in the methanol oxidation reaction. It will be shown later, in the experimental section of this thesis regarding methanol oxidation reaction, that gas-phase reactions definitely contribute to the overall reaction mechanism.

Lefferts et al.^{44,45,46,47} explained, in a series of articles, the role of silver morphology and the silver-oxygen interaction in the methanol oxidation reaction. The work in this thesis follows the trend of Lefferts¹⁴⁻¹⁷ work in many ways. It is logical to start with a thorough understanding of the silver-oxygen system and then move on to tackle the more difficult

methanol oxidation. The theory presented in this thesis differs from that suggested by Lefferts¹⁴⁻¹⁷ et al. in a number of ways. In particular, the dynamic role of sub-surface oxygen in reaction was not suggested by Lefferts et al.¹⁴⁻¹⁷ The existence of a number of oxygen species, each playing a different role in reaction, was also proposed by Lefferts. Reaction of methanol with surface atomic oxygen was believed to result in the complete oxidation of methanol to formaldehyde. Oxygen strongly bound at surface defects as well as sub-surface oxygen were also proposed to exist. Both were believed to participate in reaction, primarily resulting in the formation of direct dehydrogenation of methanol to formaldehyde and hydrogen.

Gariyban et. al.^{48,49} suggested that gas-phase radicals, in particular peroxy radicals, play an important role in the formaldehyde-synthesis reaction. This conclusion was based on the qualitative trend observed between the formation of peroxy radicals and formaldehyde for reaction between 773 and 905 K. Hydroperoxy and alkyl peroxy radicals were also observed to desorb from the catalyst surface. It was suggested that radical initiation occurs at the catalyst surface with subsequent reaction of the radical with a silver-bound oxygen species to a more stable complex. All oxygen-containing products were believed to be formed heterogeneously.

Aneke et al.⁵⁰ studied the partial oxidation of methanol over an unsupported silver catalyst with a pulse system. By varying the dead volume of the system, the authors found that gas-phase reactions play a large role in reaction. No turbulence should be present under the reaction conditions used eliminating the possibility that back-mixing effects lead to the decreased formaldehyde production upon decreasing the dead volume with glass beads. No attempt was made to quantify the extent to which gas-phase reactions play a role. It was also found that high contact times lead to the formation of complete oxidation products. This is not surprising in light of the intrinsic thermodynamic instability of gaseous formaldehyde.

Research on the contribution of gas-phase reactions in heterogeneously initialized reactions is sparse. This is an area where a great deal remains to be done. An exception to this is the oxidative coupling of methane to C₂ hydrocarbons. Lunsford et al.^{51,52} have shown that the OCM reaction is initiated at the catalyst surface. The radicals formed desorb and subsequently recombine in the gas phase. This type of free-radical chain reaction may be applicable to more systems than just OCM. It will be shown in this thesis that gas-phase reactions play a significant role in the partial oxidation of methanol to formaldehyde. The exact role of gas phase reaction is extremely hard to determine as very few reliable techniques are readily available for studying the gas-phase reaction of free radicals. Nevertheless, it will

be shown (in chapter 4) that the methanol oxidation reaction is both heterogeneously and homogeneously catalyzed.

1.5. Motivation for this Thesis

What becomes immediately clear when examining the wealth of literature presented here is that very little is actually known about the details of the formaldehyde synthesis reaction. In particular, the effect of silver morphology is hardly dealt with (Exception is Lefferts¹⁴⁻¹⁷ and Uwins⁴⁰ et al.). The excellent study provided by Lefferts et. al.(see above) is by far the most detailed study of the formaldehyde synthesis reaction. Almost none of the surface-science studies presented took the pains to look for morphological changes of the catalyst after having treated the catalyst in oxygen at elevated temperatures. It is very likely that many of these works are flawed in the assumption that the single-crystalline face which was placed in the UHV chamber prior to treatment retains it's morphology throughout the course of the study. The use of LEED as a characterization technique for the pristineness of the surface structure is not always sensitive to the formation of surface facets. These articles must be read, therefore, with great care and a critical eye.

It is the goal of this thesis, to provide strong catalytic evidence for the validity of the previously proposed models^{53,54} which were based on results obtained using surface-science methods under conditions far removed from the actual conditions of catalysis. It will be shown that by careful consideration of the pertinent reactions and reaction parameters, one may obtain a wealth of information supporting the previously-proposed models. A number of questions are answered. Is the formation of subsurface oxygen necessary for reaction? If so, what role does it play? What type of diffusion mechanism is present? What is the rate limiting step of reaction? Do surface and/or bulk defects play a role in catalysis? Is the reaction structure sensitive and if so why?

References

1. Ullman, in "Ullman's Encyclopedia of Industrial Chemistry", 5th Edition, **A11**, 619 (1988).
2. "Formaldehyde Product Bulletin", Borden Chemical Co., Columbus Ohio, Feb. 1978
3. *Kirk-Othmer*, **11**, 231.
4. Orthner L. and Gerisch E., *Biochem. Z.* **259** 30 (1933).
5. Gilman H.: *Org Synthesis Coll.*, **vol. I**, J. Wiley & Sons Inc., New York, 514 (1932).
6. Barteau M.A. and Madix R.J., *Surf Sci.* **140** 108 (1984).
7. Bao x., Pettinger B., Ertl G., Schlögl R. *Ber. Bunsenges. Phys. Chem.* **97** No.3, 97 (1993).
8. van Santen R. and de Groot C., *J. Catal.* **98**, 530 (1986).
9. Herein D., Nagy A., Schubert H., Weinberg G., Kitzelmann E., Schlögl R., *Z. Phys. Chem Bd.* **197**, 67 (1996).
10. Leffets L., van Ommen J.G., Ross J.R.H., *Appl. Cat.*, **23**, 385 (1986).
11. Bukhtizarov V.I., Prosvirin I.P., Kvon R.I., *Surf. Sci.*, **320** L47 (1994).
12. Prince K.C., Paolucci G., Bradshaw A.M., *Surf. Sci.*, **175**, 101 (1986).
13. Barteau M.A. and Madix R.J., *Surf. Sci.* **97**, 101 (1980).
14. Backx C., de Groot C.P.M and Biloen P., *Surf. Sci.* **104**, 300 (1981).
15. Backs C., de Groot C.P.M., Biloen P. and Sachtler W.H.M, *Surf. Sci.* **128**, 81 (1983).
16. Sexton B.A. and Madix R.J., *Chem. Phys. Lett.* **76**, 294 (1980).
17. Martin R.L. and Hay P.J., *Surf. Sci.* **130**, L283 (1983).
18. Engelhard H.A. and Menzel D., *Surf. Sci.* **57**, 591 (1976).
19. Au C.T., Singh-Boparai S. and Roberts M., *J. Chem. Soc., Faraday Trans. 1*, **79**, 1779 (1983).
20. Bowker M., Barteau M.A., Madix R.J., *Surf. Sci.* **92**, 528 (1980).
21. Backx C., de Groot C.P.M., Biloen, P., *Surf. Sci.* **104**, 300 (1981).
22. Grant R.B. and Lambert R.M., *Surf. Sci.* **146**, 256 (1984).
23. Campbell C., *Surf. Sci.* **157**, 43 (1985).
24. Campbell C. and Paffett M., *Surf. Sci.* **143**, 517 (1984).
25. Enbelhardt H.A. and Menzel D., *Surf Sci.* **57** 591 (1976).
26. Campell C.T., *Surf. Sci.* **157**, 43 (1985).
27. Bao X., Muhler M., Schedel-Niedrig T., Schlögl R., *Phys. Rev. B*, **54**, 2249 (1996).
28. Bao X., Barth J.V., Lempfuhr G., Schaster R., Uchida Y, Schlögl R., Ertl G., *Surf. Sci.*, **284**, 14 (1993).

29. Wang X.D., Tysoe W., Greenler R. and Truszkowska K., *Surf. Sci.* **258**, 335 (1991).
30. Wang X.D., Tysoe W., Greenler R. and Truszkowska K., *Surf. Sci.* **257**, 335 (1991).
31. Wang X.D. and Greenler R., *Phys. Rev. B* **43**, 6808 (1991).
32. Rehren C., Muhler M., Bao X., Schlögl R., Ertl G., *Z. Phys. Chem.*, **174**, 11 (1991).
33. Kilty P.A. and Sachtler W.M.H., *Catal. Rev.* **10** 22 (1974).
34. Anderson R.B. in "Catalysis" Vol. 4, Ed P.H. Emmett (Reinhold, N.Y., 1961) 140.
35. Au C., Boparai S. and Roberts M., *J. Chem. Soc., Faraday Trans. 1*, **79**, 1779 (1983).
36. Ayyoob M. and Hegde M.S., *Surf. Sci.* **133**, 516 (1983).
37. Joyner R.W. and Roberts M.W., *Chem. Phys. Lett.* **60**, 459 (1979).
38. Briggs D., Marbrow R.A. and Lambert R.M., *Surf. Sci.* **65**, 314 (1977).
39. Boronin A.I., Bukhtiyarov V.I., Vishnevskii A.L., Boroskov G.K. and Savchenko V.I., *Surf. Sci.* **201**, 195 (1988).
40. Uwins P., Millar G., Nelson M., *Microscopy Research and Technique*, **36**, 382 (1997).
41. Wachs I., Madix R., *Surf. Sci.* **76** 531 (1978).
42. Schubert H., Tegtmeier V., Herein D., Bao X., Muhler M., Schlögl R., *Catal. Lett* **33**, 305 (1995).
43. Herein D., Nagy A., Schubert H., Weinberg G., Kitzelmann E., Schlögl R., *Z. Phys. Chem* **197**, 67 (1996).
44. Lefferts L., van Ommen J.G., Ross J.R.H., *Appl. Cat.*, **31**, 291 (1987).
45. Lefferts L., van Ommen J.G., Ross J.R.H., *Appl. Cat.*, **23**, 385 (1986).
46. Lefferts L., van Ommen J.G., Ross J.R.H., *Appl. Catal.*, **34**, 329 (1987).
47. Lefferts L., van Ommen J.G., Ross J.R.H., *Proc. 9th Int. Conf. Catal.*, Elsevier Science B.V. Amsterdam Vol. **4**, 1672 (1988).
48. Garibyan T.A., Grigoryan R.R., Ya Margolis L. and Nalbandyan A.B., *Kinetika i Kataliz*, **17**, 229 (1976).
49. Grigoryan R.R., Garibyan T.A. and Nalbandyan A.B., *Arm. Khim. Zhurn.*, **34**, 832 (1981).
50. Aneke L. F., den Ridder J.J.J. and van den Berg P.J., *Recueil, J. of the Roy. Neth. Chem. Soc.*, **100**, 236 (1981).
51. Lunsford J.H., *Proc. 10th Intl. Congr. Catal.*, Budapest (Eds: L. Guzzi et al.) Elsevier, 103 (1993).
52. Lunsford J.H., *Catal. Today* **6**, 235 (1993).

53. Bao X., Pettinger B., Ertl G., Schlögl R., *Ber. Bunsenges. Phys. Chem.* **97**, No.3, 97 (1993).

54. Schubert H., Tegtmeier U., Herein D., Bao X., Muhler M., Schlögl R., *Cat Lett.*, **33**, 305 (1995).

An Overview of the Experimental Methods Used**2.1 Introduction**

Catalysis is a field of science requiring expertise in a broad spectrum of disciplines. Physical, inorganic and organic chemistry, material science, ceramics, solid-state chemistry, engineering and physics are some of the areas which combine to form the body of knowledge necessary to obtain a clear understanding of the fundamentals of heterogeneous catalysis. A large number of analytical tools are used to fully characterize all of these facets of heterogeneous catalysis. These vary from reactor studies performed with the goal of optimizing the catalytic activity of the sample in question to a variety of characterization techniques for studying the chemistry of the solid state bulk and surface properties. Table 1 categorizes the various methods used and includes a brief explanation of the advantages and disadvantages inherent to each.

The main purpose of this chapter is two-fold. It provides the reader with a general idea of the theory behind the methods used. A detailed study of the methods is not intended and the reader is referred to the relevant literature where needed. The second point is to provide a critical assessment of complications which may arise when using the technique for the silver system studied in this thesis. Where possible, calculations are performed in order to determine the limitations placed on each method under the given measuring conditions.

Table 1: Analytical Techniques Used in this Thesis

Method	Applications	Advantages	Disadvantages
Tubular Integral Reactor	Investigation of optimum catalytic conditions.	High Conversions, High Selectivity, Simple and Cheap	Impossible to perform Kinetic Analysis.
Tubular Differential Reactor	Investigation of reaction kinetics (conversion<5%)	Simple construction and cheap.	Low conversions require precise analytical equipment.
Temperature Desorption Spectroscopy (TDS)	Investigate adsorption-desorption phenomena and solid-state diffusion	To determine the presence of different adsorbed/dissolved states.	May only be performed ex-situ under „Post-Mortem“-UHV conditions.
X-ray Photoelectron Spectroscopy (XPS)	Identification of chemical compounds in the near-surface region.	Determination of composition and oxidation states of surfaces.	May only be performed ex-situ under „Post-Mortem“-UHV conditions.
X-Ray Diffraction (XRD)	Bulk compositional and structural information for crystalline materials..	High precision information about bulk-structure.	Only provides bulk-averaged information (Conc > ~3%). Material must be crystalline.
Ion Scattering Spectroscopy (ISS)	Sensitive technique for determination of surface compositions.	Very surface sensitive. Depth profiling of samples is possible.	Performed ex-situ under UHV conditions. Difficult to quantify.
Scanning Electron Microscopy (SEM)	Provides images with a maximum resolution of about 10nm.	Easy sample preparation. Both conducting and non-conducting samples may be measured.	Limited resolution. May only be performed ex-situ under vacuum conditions.
Scanning Tunneling Microscopy (STM)	Provides images with Angstrom resolution	High magnification. Provides a 3-D image of the surface (depth/height information)	Limited to conducting materials. Powder samples are difficult to analyze

2.2 Reactor Characteristics

The first two categories are dealt with in this section; tubular integral and differential reactor design. Figure 1 shows a schematic of the tubular reactor used for all measurements made in this thesis. It consists of a quartz tube which is heated by an electrical heating oven. The oven temperature is controlled to within 1 K of the set-point with a Eurotherm PID temperature controller. Ceramic wool plugs are placed in the annulus formed between reactor and oven at the top and bottom in order to minimize temperature gradients over the length of the oven. The catalyst is located in a 2 cm isothermal zone near the center of the oven and is held in place in the reactor tube by quartz-wool plugs. Quartz plugs are placed above and below the catalyst bed in order to minimize the dead volume of the reactor. Tests for the presence of homogeneous, gas-phase reactions can be made by comparing the conversions obtained with and without these plugs. It is important to note that the thermocouple

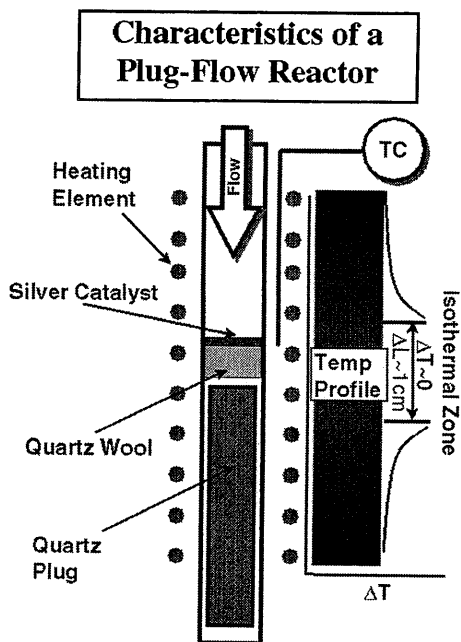


Figure 1. Schematic of the plug-flow reactor used in subsequent studies.

is located outside of the quartz tube directly next to the catalyst bed. Immersion of the thermocouple in the catalyst is optimal for accurate temperature measurements. The high activity of the K-type, Ni-Cr thermocouple for the reactions performed in this thesis makes this impossible. The accuracy of the temperature measurements is, therefore, limited as the net-exothermicity of reaction likely leads to higher local temperatures than measured. The two reactions studied here are methanol oxidation and the oxidative coupling of methane to C_2 hydrocarbons. The relevant equations are shown below.

2.3 Thermodynamics of the Reactions Studied

Methanol Oxidation:

Equation 1.	$CH_3OH \rightarrow CH_2O + H_2;$	$\Delta H = +84kJ/mol$
Equation 2.	$CH_3OH + \frac{1}{2}O_2 \rightarrow CH_2O + H_2O;$	$\Delta H = -159kJ/mol$
Equation 3.	$CH_2O \rightarrow CO + H_2;$	$\Delta H = +12.5kJ/mol$
Equation 4.	$CH_3OH + \frac{3}{2}O_2 \rightarrow CO_2 + 2H_2O$	$\Delta H = -674kJ/mol$
Equation 5.	$CH_2O + O_2 \rightarrow CO_2 + H_2O$	$\Delta H = -519kJ/mol$

Methane Coupling:

Equation 6.	$2CH_4 \rightarrow C_2H_6 + 2H_2$	$\Delta H = +66kJ/mol$
Equation 7.	$2CH_4 \rightarrow C_2H_4 + H_2$	$\Delta H = +186kJ/mol$
Equation 8.	$C_2H_4 + 3O_2 \rightarrow 2CO_2 + 2H_2O$	$\Delta H = -1,309kJ/mol$
Equation 9.	$C_2H_4 + O_2 \rightarrow 2CO + 2H_2$	$\Delta H = -257kJ/mol$
Equation 10.	$C_2H_6 + O_2 \rightarrow 2CO + 3H_2$	$\Delta H = -136kJ/mol$
Equation 11.	$C_2H_6 \rightarrow C_2H_4 + H_2$	$\Delta H = +120kJ/mol$

Secondary Reactions:

Equation 12.	$H_2 + \frac{1}{2}O_2 \rightarrow H_2O;$	$\Delta H = -243kJ/mol$
Equation 13.	$CO + \frac{1}{2}O_2 \rightarrow CO_2$	$\Delta H = -68kJ/mol$

Comparison of the methane coupling reactions with the methanol oxidation reactions show that the methane coupling reaction is, in general less exothermic than the methanol oxidation. The coupling of methane to C_2 hydrocarbons (Equations 6 and 7) is extremely endothermic.

The accuracy of the temperature measurement for the methane coupling studies should therefore be greater than for the methanol oxidation as local heating effects at the catalyst surface are minimized. This is just one of many advantages in studying the OCM reaction as opposed to the more pragmatic, but significantly more complicated, methanol oxidation reaction. This is discussed in more detail in Chapters 5 and 6 where the oxidative coupling of methane is investigated in depth.

2.4 Reactor Design

The important guidelines for the catalyst testing performed in this thesis are presented below. The mathematical niceties involved are not presented. The following books contain excellent reviews of the pertinent design criteria and present them in greater detail.^{1,2,3}

The difference between a differential and an integral tubular reactor lies in the conversions obtained. Figure 2 shows two examples of possible concentration-reactant profiles in a tubular reactor. The reactor on the left shows 100% conversion of reactant A to product B. This is typical of the methanol oxidation reaction where 100% O_2 conversion is nearly always observed. The reactor on the right shows a low conversion of reactant A at 3%. This is typical of the CH_4 conversions observed for the OCM reaction. The design Equation for a tubular reactor is derived as follows.

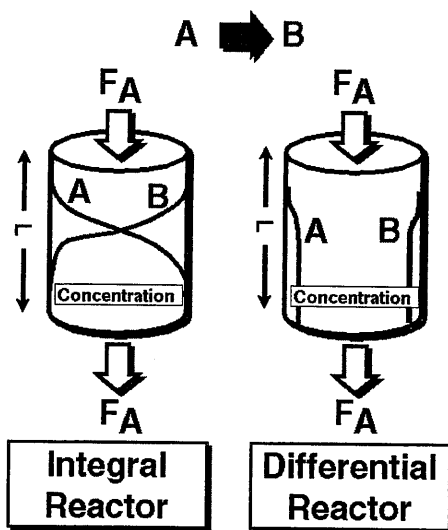


Figure 2. Schematic showing the difference between the concentration profile obtained in an integral reactor with that typical of a differential reactor.

Cutting a differential slice out of the reactor cross-section of the reactor shown in Figure 2 and performing a mass balance yields the following relationship.

Equation 14. $(\text{Flow of } A_{\text{in}}) + (\text{Generation of A}) - (\text{Flow of } A_{\text{out}}) = (\text{rate of accumulation of A})$

Equation 15.
$$F_{A0} - F_A + \int_0^V r_A dV = \frac{dN_A}{dt}$$

The integral term in Equation 15 presents an inherent difficulty in determining the actual reaction rate. This is a result of the fact that the reaction rate varies as a function of the reactor length. The observed reaction rate is, therefore, an integral value, averaged over the length of the catalyst bed. The limiting case exists for the instance where conversion is low. In this case, the variation in reactant concentration is so small that the reaction rate may safely be assumed to be constant over the length of the catalyst bed. A maximum conversion of 5% is typically assumed when defining „Differential“ reactor conditions. In this case, the integral term in Equation 15 is eliminated and the intrinsic reaction rate may be determined using Equation 16.

Equation 16.
$$\frac{dn_A}{dt} = \frac{F_{A,\text{in}} - F_{A,\text{out}}}{F_{A,\text{in}}} = X_A \times F_{A,\text{in}} ; \text{ Where } X_A = \text{conversion of reactant A}$$

One of the most important assumptions implicit to this calculation is that of the plug flow nature of the reactor. Plug-flow describes the shape of the gas velocity profile in the reactor as being approximated by a flat front. In reality, the gas velocity is often a function of the radial distance from the reactor center. Friction with the reactor walls results in a low gas velocity near the walls and a maximum at the reactor center. Dautzenberg⁴ determined the necessary criteria for plug flow. This is shown in Equation 17.

Equation 17.
$$\frac{L}{d_p} > (92.0) N_{\text{Re}_p}^{-0.23} \ln \frac{1}{1-x} ; N_{\text{re}} = \rho D v / \mu$$

L is the necessary reactor bed length, D is the pipe diameter, ρ is the gas density, ν is the gas viscosity, d_p is the catalyst particle diameter, N_{Re} is the Reynold's number and x is the conversion. Typical values of N_{Re} obtained for the reactions used in this thesis fall in the range of 25-75. Particle sizes are between 0.2 and 1mm. Methanol conversions are typically about 70% for CH_2O synthesis and methane conversions are 5% for the OCM reaction. $\frac{L}{d_p}$

ratios of 45 and 16 should therefore be used respectively. It will be shown in Chapter 3 that the decomposition of CH_2O *via* secondary reactions occurs for longer reactor beds. This places a limit on the reactor bed length for the formaldehyde synthesis reaction. There are therefore likely to be large axial variations in the catalyst surface temperature throughout the bed. This is not a problem for the OCM reaction where the $\frac{L}{d_p}$ ratios are greater than 25.

Axial variations in temperature are negligible for the setup used in this thesis (See Experimental in Chapters 4 and 4) which typically had a value of 60.

A differential and integral reactor have, therefore, essentially the same physical construction. The differential reactor has the advantage of providing information about the intrinsic reaction kinetics. The integral reactor is, however, ideal for producing high conversions and optimizing reaction conditions. The tubular reactor used in this thesis was only used in the integral mode. The calculated reaction rates are, therefore, only approximations of the intrinsic reaction rates.

2.4.1 Mass and Heat Transfer Limitations

Mass and heat transfer effects are of particular importance in heterogeneously-catalyzed reactions. This is due to the fact that adsorption of at least one reactant is necessary for reaction. In order for this to occur, the reactant must diffuse to the surface. In addition, heat must be transferred to the catalyst surface. This may occur *via* gas-phase, convective heat transfer or through conductive heating from the reactor walls into the solid catalyst bed.

Two main diffusion barriers must usually be overcome before reaction at the surface of a catalyst may occur. The first is commonly known as film layer diffusion or interphase diffusion and is shown in Figure 3. This arises from the fact that the resistance to the

convective flux of a diffusing species is slower in a stagnant medium relative to one which is flowing. Flow past a non-moving object always results in a boundary layer of fluid around the object which is essentially stagnant. This is known as the hydrodynamic boundary layer and is defined as the distance from the surface of a solid object to where the fluid velocity is 99% of the bulk fluid velocity. The thickness of this layer is inversely proportional to the linear gas velocity. The presence of boundary-layer diffusion may be tested by changing the linear gas flow in the reactor but keeping the contact time ($V_{\text{reactor}}/\text{Flow rate}$) constant. Higher gas velocities result, therefore, in decreased contributions from boundary-layer diffusion. Furthermore, the use of gases with a high thermal conductivity such as He or H_2 is preferred over that of poorly conducting gases like N_2 for the highly exothermic reactions dealt with in this thesis. The fact that He has 5 times the thermal conductivity of N_2 minimizes errors arising from local heating effects. Thermal gradients in the reactor bed are thus minimized.

The second barrier to diffusion is known as pore diffusion. The silver samples used here contain a negligible pore system. Pore diffusion is, therefore, not considered here.

The measured reaction rate is only equal to the intrinsic rate of reaction for the case in which diffusion occurs much faster than reaction. This will be shown to be a problem for studies of

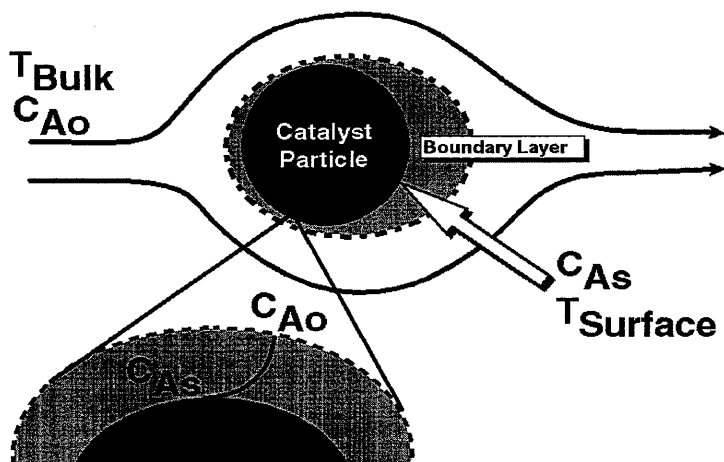


Figure 3. Schematic showing the effect of film diffusion for flow around a spherical catalyst pellet.

the partial oxidation of methanol to formaldehyde. This is a very fast reaction which is typically diffusion limited. In this case, boundary layer diffusion determines the measured reaction kinetics.

2.5 Characterization Techniques

2.5.1 X-Ray Photoelectron Spectroscopy(XPS)

XPS is an analytical tool which has proven to be invaluable in the determination of the chemical composition of the near-surface region of catalyst materials. In this thesis, XPS has primarily been used for the identification of the presence of various states of oxygen bound to silver. Figure 4 shows a schematic of a typical XPS apparatus (modified Leybold-Heraeus setup). The principle components are as follows. A movable sample holder allows for the high-pressure, high-temperature pretreatment of the sample in a variety of atmospheres. The analyzer chamber contains the X-ray source and the concentric hemispherical detector. The X-ray source is of a dual-anode setup which allow for the production of both Al K_{α} (1486.6eV, width 0.85eV) and Mg K_{α} (1253.6eV, width 0.7eV) radiation. XPS makes use of the photoelectric effect which was discovered by Hertz in 1887. Electrons may, therefore, be emitted from a solid when it is illuminated by a flux of photons with an energy greater than the kinetic energy of the ejected electrons. The relationship governing the interaction of a photon with a core level is as follows.

Equation 17.
$$E_K = h\nu - E_B - e\phi$$

Where E_K =The kinetic energy of the ejected photoelectron
 $h\nu$ =The characteristic energy of the X-ray photon
 E_B =The binding energy of the emitting core level
 $e\phi$ =The spectrometer work function

The process of photoemission is represented schematically in Figure 5. The fact that elements show unique binding energies makes XPS an excellent analytical tool for identification of

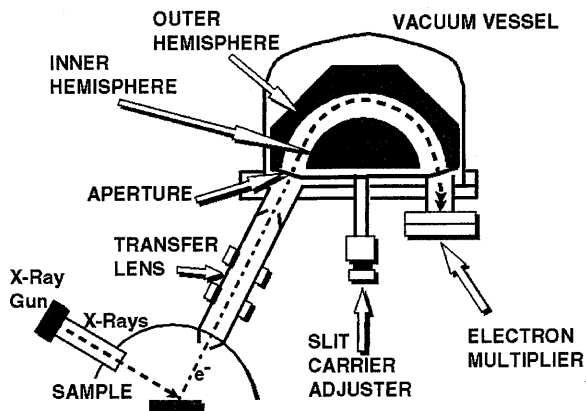


Figure 4. Schematic of the X-ray photoelectron spectrometer used in subsequent studies.

the elements present in the sample. No information on structure or symmetry can be obtained with XPS. In addition, the binding energy is a sensitive function of the oxidation state of the

material being studied. It is, therefore, possible to establish the presence of various oxide states present in the near surface region. Measurements must be conducted in ultra-high vacuum as the collision of electrons with gas molecules would result in a decreased flux as well as an error for the kinetic energy of the detected electrons. The base pressure used for the measurements in this thesis was 10^{-11} mbar. This is one inherent disadvantage to working with XPS. Samples must first be pretreated and then transferred to the vacuum chamber. XPS is therefore an inherently ex-situ method. A certain degree of speculation therefore remains as to the actual state of the surface under reaction conditions. XPS was used, in this thesis, to study the formation of sub-surface oxygen species. Measurements in Chapter 3 were made under conditions in which no surface adsorbed oxygen should be present. Samples were quenched from elevated pretreatment temperatures. The low diffusivity of oxygen in silver at lower temperatures implies that it should be possible to „freeze in“ the high-temperature state. This can be estimated as follows. Crank⁵ showed that the total amount M_t of a diffusing substance which diffuses out of a planar, semi-infinite medium may be explained by the following Equation. 18.

Equation 18.
$$M_t = 2C_0 \left(\frac{Dt}{\pi} \right)^{\frac{1}{2}}$$

The 1 x 1 cm square silver foils used were 0.2mm. The initial concentration C_0 can be estimated from the solubility of oxygen in silver. This is shown in Equation 19.

Equation 19.
$$C = S_0 P_{O_2}^{\frac{1}{2}}$$

The O_2 dosing pressures used ranged from 10^{-3} to 300mbar. The average value used was 100mbar. S_0 is the solubility of oxygen in silver and was shown by Eichenauer⁶ to be $0.747 \text{ cm}^3 O_2 / 100 \text{ gAg}$ at 1bar and 873K (typical dosing temperature). Insertion into Equation 19 yields a value of $1.046 \times 10^{-9} \frac{\text{mol} O_2}{\text{gAg}}$. Insertion of this value into Equation 18 with a calculated value of $D_{O_2, 298K} = 1.17 \times 10^{-24} \frac{\text{cm}^2}{\text{s}}$ (from Outlaw⁷) and a density of $10.5 \text{ mol } O_2 / \text{gAg}$ results in a total amount of $2.2 \times 10^{-21} \text{ mol} O_2$ desorbing in 5 minutes. This value is negligibly small in comparison to the calculated bulk concentration of $1.046 \times 10^{-9} \frac{\text{mol} O_2}{\text{gAg}}$ shown above. XPS measurements were taken at 473K in order to minimize contamination problems arising from adsorption of contaminants in the background gas (10^{-11} mbar) of the UHV chamber. A value of $D_{O_2, 473K} = 2.34 \times 10^{-16} \frac{\text{cm}^2}{\text{s}}$ results in a total desorption of $2.2 \times 10^{-21} \text{ mol} O_2$ in 5 minutes. This value is also negligibly small which is a very important point which much be taken into consideration for all ex-situ characterization techniques. The low oxygen diffusivity in silver at low temperatures implies that the values are constant in time for the XPS and ISS measurements. The stability of the species under question can also be established by repeatedly scanning the surface with XPS in the course of time. Metastable species will change under the action of the illuminating X-ray radiation and bulk diffusion. This was not observed below 573K.

Surface charging is a problem when studying electrically-insulating samples. This occurs as a result of the inability of the sample to maintain electrical neutrality during the photoionization

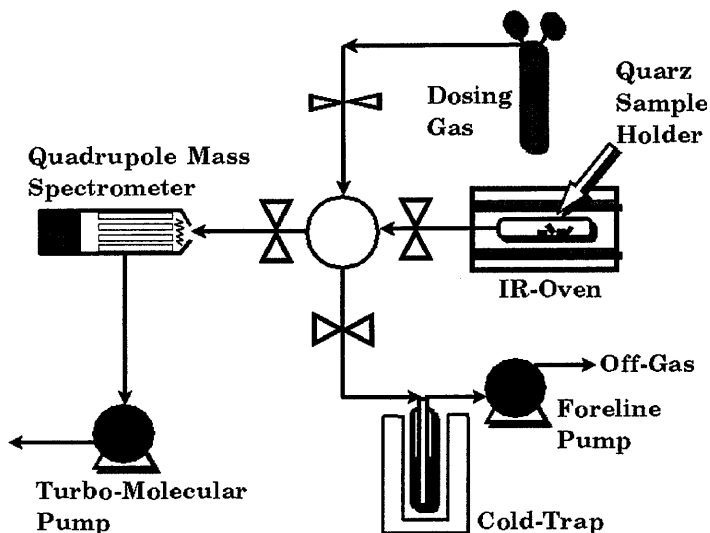


Figure 5. Schematic of the temperature-desorption spectrometer (TDS) used in subsequent studies.

process. Silver is an excellent electrical conductor and does not form stoichiometric oxides under the conditions used for the XPS measurement in this thesis. Charging effects are therefore assumed to be negligible.

2.5.2 Temperature Desorption Spectroscopy (TDS)

Temperature desorption spectroscopy (TDS) makes use of the fact that the temperature at which an adsorbate desorbs from a solid surface is proportional to the adsorbate-substrate bond strength. The TDS setup used in this thesis is shown schematically in Figure 5. It consists of a quartz sample holder which is connected to a mass spectrometer (Hiden Inc.) containing a secondary-electron multiplier (SEM) detector. The quartz holder is centered in a water-cooled, infrared oven (Stroehlein Instruments, Control 100) for treatment at elevated temperatures. The vacuum is pumped differentially, so that species desorbing from the sample are pumped to the spectrometer. The turbopump is located directly below the ionization chamber in order to maximize the sensitivity of the mass spectrometer. The

incorporation of a gas dosing system allows pretreatment of the sample in a range of pressures from 10^{-4} mbar to 1bar. Pressures higher than 10^{-4} mbar are recorded using thermal conductivity pressure gauges (Pirani - Balzer's Inc). Lower pressures ($P < 10^{-4}$ mbar) are

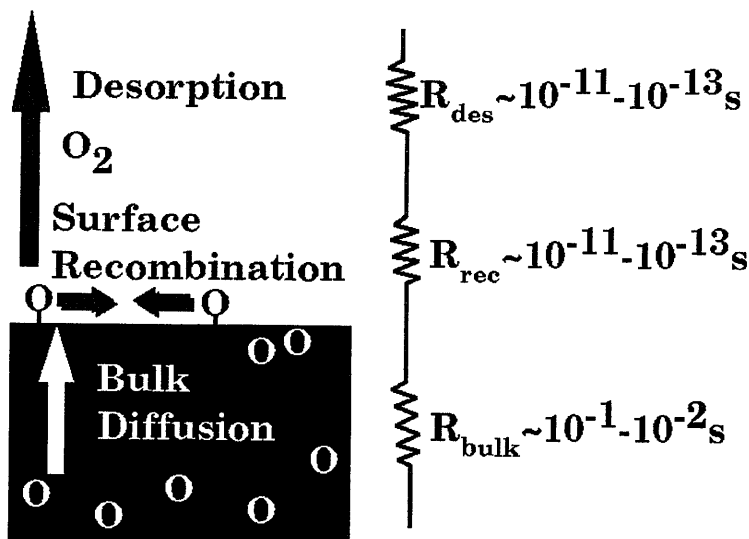


Figure 6. Schematic representation showing the relative rates of various processes involved in the thermal desorption of bulk-dissolved oxygen in silver.

measured with ionization gauges (Pfeiffer Inc). It is critical that the pumping speed of the apparatus be so high as to prevent desorbing molecules from re-adsorbing at the surface. A turbopump (Balzer's) with a pump capacity of 240L/s was used for all TDS measurements.

The TDS experiments performed in this thesis show an important deviation from typical thermal desorption. This lies in the fact that the species being considered are located in the sub-surface region of silver and not on the surface as in classical TDS. The implications of this are as follows. Typical interpretation of TD spectra is based on the Wigner-Polanyi Equation shown below.

Equation 20.
$$-\frac{d\sigma}{dt} = -\sigma_{\max} \cdot \frac{d\theta_{\sigma}}{dt} = \nu_{(x)} \exp\left(-\frac{\Delta E_{des}^*}{RT}\right) \cdot \theta_{\sigma}^x$$

Where σ = surface concentration
 θ = surface coverage

This equation and the subsequently-derived equations for determining reaction orders^{8,9} and activation energies are not applicable in the case where a bulk-dissolved species is being studied. The relative kinetics of the steps involved in the observation of a bulk dissolved species using TDS are represented schematically in Figure 6. Here the bulk, surface and gas-phase are shown schematically on the left. The relative kinetics of the various steps are represented on the right by an electrical circuit where the individual steps of in the overall desorption process are shown. The enormous differences between frequency factors for bulk diffusion ($10\text{-}10^3 \text{ s}^{-1}$) and those for surface recombination and desorption ($10^7\text{-}10^{15} \text{ s}^{-1}$) insure that segregation of oxygen from the bulk to the surface will always be rate limiting for the case of oxygen in silver.

A second complication arises from the assumption that the solid surface remains unchanged during the TD run. Silver is a metal with a relatively low melting temperature (1233K). The interdiffusion of metal atoms is assumed to be activated at the Tamann temperature ($T_{\text{tamm}}=0.5T_{\text{melt}}$). Measurements made above 600K are therefore complicated by metal reconstruction. The measurements made in this thesis are nearly all higher than this temperatures. These temperatures were chosen in order to approach, as closely as possible, the reaction conditions for both the methanol oxidation and oxidative coupling of methane. It will be shown in the following chapters that silver is in a dynamic equilibrium with the gas phase and is by no means passive.

2.5.3 Ion Scattering Spectroscopy (ISS)

Scattering techniques make use of the fact that the dynamics of an ion beam interacting elastically with a solid surface are a function of the atomic mass of the ions and atoms involved as well as the impact energy. Rutherford backscattering (RBS) and Low-Energy Ion Scattering (LEIS or ISS) are typically used. They differentiate themselves primarily in the fact that high energy noble gas ions are used for RBS (2-4MeV He⁺) and lower energy ions are

used for ISS (0.1-10keV). The more energetic RBS produces information with a depth of analysis in the μm range. In contrast to this, the less energetic ISS process provides information which lies nearly entirely in the uppermost atomic layer. Quantum effects play a more important role in the less energetic ISS method where interactions with the electrons of the material under investigation dominate. This quantum-chemical interaction complicates the quantitative interpretation of ISS data. Only qualitative interpretation were made in this thesis. The process is explained accurately enough using classical Newtonian mechanics to provide a reliable basis for qualitative comparison of results. The dynamics of the scattering process are shown in Figure 7. During the experiment, He^+ ions are accelerated through an electrical potential and strike the surface at an angle θ relative to the surface. The energy of the final scattered ion E_f is related to the masses of the surface atoms and the incident surface energy E_i through the following equation.

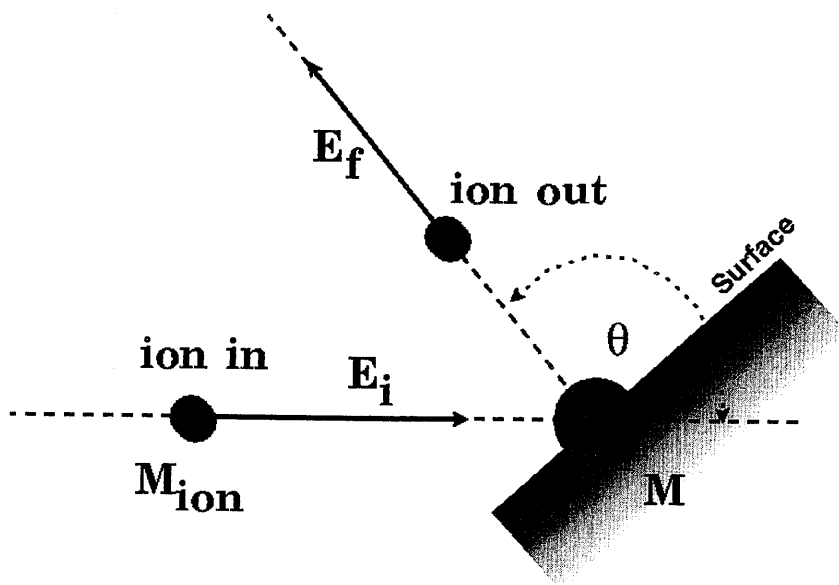


Figure 7. Schematic representation of the classical mechanics interactions occurring during an ion-scattering spectroscopy (ISS) experiment.

Equation 21.
$$\frac{E_f}{E_i} = \left[\frac{(M^2 - M_{ion}^2 \sin^2 \theta)^{\frac{1}{2}} + M_{ion} \cos \theta}{M + M_{ion}} \right]^2$$

With E_i = The energy of the incoming ion.
 E_f = The energy of the scattered ion.
 M_{ion} = The atomic mass of the incoming ion.
 M = The atomic mass of the scattering atom in the solid.
 θ = The scattering angle.

The reflected ions are measured with an electrostatic analyzer (Leybold Heraeus). During the course of an experiment, substrate ions are continuously sputtered away. Depth profiling is therefore possible with this technique. ISS is used for determining the form of the oxygen concentration profile in silver in Chapter 3.

2.5.4 X-Ray Diffraction

X-ray diffraction is a long-established technique for determining the structural properties of crystalline samples. A Stoe STADI P diffractometer was used in this thesis. X-rays are

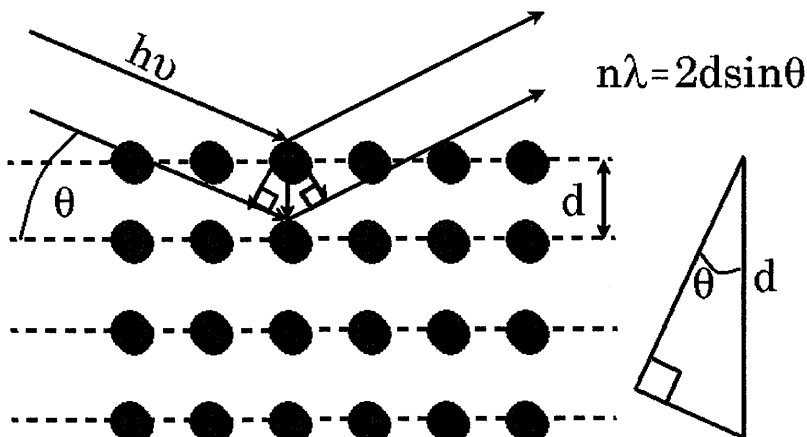


Figure 8. Schematic of the Bragg condition for the observance of X-ray diffraction lines in a crystalline solid.

emitted when a metal target is bombarded with high energy electrons. Only Cu K_{α} radiation with a HOPG-secondary monochromator was used for the work presented in this thesis. The wavelength of the emitted X-rays is on the order of Angstroms. The X-rays, therefore interact with the electron shells of the atoms in the solid under investigation. The atoms are envisaged as layers which scatter incoming X-rays as shown in Figure 8. This is an approximation of the actual scattering process which has the intrinsic fault that it is actually the interaction between the sample electron shells and the X-rays which results in the diffraction effect. Experience has repeatedly shown, however, that this is a sufficient approximation which yields a high degree of accuracy.

Diffacted X-rays are only detected (using a scintillation counter) for the instance where the diffracted X-rays are integer-multiples of the distance between the crystalline planes. This is the so-called Bragg relation and is shown in Equation 22.

Equation 22.
$$n\lambda = 2d \sin \theta ; \quad n = 1, 2, \dots$$

Where λ = The X-ray wavelength.
 d = The distance between lattice planes.
 θ = The angle between incoming X-rays and the normal.
 n = The integer reflection.

Silver is a metal which crystallizes in the face-centered-cubic arrangement. The high degree of symmetry results in a relatively simple diffraction pattern. This arises from the fact that most reflections are forbidden by the fact that X-rays diffracted from highly symmetric planes cancel out for all but integer phase shift values. The width of the peaks provides information about the degree of crystallinity, crystalline size and amount of internal strain. The intensity distribution provides information about preferred crystallite orientations and texture effects. The relation used in this thesis to distinguish between contributions from changes in crystallite size and internal strain is the Williamson-Hall equation. This is shown below in Equation 23.

Equation 23.
$$\beta_{ges} \cdot \cos \Theta = \frac{\lambda}{L_{volume}} + 4 \cdot e \cdot \sin \Theta$$

Where β_{ges} = Contributions to the FWHM from internal stress and particle-size

Decrease.

Θ = The measured Bragg angle.

λ = The X-ray wavelength.

e = The stress coefficient.

L_{volume} = The length of the unit cell volume assuming a cubic form.

By plotting $\beta_{\text{ges}} \cdot \cos \Theta$ as a function of $\sin \Theta$ one may obtain the relative particle size from the y-intercept which is equal to $1/L_{\text{volume}}$. The slope of the resulting line is equal to $4 \times (e)$.

The largest problem when using powder XRD to study electrolytic silver samples is the size of the crystallites. The samples used here consist of silver particles (0.2-0.4mm) which consist of smaller crystallites in the range of 10-100 μm . Close inspection by SEM (See Chapters 3-6) shows these small crystallites to also be polycrystalline in nature. The large size of the silver particles makes it almost impossible to obtain a good statistical distributions of crystallites in the XRD capillary. It is, therefore, impossible to study variations in the reflex intensity distribution for these samples. It is, however, possible to study changes in the FWHM and the 2Θ values obtained after various pre-treatments. This makes the above-mentioned Williamson-Hall analysis possible. In addition, calculation of variations of the unit-cell size allow the indirect observation of the incorporation of oxygen in the silver lattice under reaction conditions.

2.5.5 Scanning Electron Microscopy (SEM) and Energy-Dispersive X-ray Analysis (EDX)

Scanning electron microscopy (Hitachi S-4000) proved invaluable to the determination of the conclusions made in this thesis. This is due to the excellent topographic resolution which is obtainable with SEM. An SEM setup similar to that used in this thesis is shown schematically in Figure 9. A heated filament produces a flood of electrons which are focused through a lense-apatature system. The narrow electron beam (approximately 10nm) produced then passes through scanning coils and eventually on to the sample being studied. The resolution of the instrument is primarily limited by the diameter of the imaging electron beam. The scanning coils are electromagnets which scan the beam over the sample surface in much the same way that electrons are scanned over a television screen. A number of processes occur as a result of the interaction between the incoming electron beam and the surface. Whenever a

primary electron interacts with sample atoms both secondary electrons and X-rays are released. The former are collected in the SEM detector and an image is produced. The latter may be collected in an X-ray detector (scintillation) and used to determine the chemical composition of the compound. This is particularly useful for the determination of impurities in the silver surface.

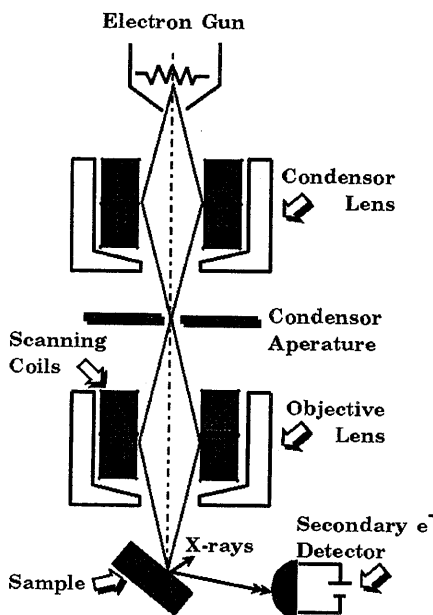


Figure 9. Schematic of the principle components of the scanning-electron microscope (SEM)

2.5.6 Scanning Tunneling Microscopy (STM)

The theory behind STM is extremely complicated and is only sufficiently described by considering the quantum effects involved. The microscope used in this thesis was purchased from Burleigh, (Model ARIS 3450). The tunneling voltage was 0.45V and the current was 2.0 μ A. operated in air and tunneled well into silver. In essence, a tip of atomic diameter is scanned over a surface while a feedback circuit constantly maintains a constant tip height. The surface morphology may therefore be derived from the voltage supplied to the piezoelectric drivers which control the tip height. Only one STM image is shown in this thesis therefore the details of the method are not provided here. The reader is referred to a

number of excellent sources of information containing a great deal more specific information on the STM technique.^{10,11,12}

2.6 Summary

Catalysis is a multifaceted field which integrates a wide spectrum of scientific disciplines. Obtaining a solid understanding of a catalyst requires excellent characterization of the catalyst before, after, and if possible, during catalytic reaction. This characterization includes both the morphology and electronic properties of bulk and surface phenomena. Reliable catalytic measurement form the foundation of any good catalytic study. A knowledge of the pertinent reaction reactor parameters is critical and necessitates the prudent choice of the appropriate laboratory reactor for the problem at hand.

References

1. Fogler Scott H., „Elements of Chemical Reaction Engineering“, 2nd Ed. PTR Prentice Hall, Enlewood Cliffs, New Jersey 07632, ISBN 0-13-263534-8 (1992).
2. Walas S.M., „Reaction Kinetics for Chemical Engineers“, Neq York, McGraw Hill, (1959).
3. Levenspiel O., „Chemical Reactor Engineering“, wnd ed. New York, Wiley, (1972).
4. Dautzenberg F., „Ten Guideline for Catalyst Testing“, American Chemical Society 105 ISBN 0097-6156/89 (1989).
5. Cranck J., „The Mathematics of Diffusion 2nd Ed.“, Clarendon Press, Oxford, ISBN 0-19-853411-6.
6. Eichenauer W. and Müller G., *Z. Metallkde.* **53** 321-324 (1962).
7. Outlaw R., Wu D., Davidson M., Hoflund G., *J.Vac.Sci.Tech. A* **10(4)** 1497-1502 (1992).
8. Redhead P., *Vacuum* **12** 203-211 (1962).
9. Menzel D., „Desorption Phenomena“ in: R. Gomer's „Interactions on Metal Surfaces“, Topics in Applied Phsics, vol.4. Springer, Berlin Heidelberg, New York, pp 101-142.
10. Bonnell D., „Scanning Tunneling Microscopy and Spectroscopy, Theory, Techniques and Applications“, VCH Publishers, Inc. New York, N.Y., ISBN 0-89573-768-X.
11. Flegler, Heckman, Klomparens, „Elektronenmikroskopie, Grundlagen, Methoden, Anwendungen“, Spektrum Akeademischer Verlag GmbH Heidelberg, Berlin, ISBN 3-86025-341-7.
12. Brune E., Hellborg R., Whitlow H., Hunderi O., „Surface Characterization“, Wiley-VCH Verlag GmbH, ISBN 3-527-28843-0.

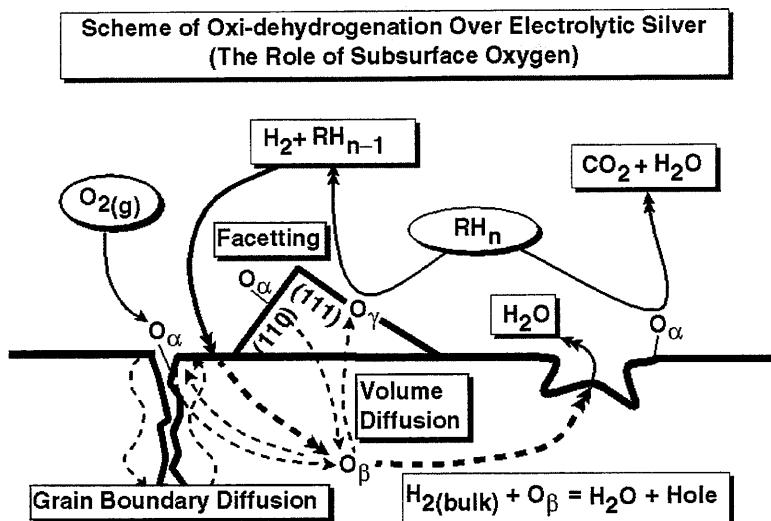
The Correlation of Sub-Surface Oxygen Diffusion with Variations of Silver Morphology in the Silver-Oxygen System

Abstract

Silver undergoes pronounced morphological changes following high-temperature treatment in various gas atmospheres. SEM results show that high-temperature treatment in oxygen leads to pronounced faceting of the silver surface. Two distinctly different forms of sub-surface oxygen have been identified and the mechanism leading to their formation clarified. The first of these species is O_a . It is bulk-dissolved oxygen which diffuses interstitially through low-resistance paths such as grain boundaries and higher-indexed crystalline planes. TDS analysis reveals that high temperature oxygen pretreatment results in the formation of crystalline surfaces exhibiting different oxygen diffusion barriers. At elevated temperatures, pure thermal reordering dominates over oxygen-induced restructuring of the silver bulk and surface. The near-surface region is, therefore, comprised primarily of low-indexed crystalline planes. At temperatures in excess of 923K, bulk-dissolved, atomic oxygen (O_b) segregates into these low-indexed planes. This likely occurs *via* an interstitialcy diffusion mechanism where oxygen substitutes for silver atoms in the lattice. This intercalated oxygen is referred to as O_i . A comparison of TDS and XPS results shows that annealing of the silver in vacuum results in surface restructuring to low-indexed planes which subsequently results in a marked increase the amount of O_i observed by TDS. ISS Depth profiling of silver foils treated under various conditions shows that the diffusion coefficient is a positive function of the oxygen concentration. This is a direct result of the oxygen-induced recrystallization of the silver. In-situ XRD shows that oxygen located in octahedral holes of silver diffuse preferentially in the [110] direction. This requires the anisotropic displacement of silver atoms which culminates in a slight expansion of the silver unit cell size. The resulting anisotropic strain in the lattice results in the formation of silver crystallites exhibiting a needle-like morphology. These structures were subsequently imaged with STM.

surface contains a high density of dangling bonds which results in an increase in the surface free energy.^{10,11} Preferential adsorption of oxygen on rough surfaces results in an adsorbate-induced decrease in the surface free energy which exerts a stabilizing influence leading to their subsequent growth. It is to be expected that moderate temperatures and high oxygen pressures should favor the formation of such structures.

It has been shown that two distinctly different oxygen species may be formed in the subsurface region of silver as a result of the gas-metal interaction.¹⁴⁻¹⁷ These species differentiate themselves in both their location and bonding states. They have been characterized with a variety of spectroscopic techniques.¹⁴⁻¹⁷ The mechanism leading to the formation of these species is, however, poorly understood. In this chapter, a model is proposed, which allows for a quantitative understanding of the diffusion process which ultimately leads to the formation of these various oxygen species. The first of these sub-surface species is known as O_p . This species is formed when dissociatively-adsorbed, atomic surface oxygen (O_a) diffuses into the bulk. A second species O_v is formed at higher temperatures. It is supposed that O_v is formed *via* the subsequent segregation of O_p to the surface.¹⁴⁻¹⁷ The reasoning behind this mechanism is presented here. It is shown that the competing effects of thermal reordering and oxygen-induced restructuring result in the formation of different crystal structures whose extent of formation shows a strong dependence on oxygen partial pressure and temperature.



Scheme 1. Proposed scheme for the participation of various oxygen species in high-temperature, silver-catalyzed partial oxidation reactions.

The partial oxidation of methanol and the oxidative coupling of methane (OCM) to C_2 hydrocarbons are two reactions which are believed to be catalyzed by O_γ ²². The assumption that the segregation of O_β to the surface region is necessary for O_γ formation implies that the kinetics of this step should play an important role in the overall reaction kinetics for reactions catalyzed by O_γ . This study lays the groundwork necessary for the development of a kinetic model which explains the role of O_β and O_γ reacting under steady-state reaction conditions. Subsurface oxygen is continuously produced *via* bulk dissolution and consumed *via* surface segregation and reaction. An outline of the proposed OCM mechanism is shown in Scheme 1.

3.2 Experimental Section

Materials: Oxygen (5.0), helium (5.0) and methane (3.5) were used for pretreatments. A 99.999% pure silver foil purchased from Goodfellow was used for the XPS, SEM and STM studies. Fine Ag powder was produced by decomposing a fine Ag_2O powder from Aldrich

(99.9%) *in situ* with methanol (16ml/min CH_3OH +100ml/min He). This method of in-situ reduction resulted in a thin, polycrystalline layer supported on a stainless steel resistance heater. Oxidation was performed by flowing 100ml/min O_2 over the sample. Methanol was not dried prior to use. Electrolytic silver was generously provided by BASF AG and was used for the TDS runs.

XPS: The sample was cleaned by repeated cycles of oxidation (573K, 100mbar O_2), flashing (873K) and pumping followed by Ar^+ sputtering (1 kV, 2 μA). Significant quantities of impurities ($\text{C}_{\text{tot}} < 5\text{at}\%$, $\text{Na} < 2\text{at}\%$, $\text{K} < 1\%$) segregated to the surface upon heating. Two days of repeated sputtering cycles were necessary to obtain an acceptable purity. It is impossible to remove all of the impurities present. XPS was performed with a modified Leybold LHS 12 MCD system. The XPS spectra were obtained with Mg K_{α} radiation ($h\nu = 1253.6\text{eV}$) using a fixed analyzer pass energy of 48 eV. This results in a depth of analysis of approximately 30 angstroms. Surface compositions were calculated after performing a Shirley background subtraction and were quantified using the respective atomic correction factors. ISS spectra were generated using a scanning defocused 100 eV He^+ primary beam. The He^+ current was 1 μA which results in a flux of about 6×10^{12} ions/ cm^2s . All photoelectron spectra were recorded at 573K in order to minimize interference from adsorbed carbon contamination. TDS and XPS were made in separate apparatuses as the available XPS facilities do not include the possibility of performing TDS.

SEM: SEM images were taken with a Hitachi S-4000 SEM equipped with an EDX for element identification. Samples were first polished with diamond paste and then treated for 1 minute in an ultrasound bath of acetone in order to remove embedded diamond particles. Longer treatment times in the ultrasound bath led to severe deformation of the silver foil.

STM: STM images were taken with a Burleigh STM (model ARIS-3450) with a PID feedback controller which was interfaced with a PC. The tunnelling voltage was 0.45V and the current was 2.0 μA . Tips were cut to size and were made of Pt/Ir (80/20).

TDS: TDS measurements were made in an UHV chamber with an average background pressure of 3×10^{-8} mbar. The vacuum was pumped by oil-free Balzer's turbopumps with a pump rate of 240L/s. Analysis of the background gas shows water to be the primary impurity present. EDX analysis showed the presence of small amounts of Na, Cl, Si and C contaminants in the electrolytic silver. Monitoring of desorption products was made with a Hiden (Hal2) quadrupole mass spectrometer coupled to a Next workstation. A sampling rate of 0.65 scans/s was used. A water-cooled, infra-red oven was used for sample heating. The thermocouple (Type K) was placed immediately below the sample and was in direct contact with the quartz holding tube. Linear heating ramps from 373K to 1273K with a maximum heating rate of 2.5K/s were possible with this setup. The sample was treated in flowing oxygen (purity 5.0, 17ml/min) at 973K overnight in order to minimize problems arising from carbon contamination. The sample was subsequently transferred through air to the UHV setup. Oxidation-reduction cycles were performed until the CO_2 signal reached an acceptable level (approximately 2% of max O_2 signal). This cleaning procedure typically lasted one week. Dosing pressures for the temperature-programmed desorption experiments ranged from .01-300mbar. Three dosing temperatures of 573K, 773K, and 973K were used. All exposures were made for 5 minutes. Longer exposure times did not show an increased oxygen uptake for samples treated in excess of 573K indicating rapid equilibration of the silver and gas. One gram of silver was used for all runs. The oxygen pretreatment temperatures are equal to or exceed the thermal desorption temperature of O_α ($T=573\text{K}$). This, in combination with the fact that the unsupported silver samples have a very low surface area ($<0.001\text{m}^2/\text{g}$) and a low sticking coefficient means that surface-bound atomic oxygen, O_α , should not be observed for these runs. It is also important to note the extremely high dosing pressures used here ($P<300\text{mbar}$). The dosing pressures and temperatures used here are much higher than the Langmuir exposures typically used in surface-science experiments. The sample was evacuated for 5 minutes prior to taking each run. The fact that the spectra are not baseline resolved for runs made in excess of 10mbar is due to the inability to completely pump off all of the oxygen within this time. The pumping time was held constant at 5 minutes prior to taking each TD spectrum as reaction with bulk-dissolved carbon results in CO_2 formation for longer holding times. These high pressures were chosen with the intention of approaching, as closely as possible, the actual reaction conditions used in the methanol oxidation reaction and the oxidative coupling of methane to C_2 hydrocarbons (1-10% O_2 , total pressure=1bar).

XRD: A Stoe STADI P diffractometer using $\text{Cu K}\alpha$ -radiation and a Bragg-Brentano geometry was used for the powder measurements. This included a HOPG-secondary monochromator and a scintillation counter. *In-situ* XRD was measured in a modified Bühler HTK 2.0 chamber. Measurements were made by taking the first point at room temperature and then heating in 100K steps beginning at 373K. The sample was held at the set temperature for 30 minutes prior to measurement. The heating rate was 10K/min.

3.3 Results and Discussion

3.3.1 SEM Analysis of Pretreated foil

Figure 1a shows a micrograph of the surface of a polished silver foil subsequent to treatment in flowing He for 4 days. The surface consists of broad flat areas and show very few grain boundaries. The high-temperature treatment has obviously resulted in significant annealing of the surface. The surface is lightly faceted in some regions but is overwhelmingly flat and has a slightly “melted” appearance. Experiments made with He(Purity) without an oxisorb filter show a completely faceted surface (not shown). Only a minimal amount of oxygen is required, therefore, to achieve surface faceting. The reference measurement in oxygen-free He shows clearly that facetting occurs at best to a small extent in the absence of oxygen. Figure 1b is an image of the same foil after treatment for four days in oxygen at 1023K. The treatment has resulted in massive morphological restructuring of the silver surface. The originally flat surface is now covered with pyramidal-like structures in the μm size range. All structures located within a single crystalline area are oriented in the same direction. Note that the orientations on opposite sides of the grain boundaries are different. Different starting surfaces obviously show different susceptibilities to facetting. Previous work has shown the preferential crystallographic orientation of these surface structures to be a function of both oxygen pressure and treatment temperature.¹⁴ Figure 1c shows an image of the foil subsequent to treatment in the OCM reaction for 4 days at 1023K. The surface structures produced subsequent to oxygen pretreatment appear nearly identical to those formed during catalytic reaction. The unambiguous assignment of the crystallographic orientations of the facet faces is, unfortunately, not possible using SEM data alone. However, the regular

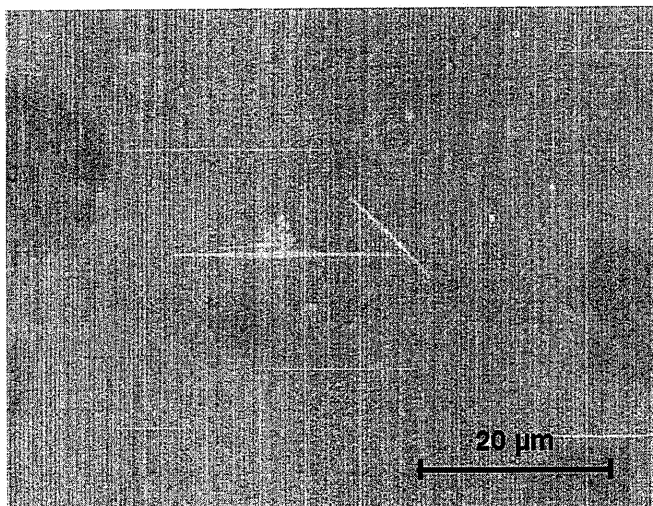


Figure 1a. Scanning electron micrograph of the surface of a silver foil treated for 4 days in flowing He.(150 ml/min) at 1023K.

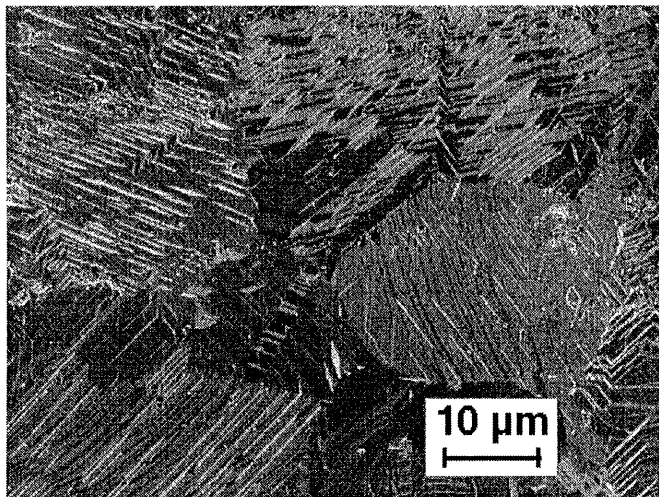


Figure 1b. Scanning electron micrograph of silver foil after treatment in flowing oxygen for 4 days; 10% O₂ in flowing He, flow rate 150 ml/min, 1023K

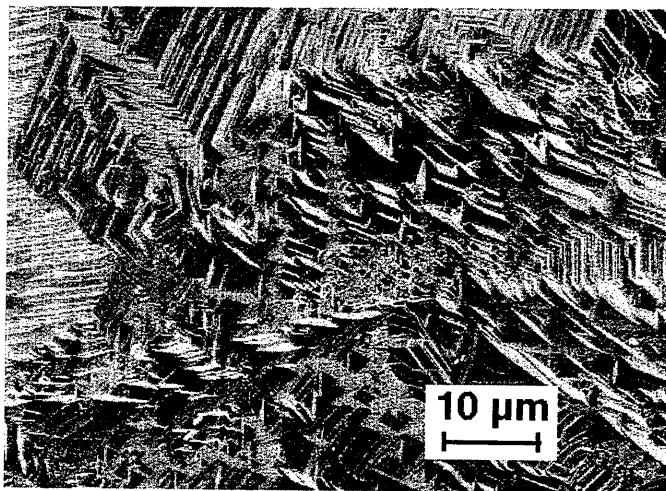


Figure 1c. Scanning electron micrograph of silver foil after use in the oxidative coupling of methane (OCM) reaction; 8.2 vol% O_2 , 46 vol% CH_4 , 45.8 vol% He, flow rate is 150 ml/min at 1023K

periodicity of the geometrically equivalent surface structures implies a preferential orientation of the crystallites. The similarity of the surface structures seen in Figures 1b and 1c shows that a solid understanding of the oxygen/silver interaction is essential to understanding the morphology-activity relationship for the silver-catalyzed OCM reaction.

3.3.2 TDS as a Tool for Studying Structural Changes

As stated in the introduction, the formation of O_γ is believed to occur *via* the migration of bulk-dissolved oxygen (O_β) to the surface.¹⁴⁻¹⁷ The question then arises as to why surface segregation of bulk oxygen should lead to the formation of an oxygen species exhibiting uniquely different chemical properties (O_γ) and not just to chemisorbed surface oxygen (O_a). The answer to this question lies in the intimate connection between thermal reordering of the silver metal and oxygen diffusion in the silver bulk. Both are activated processes exhibiting an Arrhenius-type temperature dependence. A solid understanding of the kinetics of both these processes is essential to elucidating the mechanism leading to the formation of O_γ . The

strong structural dependence of gas diffusivity makes temperature-programmed-desorption spectroscopy (TDS) a sensitive probe for studying morphological changes induced during the pretreatment. A thorough TDS investigation of the influence of oxygen pretreatment on the diffusive properties of oxygen in silver was, therefore, carried out with the goal of understanding the nature of the formation of both the O_β and the O_γ species.

3.3.3 Pretreatment at 573K

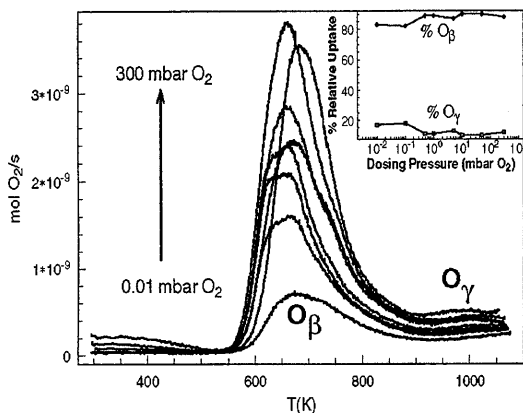
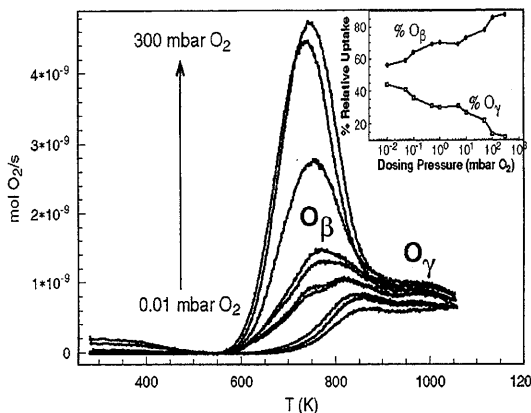


Figure 2a. TDS
for dosing at
573K

Figures 2a-c show oxygen-TD spectra for electrolytic silver samples pretreated in oxygen at various pressures and temperatures. A series of TD spectra obtained after having exposed the sample in various O_2 pressures at 573K for 5 minutes are presented in Figure 2a. The first broad, asymmetric peak centered at approximately 650K is assigned to O_β desorption. The weaker peak desorbing above 873K is assigned to O_γ . The O_β signal results from diffusion and desorption of bulk-dissolved oxygen diffusing along low-resistance diffusion paths such as high-indexed crystal planes and grain boundaries. The broadness and asymmetry of this peak are to be expected as a polycrystalline silver sample offers a variety of paths for oxygen diffusion. A number of authors^{3,4,7,8,11,13-17} have assigned this species to bulk-dissolved oxygen. Two important pieces of evidence presented here support this. First, the signal does not saturate for dosing pressures made up to 300mbar O_2 . Second, the calculated uptakes are far in excess of monolayer adsorption assuming a (111) oriented surface with 100% coverage.

Attempts at curve fitting fails as one may fit any number of curves of various line profiles. The point common to all the diffusing species resulting in the O_β desorption peak is that the diffusion mechanism resulting in their formation likely occurs as a result of interstitial hole-jumping and/or grain boundary diffusion.^{5,6,9} The sizes of both the O_β and the O_γ desorption signals increases for increasing dosing pressures. The O_γ signal increases, however only slightly. This implies that it is limited to the near-surface region. The O_β desorption temperature shows a very weak dependence on the dosing pressure for exposures made at 573K. The broadness of the peak complicates a precise determination of the desorption temperature. The weak dependence of the desorption-temperature maximum on exposure cannot simply be attributed to a first-order desorption of oxygen as the desorbing species originates from a bulk-dissolved species (O_β)^{3,4,6,7,8,14} which must first diffuse to the surface. The desorption rate is therefore limited by the diffusive flux of oxygen to the surface. Pre-exponential factor for the recombinative desorption of surface-bound atomic oxygen are typically on the order of 10^9 - 10^{15} (s^{-1})²³. The diffusion kinetics dictate the peak form as well as the temperature desorption maximum. This is a critical point to be considered when interpreting thermal desorption spectra made under conditions where sub-surface species are produced. The O_γ desorption signal beginning at approximately 950K is very weak. The inset in Figure 2a shows the % value of the total O_2 desorption signal attributed to O_β and O_γ . There is no substantial variation in the relative integral desorption signals for both species. The insensitivity of the relative amounts of O_γ and O_β to dosing pressure at this temperature suggests that no significant morphological changes occurred during the pretreatment. SEM images show no faceting of the surface for Ag foils treated in oxygen at this temperature (data not shown).

3.3.4 Pretreatment at 773K



**Figure 2b. TDS
for dosing at
773K**

Figure 2b shows that the situation is drastically different for oxygen pretreatments made at 773K. Low-pressure dosing results in an O_β desorption maximum at 850K. This is nearly 200K higher than the desorption maximum for the identical dosing pressures seen in Figure 2a. Increasing the dosing pressure results in a gradual shift of the O_β desorption peak maximum to lower temperatures. The O_β desorption maxima for high pressure doses ($P > 5$ mbar) is approximately 50K higher than those obtained with the identical dosing pressures at 573K in Figure 2a. The weak desorption maximum for O_γ remains approximately constant for all dosing pressures. The desorption temperature for O_β does not shift to lower temperatures for dosing pressures higher than 10 mbar. The relative amounts of O_β and O_γ formed subsequent to dosing at 773K are shown in the inset of Figure 2b. The relative amount of O_β increases monotonically and that for O_γ decreases monotonically. This behavior is very different from that which is observed in the inset of Figure 2a for doses made at 573K. The large variation in $\%O_\beta$ and $\%O_\gamma$ as a function of dosing pressure suggests that significant restructuring of the catalyst has taken place during pretreatment. This correlates well with the onset of faceting seen in SEM (data not shown).

3.3.5 Pretreatment at 973K

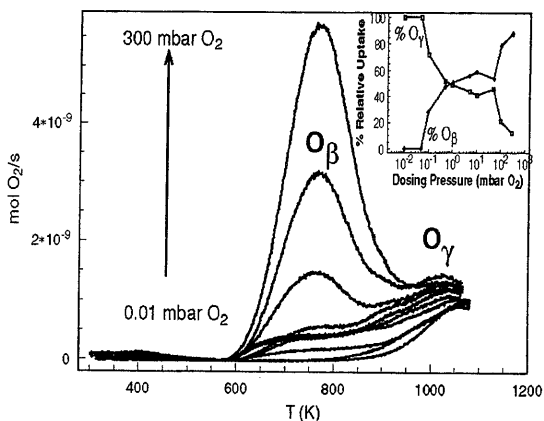


Figure 2c. TDS
for dosing at
973K

Figure 2c shows a set of desorption spectra obtained after dosing at 973K. There is a slight increase in the signal around 400K. This is likely due to the decomposition of carbonates formed at the surface. Again, the situation is very different from that shown in Figures 2a and 2b. Only O_γ appears to initially be populated for oxygen dosing pressures lower than 0.1 mbar. The desorption temperature maximum is initially about 1050K. The O_γ signal shows a maximum desorption temperature of 1073K. The O_β species populates first at higher dosing pressures and the desorption maximum shifts again to lower temperatures for increasing exposures. The O_β temperature-desorption maximum obtained for doses made in excess of 10 mbar is constant and is approximately the same as that observed for similar doses made at 773K seen in Figure 2b. The relative amount of O_β and O_γ produced is shown in the inset of Figure 2c and exhibits yet another trend. There are two obvious inflection points. The first appears slightly below 10⁻¹ mbar O₂ and the second at 50 mbar O₂. Again, this variation suggests that the silver morphology has changed during the oxygen pretreatment. The variation at 973K is however different than that seen in the inset of Figure 2b for doses made at 773K.

3.3.6 Interpretation of the TD Spectra and SEM Micrographs

The observed trends for all dosing temperatures and pressures can be explained by taking into account both the pure thermal reordering of silver as well as the oxygen-induced reordering. Dosing at 573K showed no change in the relative amounts of O_β and O_γ formed as a function of dosing pressure indicating that the surface remains unchanged. 573K is not sufficiently high to result in substantial mass transfer of silver. This temperature is approximately 200K lower than the Tamman temperature which must be reached for the kinetics of silver interdiffusion to be significantly fast.⁹ The strong pressure dependence of the temperature desorption maxima recorded after oxygen exposures made at 773K indicates that changes in the silver morphology occur at this temperature. The observed decrease of the O_β desorption maximum temperature with increasing oxygen pressure indicates that the diffusion resistance decreases with increasing dosing pressure. It has been shown by *in-situ* XRD that incorporation of oxygen into silver induces a distortion in the (110) silver planes which results in an optimum fit for oxygen diffusion in the silver bulk.¹⁴ The incorporation of oxygen into the silver lattice has also been shown to cause an increase in the unit cell constant for silver particles supported on alumina²². This temperature provides an optimum where oxygen-induced restructuring dominates over pure thermal reordering resulting in decreased diffusion resistance. The increased O_β desorption temperature for exposures made at pressures below 1.0mbar seen in Figure 2b results from the fact that pure thermal reordering kinetics dominate at low oxygen pressures. The decreased O_β desorption temperature obtained for increasing oxygen dosing pressures results from the increased role of oxygen-induced restructuring at higher pressures. The oxygen-induced restructuring is obviously a strong function of the dosing pressure. It is interesting to note that the maximum desorption temperature remains constant for all pretreatments made at pressures greater than 10mbar. This point will be touched upon again later. The behavior seen in Figure 2c provides a clear indication that increasing the dosing temperature to 973K results in a situation where the thermal rearrangement of silver becomes the dominating process. This explains the fact that only O_γ is formed for dosing pressures lower than 0.1mbar made at 973K. Increasing the dosing pressure results in oxygen-induced restructuring which subsequently causes the desorption maximum to shift to lower temperatures. This behavior cannot be explained by a simple

second-order thermal desorption model as the species evolved originate from oxygen located in the bulk and not on the surface. Again, the desorption of oxygen is limited by the diffusive flux of O_2 from the bulk to the surface.

3.3.7 Activation Energies of Diffusion/Desorption

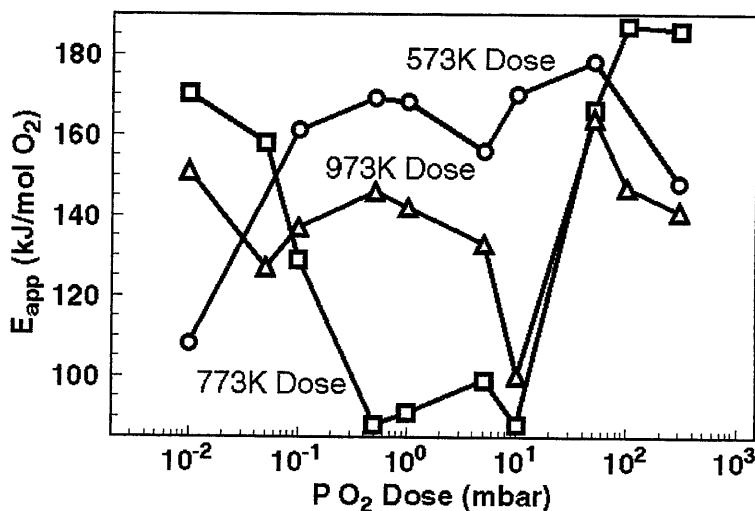


Figure 3. Calculated activation energies of diffusion/desorption for the thermal desorption spectra shown in Figures 2a-c

Figure 3 shows the desorption/diffusion activation energies for these measurements calculated using the front-line method.¹⁵ This involves plotting the initial portion of the desorption curve in the Arrhenius form. The log of the desorption rate appears on the y-axis and the inverse temperature on the x-axis. The activation energy is obtained from the slope of this plot. A critical assumption is that the concentration-dependent activation energy varies negligibly during the initial stages of desorption. These activation energies are not attributed to energies of activation for single mechanistic steps. They are, rather, values for the overall barrier which must be overcome when oxygen segregates from the bulk (bottom of the potential well) to the desorbed molecular oxygen species (highest energy state). The observed

activation energies represent, therefore, the activation energies of surface (segregation)+(recombination)+(desorption) of bulk-dissolved oxygen. The fact that the height of the diffusion barrier is a function of the crystallite orientation⁶ means that these values are an excellent indicator as to the type of crystalline structures present. More densely packed structures present a higher diffusion barrier. Unfortunately, there are only a handful of studies in the literature regarding the kinetics of oxygen diffusion in silver single crystals.^{5,6,10} The unambiguous determination of the exact crystal structures present is, therefore, impossible based on these values alone. A comparison of results obtained here with the existing reference material is sufficient, however, to build a model which explains the qualitative trends observed.

Figure 3 shows that the activation energy of desorption/diffusion for all dosing temperatures goes through a minimum at approximately 10 mbar for all runs. Doses made at pressures in excess of 10mbar show an increase in activation energy, essentially returning to the value observed for the low pressure doses (10^{-2} mbar). The exceptionally small activation energy of 110kJ/mol for the 10^{-2} mbar dose made at 573K is likely due to the fact that the desorption signal of surface-bound oxygen, O_a ¹⁴ dominates over the desorption signal of bulk-dissolved O_b at this low exposure pressure and temperature. The lack of consistent data as to the exact activation energy of desorption complicates this interpretation. The subsequent doses made at higher pressures and temperatures results in increased formation of O_b which overwhelms the O_a signal whose intensity is limited to single monolayer coverage.

The high activation energy for oxygen diffusion for exposures made at pressures lower than 10^{-2} mbar arises from the fact that pure thermal reordering dominates at low oxygen partial pressures. An increased diffusion barrier to O_b segregation results from the formation of thermodynamically-stable low-indexed surface planes which prevail under these conditions. This explains the relatively high thermal desorption maxima for the low pressure doses seen in Figures 2b and 2c. Increasing the pressure to approximately 10mbar results in a decrease in the observed activation energy. The extent of the E_{app} decrease shows a strong temperature dependence as well. Of the three dosing temperatures used here, dosing at 773K represents the optimum temperature for achieving a minimum in the diffusion barrier. This decrease in the

diffusion barrier for increasing dosing pressures agrees excellently with the observed decrease in the thermal desorption maximum seen in Figures 2b and 2c for dosing pressures lower than 10mbar. This optimum pretreatment temperature for oxygen diffusion coincides well with the Tamann temperature of silver (754K). 773K is therefore sufficiently high to allow efficient structural reorientation of the silver but is not so high as to have the effect of suppressing the oxygen-induced reconstruction. The oxygen atmosphere essentially guides the progress of the silver reconstruction. In this case, oxygen adsorbate-induced changes in the surface-free energy provide the thermodynamic driving force for morphological changes which are kinetically limited for temperatures below the Tamann temperature.

The increase in activation energy for doses made at pressures higher than 10mbar represents yet another drastic change in the barrier to oxygen diffusion. This effect results from the structural transformation of the facets from a preferential [110] orientation to a [331] orientation as observed by *in-situ* XRD.¹⁴ A normally bulk-sensitive analytical tool like XRD may be used for determination of the average surface orientation as the massive μm sized facets account for a substantial part of the silver bulk. The (331) surface structure is a more densely packed terminating structure than the (110) structure. It consists of (111) terraces with (110) oriented steps. It is, essentially, an open variety of the (111) surface. The fact that it is a more densely packed structure results in the higher activation energy of diffusion seen in Figure 3. The restructuring of the catalyst to the (331) terminating structure at high oxygen potentials also explains the fact that the desorption maxima for these high-pressure doses do not continue to shift to lower temperatures for doses made at pressures higher than 10mbar. It also correlates well with a subsequent rise of the calculated activation energies to approximately 160kJ/mol O_2 seen in Figure 3.

3.3.8 In-situ XRD-The Temperature Dependence

In-situ analysis of the fine silver powder was performed in order to gain information about bulk transformations occurring as a result of high-temperature treatment in oxygen. Measurements were made under a pure oxygen atmosphere as well as a 14% methanol in helium mixture. These represent the extremes of oxidation and reduction. Previous work^{3,14,16,17} has shown that methanol is an excellent reducing agent for silver.

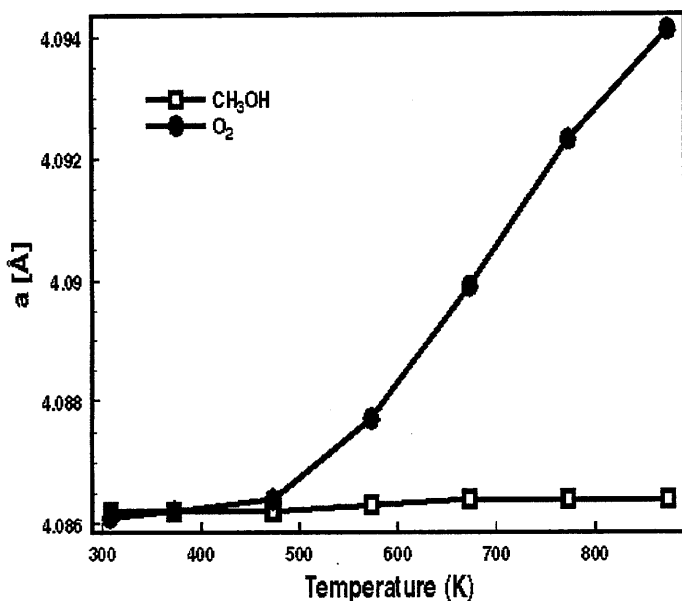


Figure 4. Variation of the unit cell constant as a function of temperature and gas-phase composition. The values have been corrected for the thermal expansion. (Open Squares: 16ml/min CH₃OH in 100ml/min He; Closed Circles 100ml/min O₂)

The methanol run, therefore serves as a suitable reference. Figure 4 shows the results obtained for variations of the unit-cell constant as a function of temperature. The thermal expansion of silver was subtracted for both runs. Unit cell expansion indicates the incorporation of oxygen into the bulk. Oxygen is known to occupy octahedral holes in the fcc lattice of silver^{5,6}. The direct determination of the oxygen positions by powder X-ray diffraction is impossible as the x-ray scattering factor (f-factor) for silver dominates over that of oxygen in this low concentration regime ($C_{O_2} < 100\text{ppm}$). The onset of the unit cell expansion correlates excellently with the thermal desorption of O_p shown in Figures 2a-c. It is critical to note that no stoichiometric oxide is formed here. Ag_2O , the most stable silver oxide, decomposes thermally above approximately 573K. No additional reflections characteristic of

stoichiometric silver oxides were found. The unit cell expansion is, therefore, a secondary effect occurring as a result of the incorporation of oxygen into the bulk.

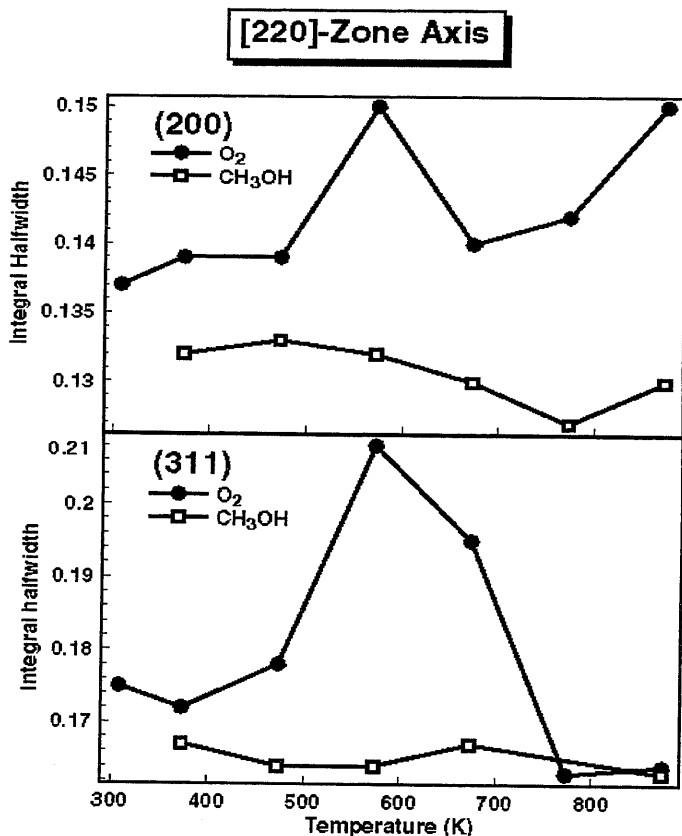


Figure 5a. Variation of the integral halfwidth as a function of temperature and gas-phase composition (Open Squares: 16ml/min CH_3OH in 100ml/min He; Closed Circles 100ml/min O_2)

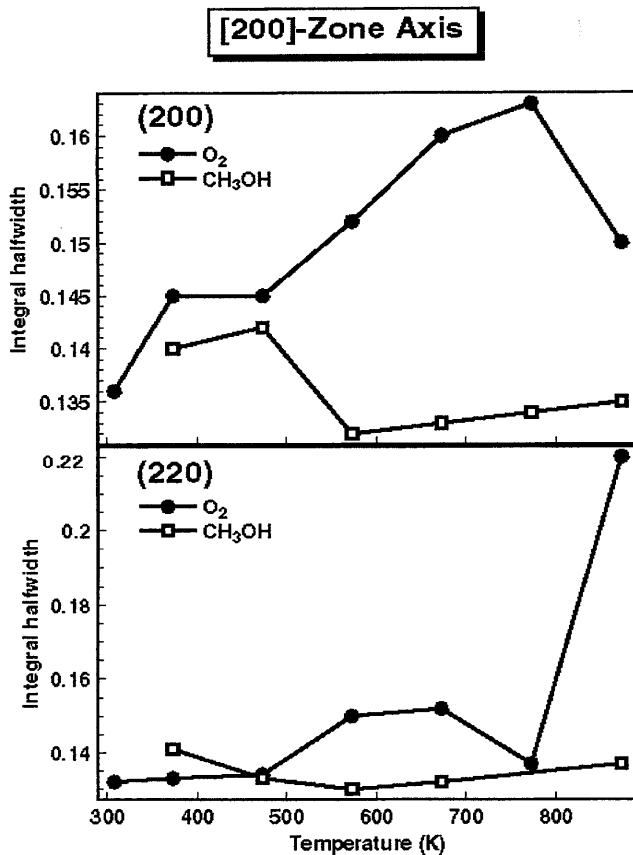
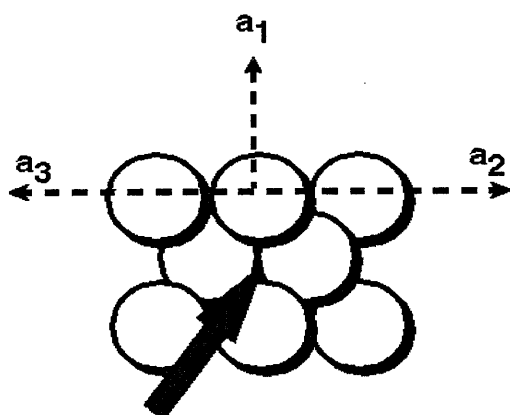


Figure 5b. Variation of the integral halfwidth as a function of temperature and gas-phase composition (Open Squares: 16ml/min CH₃OH in 100ml/min He; Closed Circles 100ml/min O₂)

Figures 5a and 5b show the variation of the (111) and the (311) integral halfwidths as a function of temperature for both the oxygen and methanol runs. Figure 5c and 5d show the variation of the (220) and (200) integral halfwidths. The figures are grouped according to their respective zone axes. The zone axis represents the axis formed by the two intersecting planes shown. The increase of the integral halfwidth seen in Figures 5a-d at 573K

corresponds exactly with the onset of O_p desorption shown in Figures 2a-c and the increase in the unit cell constant shown in Figure 4. The variations arise, therefore, as a result of oxygen diffusion into the silver. An increase in the integral halfwidth indicates the formation of defects or the building up of stress in the crystal lattice. The integral halfwidths of the reflexes forming the [220] zone axis in Figures 5a,b and the () plane in d vary in a similar way. The (200) reflection shows a different trend. A model which explains these qualitative trends is shown in Figure 6a. The similar trends of the (111), (311) and (220) reflexes indicates an increase of strain or a decrease in crystal size along the [110] direction. This behavior is therefore a strong argument for the diffusion of oxygen along the [110] direction into the bulk. The decrease of the reflexes above 573K and the increase of the (200) reflection indicates a reorganization of the anisotropic defect distribution caused by the [110] oxygen diffusion. This is a result of the thermal reorganization of the defects. In addition, the model predicts that long needle-like microcrystals are formed with the orientation shown in figure 6b. This morphology develops as result of the anisotropic strain induced by the incorporation of O_p via diffusion in the [110] direction through the distorted unit cell. The anisotropy arises from the fact that the atoms oriented along the a_1 vector shown in Figure 6a are not disturbed by the displacement of the face-centered atoms in the a_2 and a_3 vectors. Figure 6c is an illustration of the macroscopic polycrystalline silver grains as expected from XRD data. Diffusion is favored along the grain boundaries formed between the crystallites. The unit cell constant increases upon the incorporation of oxygen into the silver leading to increasing stress between the microcrystalline domains causes rupture and subsequent crack formation. The formation of more and larger crystal grains result which in-turn enhances further bulk diffusion. This is a type of autocatalytic process where oxygen incorporation in the bulk results in an increased diffusivity for oxygen.



Octahedral Site

Figure 6a. Ball model cut through the silver (110) plane. Suggested mechanism for oxygen-induced bulk restructuring.

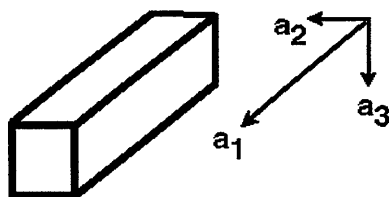
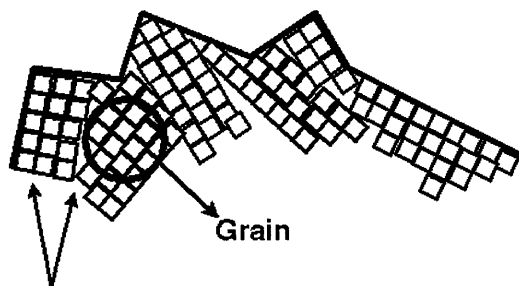


Figure 6b. The suggested shape of the microcrystals formed as a result of the oxygen pre-treatment of silver.



Grain Boundaries

Figure 6c. The suggested morphology of the polycrystalline silver subsequent to high-temperature treatment in oxygen.

3.3.9. STM Results

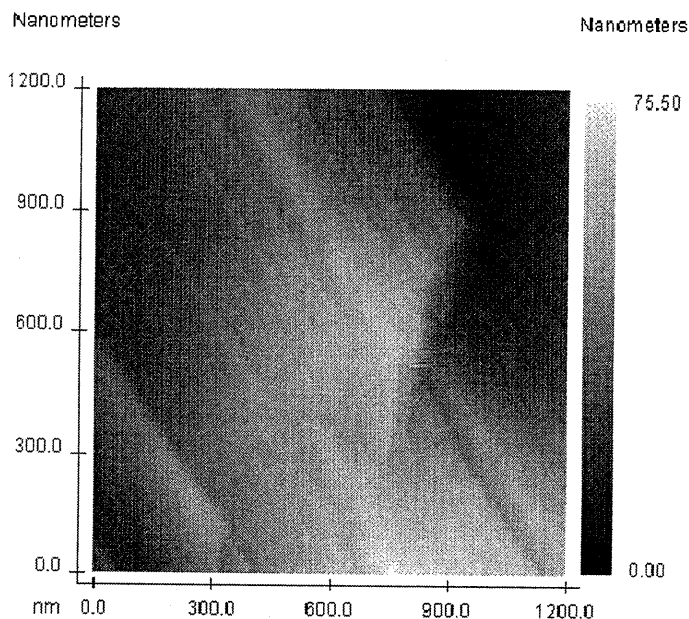


Figure 7. Scanning tunneling microscopy image of a silver foil pretreated in 10% O_2 in He, total flow of 150 ml/min for four

Figure 7 shows an STM image of the silver foil surface following treatment in a 10% O_2 atmosphere in helium. The presence of large crystallites composed of smaller columnar crystallites is self evident. The large crystals imaged with STM are similar to those found with SEM and are typically in the μm size range. The smaller crystallites vary in size and exhibit a surface roughness of approximately 3-5nm. This image is typical of images taken at almost every point on the surface. The main difference in the scans is the shape of the μm -sized crystal structure formed. In all cases, the large crystals are composed of columns of smaller microcrystals. This confirms the model derived on the basis of the XRD data.

3.3.10 TDS vs. XPS-The Evidence for Surface Diffusion Inhibition

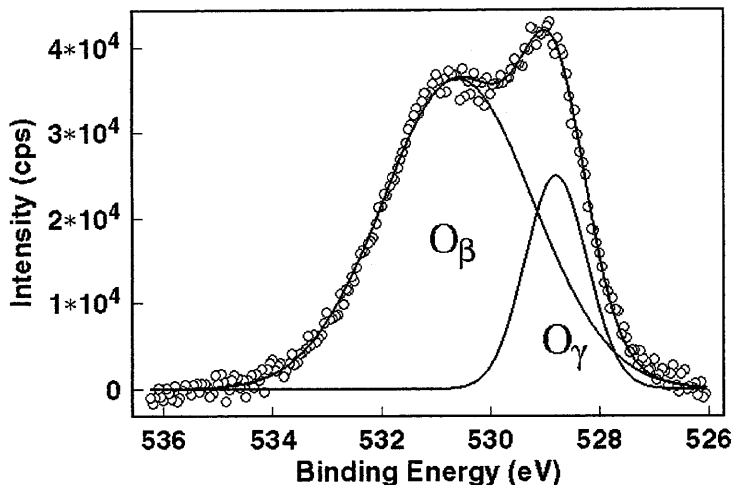


Figure 8. X-Ray Photoelectron spectrum for silver pretreated in 100mbar O_2 at 873K

The idea that O_γ is formed by segregation of O_β to the surface *via* diffusion through low-indexed crystalline planes was tested. The sample was heated to 873K in vacuum for 30 minutes. This vacuum treatment results in extensive annealing and thus to the formation of low-indexed terminating surface structures¹⁸. These structures offer increased resistance to oxygen diffusion. TDS and XPS analysis were performed on the sample prior to and after this vacuum treatment. TDS provides information about the thermal stability of all oxygen species present in the bulk whereas XPS provides chemical information about species located in the near-surface region (30 angstroms). With this combined information, one can effectively differentiate between processes occurring in the subsurface and surface regions. In the XPS measurements, O_β was assigned to the peak centered at 531eV and O_γ to the peak centered at 529eV¹⁶. A typical spectrum with subsequent peak deconvolution and assignments is shown in Figure 8.

The large FWHM for O_β relative to O_γ supports the argument proposed earlier, based on the TDS spectra, that O_β is bulk-dissolved oxygen located both in the grain boundaries as well as in crystallites of various orientations. The resulting heterogeneity of the O_β electronic environment results in a broadening of the XPS signal (Figure 8) as well as the TDS signal (Figure 2a-c). The results of both experiments are combined and are shown in Figure 9.

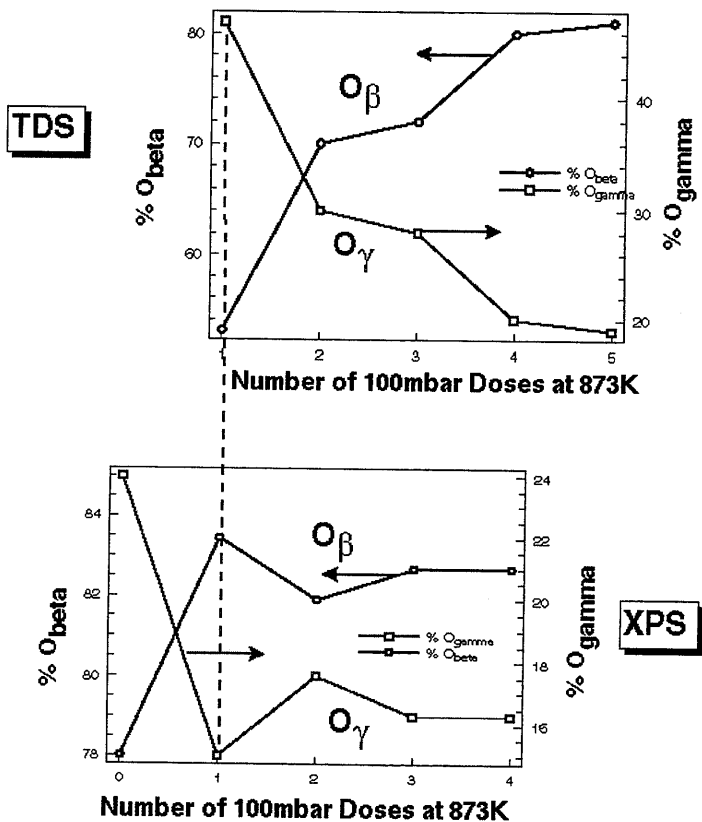


Figure 9. Integrated intensities for O_β and O_γ for TDS and XPS of silver initially treated for 30 minutes at 873K in vacuum and then subsequently dosed with 100 mbar O_2 at 873K.

It is immediately obvious that treatment of the silver in vacuum prior to oxygen dosing results in a drastic change in the O_β/O_γ ratio detected by TDS. O_γ usually accounts for about 20% of the thermal desorption signal under these conditions. Dosing oxygen subsequent to vacuum treatment results in a fourfold increase of the integrated O_γ intensity, which now represents more than 80% of the total desorption signal. Figure 9 shows that continued exposure to oxygen eventually returns the surface to its original state where O_β is the dominant signal. The changes of the relative XPS intensities clearly indicate that the drastic variation of the TDS oxygen desorption signals, seen in the upper half of Figure 9, results from partial blocking of O_β segregation to the surface. This occurs as a result of the surface restructuring during the vacuum pretreatment. There is a large decrease of both the O_β (531eV) and O_γ (529eV) signal intensities immediately following the vacuum treatment (first point prior to O_2 exposure). The silver is depleted of most of the O_β which results in O_γ being the dominant signal at this point (exhibits the highest thermal stability). Subsequent dosing of oxygen shows a slight increase of the XPS signal for O_β relative to O_γ . The O_γ signal observed in XPS is assigned to oxygen intercalated in the uppermost (30 Angstroms) silver layers. The fact that the integral O_γ signal intensity observed with XPS does not show the same trend as observed by TDS arises from the fact that oxygen located deeper in the silver bulk is not observable using XPS. This must be taken into account when assigning species observed by both techniques. The integral O_γ desorption signal observed by TDS represents the total flux of oxygen contained in the bulk which diffuses through low-indexed crystalline planes formed at the surface during the pretreatment or during the TD experiment itself. XPS shows, essentially, a snapshot of the surface subsequent to pretreatment. Therefore, the O_γ observed by XPS is attributed to the O_γ observed by TDS only in that moment when the oxygen has segregated from the bulk into the uppermost atomic layers of silver where it may be detected. Extreme caution must be used when interpreting spectra attributed to sub-surface species. The integral areas of O_γ and O_β measured by both XPS and TDS agree excellently after having repeatedly exposing the silver to oxygen ($O_\beta=84\%$, $O_\gamma=16\%$). These values represent the values expected after the silver has equilibrated with the surrounding gas atmosphere. The similarity of the values obtained with both methods indicates that under conditions of equilibration, O_γ is confined to the uppermost silver layers.

3.3.11 ISS-Evidence for the Reconstruction/Diffusion Relationship

Further evidence for this interpretation was obtained by performing ion-scattering-spectroscopy (ISS). The first run was made after dosing 100mbar O_2 at 873K subsequent to having equilibrated the sample by repeatedly dosing with oxygen at 100mbar and 873K. The concentration profile represents the same situation as that found after having performed multiple oxygen exposures (Figure 8). A second run was made by first heating in vacuum at 873K and then dosing 100mbar O_2 at 873K. The normalized results are shown in Figure 10.

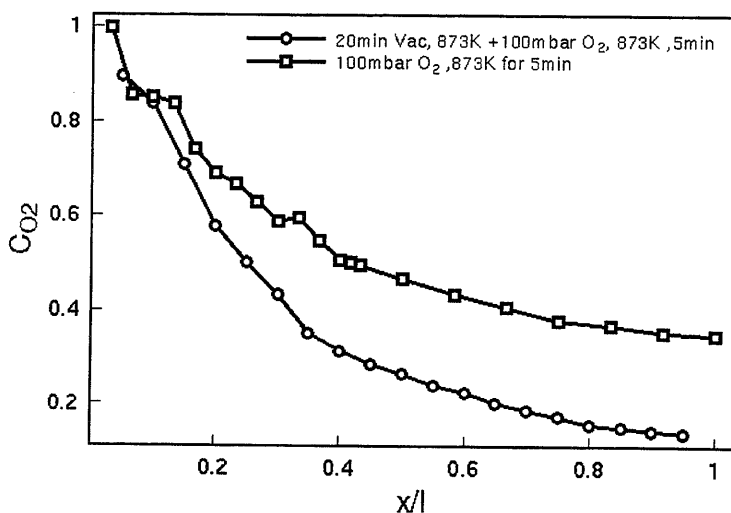


Figure 10. Results of depth profiling analysis obtained with He⁺ ion-scattering spectroscopy of silver equilibrated with oxygen (open circles) and silver dosed with oxygen subsequent to heating under vacuum (open squares).

A comparison of these runs should reveal whether surface annealing results in a surface diffusion barrier to the segregation of oxygen from the bulk. The oxygen concentrations in the near-surface region are identical for both runs. The variation of the total oxygen content as a function of depth is very different for both pretreatments. The concentration-depth profile distribution for the oxygen-equilibrated sample shows a gradual decrease in the oxygen signal as a function of depth. The sample subjected to vacuum treatment prior to oxygen dosing

shows an initial steeply dropping slope which eventually plateaus at greater depth. Bulk-dissolved oxygen was obviously forced into a thin layer in the near-surface regime during segregation as a result of the formation of the diffusion barrier formed during vacuum annealing. The form of the depth profile also yields important information. In this case, the 0.1mm thick silver foil is considered to be a semi-infinite medium subjected to the initial boundary conditions $C(O_2)_{x=0} = S_{O_2} \times P(O_2)$, $C(O_2)_{x=1/2L} = 0$. S_{O_2} is the solubility of oxygen in silver and $P(O_2)$ is the gas phase oxygen pressure. Normal Fickian diffusion predicts a linear decrease in oxygen concentration as a function of depth.^{9,6,19} The nonlinearity of the concentration-depth profile provides strong evidence that the diffusion coefficient is concentration dependent. The concave-up curve form indicates that the diffusion coefficient is a positive function of oxygen concentration. This agrees excellently with the supposition that oxygen induces a recrystallization of the bulk at elevated temperatures, which subsequently results in an enhancement of oxygen diffusion. It is to be expected, therefore, that oxygen diffusion is favored for those parts of the silver bulk which have incorporated the largest amount of oxygen (O_p) and, therefore, are the most strongly reoriented (high O_p concentration).

3.4 Discussion

A comparison of two earlier studies (6,20) with the present results supports the arguments presented here. The first is a publication regarding the diffusion of oxygen in both polycrystalline silver and silver (110).⁶ The second is a study dedicated to the determination of the temperature dependence of the silver interdiffusion coefficient using isotope-marked tracers.²⁰ These studies yield some very important information about the silver-oxygen system. Outlaw⁶ showed that the Arrhenius-temperature dependence of oxygen diffusion in silver exhibits two distinctly different linear regimes. Hoffman et al.²⁰ showed that the interdiffusion coefficient of silver also exhibits similar behavior. The results of both of these studies are depicted graphically in Figure 11.

Above 623K, the oxygen diffusion coefficient exceeds that of silver-self diffusion. This temperature coincides excellently with the onset of O_p desorption seen in Figures 2a-c and with the unit cell expansion seen in Figure 4. Above this temperature, the kinetics of oxygen

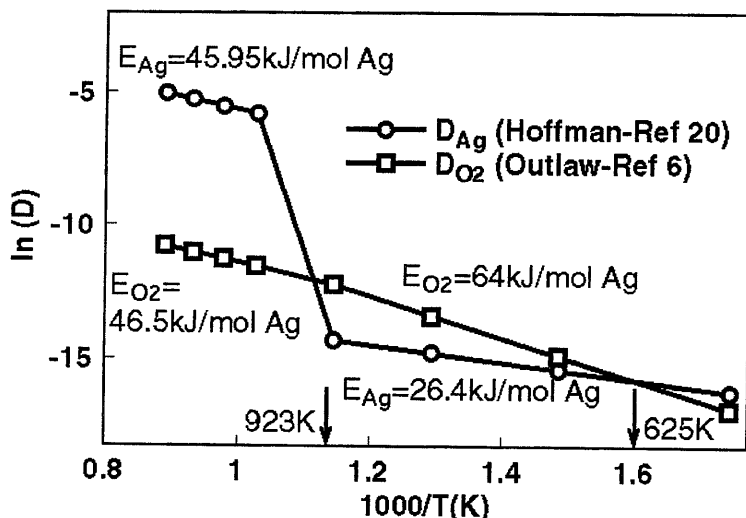


Figure 11. A comparison of data obtained from Outlaw and Hoffman regarding the temperature dependence of the oxygen diffusion coefficient in silver and the silver interdiffusion coefficient.

diffusion exceed that of thermal reordering resulting in an 'activation' of O_p desorption during the TDS. The discontinuity in the Arrhenius plot observed upon reaching 950K represents the point at which interdiffusion of silver occurs at approximately 300 times the rate of oxygen diffusion. It is interesting to note that the activation energy of silver interdiffusion and oxygen diffusion in silver are identical beyond the inflection point at 923K. This implies that both oxygen and silver must overcome identical energetic barriers for diffusion. This is a strong indication that oxygen diffusion under these conditions is not limited by dissociative chemisorption of oxygen.⁶ These are the conditions under which O_i is formed. Conditions under which the kinetics of thermal silver reordering plays the bigger role and result in the growth of closely-packed, thermodynamically-stable surface structures. Oxygen is therefore forced to diffuse through these structures *via* volume diffusion which ultimately leads to O_i formation. The high temperatures necessary for activation of interstitialcy diffusion will always lead to the structural rearrangement of the silver. Surface transformations typically occur at a lower temperatures than bulk transformation resulting in the formation of low-

indexed terminating surface structures which offer a high barrier to the surface segregation of oxygen. This explains the fact that O_i is only found in the (111) terraces of silver⁽¹⁶⁾ and appears to occupy only the uppermost silver layers.

Figure 12 shows a ball model of the (110) and (100) surfaces. The channels in the [110] direction are clearly visible. It is these channels which act as the path of least resistance for the interstitial transporation of oxygen *via* octahedral hole jumping. Diffusion of oxygen in directions other than this occur via an interstitialcy mechanism at temperatures greater than 923K.

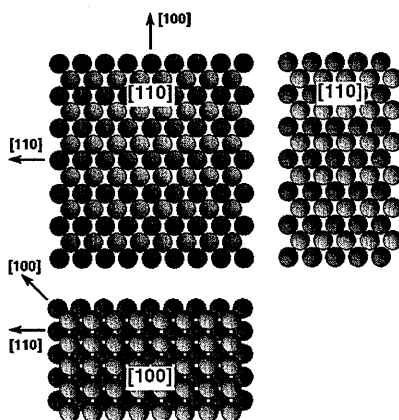


Figure 12. Ball model showing various sphere packings for silver.

3.5 Conclusions

Two distinctly different types of subsurface atomic oxygen are formed in oxygen-pretreated, polycrystalline silver. The first is termed O_b and refers to bulk-dissolved oxygen which diffuses along grain boundaries or *via* interstitial hole-jumping through loosely-packed, high-index crystalline planes. O_i is formed at elevated temperatures under conditions at which interstitialcy diffusion becomes possible and results in the substitution of silver atoms by oxygen. The catalytically active O_i species is essentially O_b in that moment when oxygen segregates from the bulk to the surface *via* volume diffusion of oxygen through low-indexed terminating crystalline planes. Formation of both species is a strong function of temperature and oxygen pressure. The interaction of oxygen with silver results in a substantial decrease in the diffusion barrier for oxygen pressures in the range of $1.0\text{mbar} < P_{O_2} < 10\text{mbar}$. This effect is caused by oxygen-induced recrystallization which leads to the formation of higher-indexed crystalline planes, a reorientation of the facets, and the formation distortion of the unit cell

forming channels in the [110] direction through which oxygen may diffuse. Dosing at pressures above 10mbar O_2 leads to a marked increase in the barrier to oxygen diffusion. This is due to a texturing of the facets to a predominantly (331) terminating surface. This study lays the groundwork for understanding the role played by these oxygen species in silver-catalyzed oxidation reactions. The strong dependence of oxygen diffusion kinetics on morphology is expected to have a direct impact on the reaction kinetics of the oxidative coupling of methane, which is believed to be catalyzed by O_r .

References

1. Ullman, in "Ullman's Encyclopedia of Industrial Chemistry", 5th edition, **A11**, 619. (1988).
2. Sperber H., *Chemie-Ing.-Technology*, **41(17)**, 962 (1969).
3. Lefferts L., van Ommen J.G. and Ross J.R.H., *Appl. Catal.* **31**, 291 (1987).
4. van Santen R.A. and Kuipers H.P.C.E, *Adv. Catal.* **35**, 265 (1987).
5. Eichenauer W. and Pebeler A., *Z. Metallkade.* **48**, 373. (1957).
6. Outlaw R.A., Wu D., Davidson M.R. and Hoflund G. B., *J. Vac. Sci. Technol. A* **10(4)**, 1497 (1992).
7. Rovida G., Pratesi F., Maglietta M. and Ferroni E., *Surf. Sci.* **43**, 230 (1974).
8. Backx C., de Groot C.P.M. and Biloen P., *Surf. Sci.* **104**, 300 (1981).
9. Schmalzried H., in "Chemical Kinetics of Solids", VCH Verlagsgesellschaft Weinheim. (1995).
10. Wei Ta-Chin and Phillips J., *Adv. In Catal.* **41**, 359 (1995).
11. Bao X., Barth J.V., Lempfuhr G., Schuster R., Uchida Y., Schlögl R. and Ertl G., *Surf. Sci.* **284**, 14. (1993).
12. Bonnel D.A., in "Scanning Tunneling Microscopy and Spectroscopy, Theory, Techniques and Applications", VCH Publishers, Inc., ISBN 0-89573-768-X. (1993).
11. Bao X., Lempfuhr G., Weinberg G., Schlögl R. and Ertl G., *J. Chem. Soc. Faraday Trans.* **88**, 865 (1992).
12. Herein D., Nagy A., Schubert H., Weinberg G., Kitzelmann E. and Schlögl R., *Zeitschrift für Physikalische Chemie, Bd.* **197**, 67. (1996).
13. Xinhe Bao and Jingfa Deng, *J. Catal.* **99**, 391 (1986).
14. Xinhe Bao, Muhler M., Schedel-Niedrig Th. and Schlögl R., *Phys. Rev. B*, **54**, 2249. (1996).
15. Schubert H., Tegtmeier U., Herein D., Bao X., Muhler M. and Schlögl R., *Catal. Lett.* **33**, 305 (1995).
16. Somorjai G. A., in "Introduction to Surface Chemistry and Catalysis", John Wiley & Sons, Inc., ISBN 0-471-03192-5. (1994).
17. Crank J., "The Mathematics of Diffusion", Oxford University Press, ISBN 0-19-853411-6. (1975).

18. Hoffman R.E. and Turnbull D., *J. Appl. Phys.* **22**, 634. (1951).
19. Stranski I.N. and Krastanov L., *Sitzungsber. Akad. Wissenschaft Wien*, **146**, 797. (1938).
20. Yanase A., Komiyama H. and Tanaka K., *Surf. Sci. Lett.* **226**, L65 (1990).
21. Czanderna A., Chen S. and Biegen J., *J. Catal.* **33**, 163 (1974).

The Dynamic Restructuring of Electrolytic Silver During the Formaldehyde Synthesis Reaction

Abstract

The partial oxidation of methanol to formaldehyde was studied over an industrial electrolytic silver catalyst. Special attention was paid to the influence of reaction-induced restructuring of the silver surface and bulk on the activity for the partial oxidation of methanol to formaldehyde. Drastic differences are observed in the performance exhibited by fresh samples and those which have been previously treated at high temperature ($T > 873\text{K}$) reaction conditions. The temperature dependence of the conversion for a fresh catalyst shows a pronounced hysteresis which can be separated into 3 temperature regimes. These regimes are strongly correlated with various morphological changes induced in the silver during reaction. SEM images reveal that heating silver in an excess of methanol to 773K results in the destruction of grain-boundary defects. Comparison of the various hysteresis profiles with TDS analysis of silver pretreated at high temperature in oxygen shows that elimination of these defects results in the inhibition of oxygen diffusion from the bulk to the surface in the temperature region between 673K and 873K . The formation of holes resulting from reaction of bulk-dissolved hydrogen and oxygen indicates that diffusion along these defect structures supplies bulk oxygen for the catalytic reaction. Hole formation above 923K is no longer restricted to grain boundaries indicating that volume (interstitialcy) diffusion replaces grain-boundary diffusion at elevated temperatures. This incorporation of oxygen into the silver lattice results in the formation of O_i which exhibits an increased conversion of methanol with a higher selectivity to formaldehyde. This restructuring completely eliminates reaction hysteresis in samples treated in the reaction mixture at temperatures in excess of 873K . This leads to an improvement in the catalytic performance of silver for this extremely structure-sensitive reaction.

4.1 Introduction

It was mentioned in the general introduction on pages 1-17 that the partial oxidation of methanol to formaldehyde is conducted at significantly higher temperatures (in excess of 800K) than the ethylene epoxidation (EO) reaction (approximately 523K). In addition, the formaldehyde-synthesis reaction is carried out over unsupported, electrolytically prepared silver as opposed to the Al_2O_3 -supported silver used for the EO reaction. These extreme differences in temperature and catalyst show the extreme versatility of silver as a partial oxidation catalyst, but hint that the mechanisms involved differ significantly. This arises, in part, from the fact that silver is capable of accommodating a variety of catalytically-active oxygen species^{1,2,3}. The formation of these species was shown in the last chapter to be a complex function of temperature, partial pressure of oxygen, type of silver and pretreatment history. Both the silver surface and bulk undergo drastic morphological changes during reaction which ultimately lead to inhibition or promotion of the catalytic activity.

The goal of the work presented in this chapter is to show that restructuring of silver resulting from the gas-solid interaction leads to the activation of silver for the partial oxidation of methanol to formaldehyde. It is shown that silver plays a dynamic role in the reaction, adapting to its thermal and chemical environment on the time scale of the experiments performed here.

4.2 Experimental

Electrolytic silver (BASF-AG, 99.999%), silver powder (Chempur 99.9%) and silver foil (Goodfellow 99.9995%) were tested. Qualitative elemental analysis using EDX showed the presence of small amounts of C, Si and Cl contamination in all samples (data not shown). It is impossible to quantify their concentration with this technique. Silver is, however, the dominant component observed. The silver foil used for the scanning electron microscopy experiments was polished with diamond paste down to a grain size of 100 nm. Catalytic experiments were carried out in two different tubular quartz reactors. Both reactors were 20cm long. The first had an inner diameter of 4mm and the second 8mm. Samples were held in place with quartz-wool plugs and were located in a 2cm isothermal zone near the center of the oven. A thermocouple (Type K) was attached to the outer wall of the quartz tube directly adjacent to the sample with stainless steel wire. Blank runs showed that the thermocouple exhibits high catalytic activity. This makes direct placement of the thermocouple in the catalyst bed impossible. Quartz chips (0.05mm diameter) were used to dilute certain samples in order to differentiate when local heating effects play a significant role. Heating was provided by a single-zone oven (i.d.=15mm, length=30cm) with an isothermal section approximately 2cm long which was controlled by a Eurotherm temperature controller (model 902). The reactor was insulated by placing ceramic wool at both the entrance and exit to the oven and then wrapping in quartz tape. Catalyst particle sizes tested were .2-.4mm, .75-1mm, and 20 microns. Space velocities varied from $22,000 \text{ hr}^{-1}$ to $6.7 \times 10^5 \text{ hr}^{-1}$. The total gas flow through the reactor was kept constant at 265 ml/min and the space velocity was varied by changing the bed height. The linear gas velocity was therefore 8.83cm/s for runs made with the 4mm i.d. reactor and 2.2cm/s for the 8mm i.d. reactor. Pressure drops across the catalyst bed were less than the maximum sensitivity of the diaphragm manometer used (0.1bar). The ratio $(8.8 \text{ vol } \% \text{ CH}_3\text{OH})/(3.5 \text{ vol } \% \text{ O}_2)$ of 2.5 is slightly higher than 2.0 which is used in the industrial process (1). The methanol-rich conditions were chosen in order to minimize local heating effects resulting from the high exothermicity of the complete oxidation reaction which is known to be favored at higher oxygen partial pressures (1,7,14). The following definitions are used throughout this chapter:

- % Conversion = $\text{mol}(\text{Product})/\text{mol}(\text{MeOH in feed}) \times 100\%$
- % Selectivity = $\text{mol}(\text{Product})/(\text{mol}(\text{MeOH in feed}) - \text{mol}(\text{MeOH out})) \times 100\%$

Complete conversion of oxygen occurs for restructured samples having undergone reaction at temperatures in excess of 873K. This makes the determination of the intrinsic reaction rate on a surface area basis impossible. For this reason, all data are shown as % conversion of reactant or % yield of product. Analysis of the products was made by on-line gas chromatography. A mol-sieve (5A) (Supelco-5') and a carboxen (Supelco-16') packed column (1/8" diameter) were used for separation of both high and low boiling point compounds. Quantitative analysis of all compounds except water was possible with this setup. Heating rates of 0.5 K/min and 1K/min combined with a sampling time of 30 min results in a temperature resolution of 15K and 30K respectively. The fact that the values obtained for these extremely slow heating rates (for reaction over aged catalysts) are representative of the steady-state values was confirmed by the fact that the activation energies and conversions calculated using the different heating rates (1K/min) and (0.5K/min) are identical within an acceptable margin of error.

Temperature-desorption spectroscopy (TDS) measurements were made in an ultra-high vacuum (UHV) chamber with a background pressure of 3×10^{-8} mbar. Mass scans showed the background gas to be primarily composed of H₂O (data not shown). Monitoring of desorption products was made with a Hiden (Hal2) quadrupole mass spectrometer coupled to a Next workstation. A sampling rate of 1s was standard. A water-cooled, infrared oven was used for heating. The thermocouple (Type K) was placed immediately below the sample and was in direct contact with the quartz holding tube. Linear heating rates from room temperature to 1000K were possible with this setup. A heating rate of 1K/s was used for all TDS runs. A special pretreatment procedure was used in order to minimize the amount of carbon present in the samples. This consisted of treating the sample in the reactor with flowing O₂ (17ml/min) at 973K overnight and then transferring to the UHV chamber through air and subsequently performing numerous oxidation-reduction cycles (10mbar O₂/ heating in vacuum to 1073K). This had to be done for approximately one week in order to minimize the CO₂ evolution after O₂ dosing. It is impossible to remove all carbon impurities.

The scanning electron microscope (SEM) images were taken with a Hitachi S-4000 SEM equipped with an EDX for element identification.

4.3 Results

4.3.1 The Conversion Obtained Over an Aged Catalyst

The catalytic activity of electrolytic silver was tested for the methanol oxidation reaction. Fresh catalysts exhibit a pronounced reaction hysteresis (See Figure 2) which will be explained in more detail later. For simplicities sake, the aged catalyst will first be presented.. Reproducible catalytic results were obtained after repeating three high-temperature reaction ($T > 923\text{K}$) cycles with subsequent cooling to 423K in the reaction mixture. No deactivation of the catalytic activity was observed for samples subjected to this pretreatment. A typical run made with a used silver catalyst is shown in Figure 1.

Figure 1 shows that the used silver catalyst is active above 500K . The exothermicity of the prevailing net-oxidation reaction results in a temperature rise of approximately 50K (observed during the measurement). A comparison of the catalytic activity of used silver samples using N_2 instead of He as the carrier gas shows (5x reduction in heat conductivity) showed the same conversion for both oxygen and methanol. This is evidence that local-heating of the catalyst bed is not responsible for CO_2 formation. The formation of complete oxidation products is attributed to the reaction of methanol with the weakly-bound atomic surface oxygen species O_a (See Chapter 3.).

Above 500K , the methanol conversion and CO_2 yield drops off and the formaldehyde yield increases. Oxygen is completely consumed at temperatures above 500K . The complete conversion of oxygen implies that only a portion of the catalyst bed is being used for reaction. This is also the case for catalyst beds which are only 1mm thick. Incomplete oxygen conversion above 573K is only obtained for samples containing an extremely small amount of silver thinned with quartz (0.06g Ag in 0.24g SiO_2 , $0.4\text{--}0.7\text{mm Ag}$ particles in $0.2\text{--}0.4\text{mm SiO}_2$

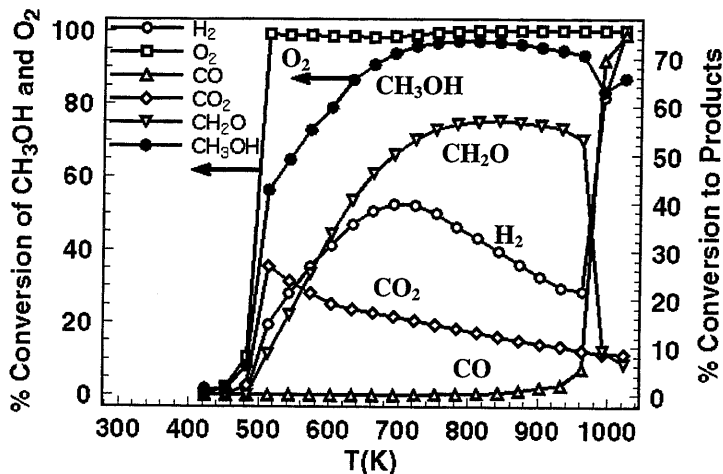


Figure 1. % Conversion of methanol to selected products over an aged electrolytic silver catalyst. Heating rate 1K/min, 0.3g Ag (0.75-1mm), 3.5 vol% O₂, 8.8 vol% CH₃OH, 87.7 vol% He, S.V.= 3.63×10^5 hr⁻¹.

particles) or for fresh silver samples which have not undergone previous high-temperature reaction treatment. Channeling of reactants through such a thinned catalyst bed is likely under these conditions and the results are therefore not shown here. This problem has been mentioned by a number of authors^{5,6,23} and makes it impossible to conduct a kinetic analysis of the methanol oxidation reaction with this reactor set-up. Determining the kinetics of the partial oxidation of methanol to formaldehyde over silver under conditions comparable to those used in industry is a challenge which has yet to be met. The methanol conversion rises with increasing conversion to formaldehyde and levels off at 55% at 773K. The abrupt drop in formaldehyde production and subsequent formation of H₂ and CO at 973K is due to the gas-phase decomposition of methanol and formaldehyde. This has also been observed by other authors¹⁰. This temperature represents the upper-temperature limit for all experiments presented here.

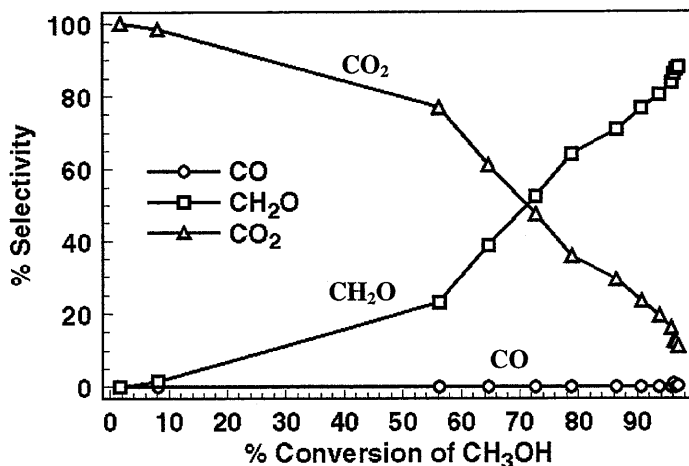


Figure 2. % Selectivity of methanol to formaldehyde as a function of methanol conversion: Heating rate 1K/min, 0.3g Ag (0.75-1mm), 3.5 vol% O₂, 8.8 vol% CH₃OH, 87.7 vol% He, S.V.= 3.63×10^5 hr⁻¹.

The product selectivity is shown as a function of methanol conversion in Figure 2. The high selectivity to CO₂ for methanol conversions lower than 80% show that total oxidation is favored at lower temperatures. A strong shift in formaldehyde selectivity from 20% to 80% at 55% methanol conversion occurs just above 500K (Compare with Figure 1). This temperature agrees well with the on-set of the O_β desorption at 573K shown in Figure 2a-c in Chapter 3 pages 28-31.

4.3.2 Catalytic Activity of a Fresh Catalyst

Figure 3 shows the first run obtained using the fresh catalyst charge which was subsequently used to produce the data in Figure 1. The onset temperature for reaction over the fresh catalyst (500K) is 50K higher than that of the aged one. The fresh catalyst initially shows nearly identical activity to the aged catalyst shown in Figure 1. Reaction over the fresh catalyst in Figure 3 shows, however, a strong deactivation in catalytic activity with heating above

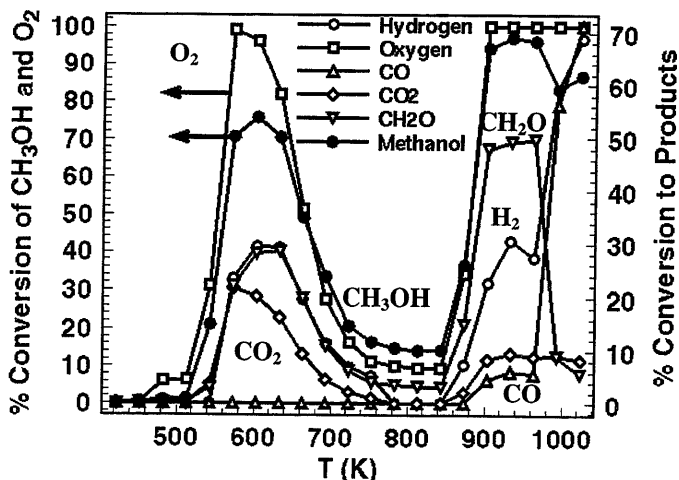


Figure 3. % Conversion of methanol to selected products over a fresh electrolytic silver catalyst. Heating rate 1K/min, 0.3g Ag (0.75-1mm), 3.5 vol% O₂, 8.8 vol% CH₃OH, 87.7 vol% He, S.V.= 3.63×10^5 hr⁻¹.

573K. This deactivation leads to a minimum in methanol conversion (13%) at 800K. Above this temperature, the methanol conversion rises sharply and plateaus at 95%. The gas-phase mixture decomposes homogeneously (See section 3.1.2) above 973K producing primarily CO and H₂.

4.3.3 The Hysteresis of Reaction

4.3.3.1 Cycle 1 (423-573-423K)

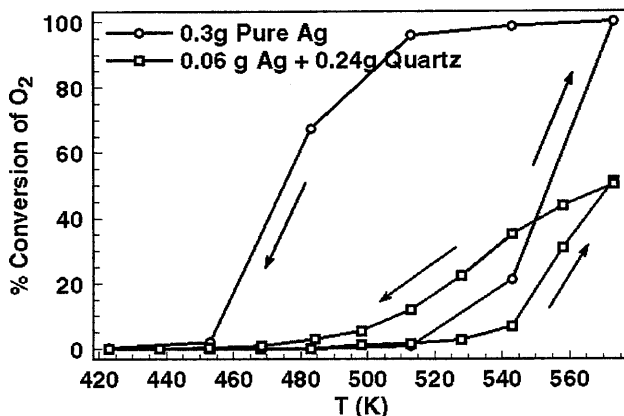


Figure 4. Comparison of hysteresis profiles for samples with and without thinning by quartz chips at two different heating rates, (0.75-1.0mm), 3.5 vol% O₂, 8.8 vol% CH₃OH, 87.7 vol% He, S.V.= 1.68×10^5 hr⁻¹

Temperature cycle experiments were performed in order to provide more information about the cause of the deactivation. The presence of hysteresis indicates either a temperature bi-stability of the system or an intrinsic change of the catalyst activity such as the creation and/or destruction of active sites. The chosen end-temperatures for the temperature cycle experiments correspond to the first maximum in methanol conversion at 573K, the minimum at 773K and the second maximum in methanol conversion at 873K in Figure 3. Runs were made with heating and cooling ramps of either 1K/min or 0.5K/min. The 0.5K/min run was diluted with quartz chips. Comparison of these runs allows the differentiation between reaction hysteresis effects caused by local heating and those which are due to intrinsic changes in the catalyst sample. The results are shown in Figures 4-8.

Figure 4 shows the methanol-conversion hysteresis obtained for the temperature cycle 423K-573K-423K using the two different heating rates of 0.5K/min and 1K/min with and without diluting with quartz chips. This data reveals that the reaction hysteresis observed in this temperature range is likely a temperature artifact. The reaction of methanol and oxygen over silver is highly exothermic in this temperature range due to the highly oxidative nature of the O_a oxygen species formed on the silver surface^{4,5,6,7}. Reaction with O_a results in the oxidative dehydrogenation of methanol to formaldehyde which is 243kJ/mol more exothermic than the pure dehydrogenation route (+84kJ/mol). The heating portion of the cycle in Figure 4 is likely to be more representative of the true temperature-conversion profile than the cooling branch. This results from one very important weakness of this experimental set-up. The high activity of the K-type thermocouple makes it impossible to have the thermocouple in direct contact with the catalyst bed. This, combined with the fact that the quartz wall separating the thermocouple from the bed is a poor thermal conductor means that a large error is present for the temperatures measurements made here. The only way to truly know the temperature at the catalyst surface is to use a temperature-sensitive infra-red camera. Performing this type of hysteresis run, however, provides an estimation of the accuracy of the temperature measurements made here. (calculate adiabatic temp rise)

4.3.3.2 Cycle 2 (423-773-423K)

Figures 5 and 6 show the hysteresis observed for methanol conversion and formaldehyde yield in the temperature cycle between (423-773-423K/0.5K/min). The maximum temperature for this cycle coincides with the observed minimum in catalytic activity shown in Figure 3. Both the conversion for methanol and formaldehyde pass through a maximum at 660K and then decrease with increasing temperature.

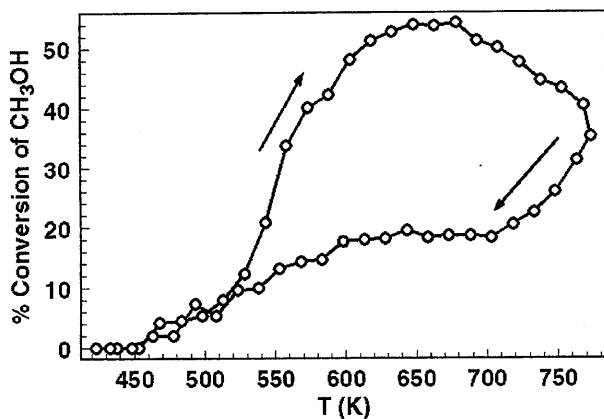


Figure 5. % Conversion of CH_3OH for the cycle (423-773-423K), 0.5 K/min, 0.06g Ag+0.06g SiO_2 , 4.3 vol% O_2 , 7.1 vol% CH_3OH , 88.6 vol% He, S.V.= $1.68 \times 10^5 \text{ hr}^{-1}$

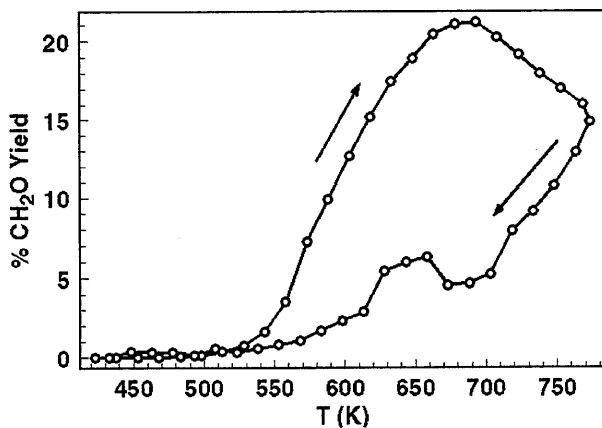


Figure 5. % Yield to CH_2O for the cycle (423-773-423K), 0.5 K/min, 0.06g Ag+0.06g SiO_2 , 4.3 vol% O_2 , 7.1 vol% CH_3OH , 88.6 vol% He, S.V.= $1.68 \times 10^5 \text{ hr}^{-1}$

4.3.3.3 Cycle 3 (423-948-423K)

Figures 7 and 8 show the reaction hysteresis observed for methanol conversion and formaldehyde yield for the temperature cycle 2 (423-948-423K//0.5K/min). A deactivation of the catalyst similar to that observed for the ascending temperature branch in cycle 2 (Figures 5 and 6) is also seen for the ascending branch in this case. The first small maximum in methanol conversion obtained at 650K for this temperature cycle is 30% lower than that shown in cycle 2 (Figure 5). The deactivation in methanol conversion and formaldehyde yield observed for the ascending branch from 423K to 948K (see Figures 7 and 8) is not observed for the descending branch. The high-temperature treatment has irreversibly modified the catalyst. Subsequent runs made with this catalyst show no hysteresis and exhibit temperature-conversion plots whose form is identical to that shown in Figure 4

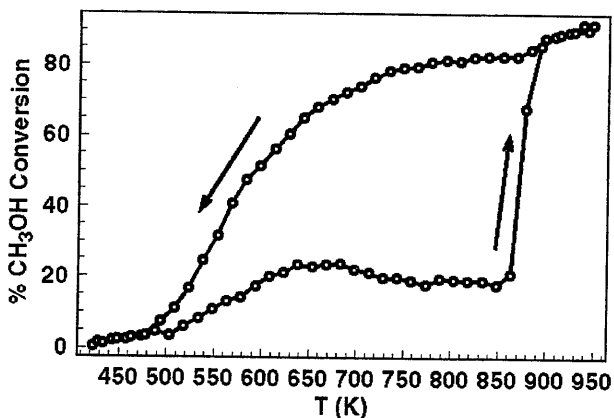


Figure 7. % Conversion of CH_3OH for the cycle (423-948-423K), 0.5k/min, 0.06g Ag+0.06g quartz, 4.3 vol% O_2 , 7.1 vol% CH_3OH , 88.6 vol% He, S.V.= $1.68 \times 10^5 \text{ hr}^{-1}$

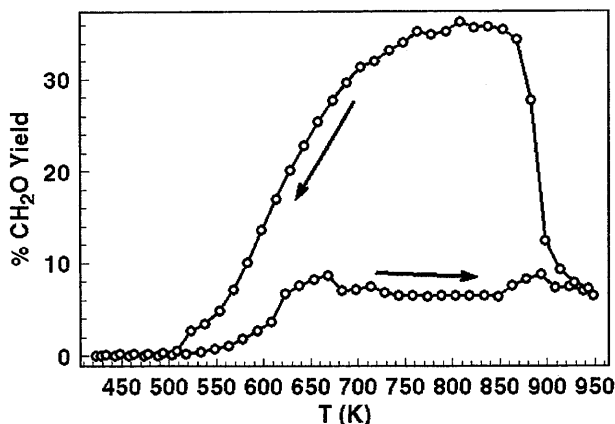


Figure 8. % Yield to CH₂O for the cycle (423-773-423K), 0.5k/min, 0.06g Ag+0.06g quartz, 4.3 vol% O₂, 7.1 vol% CH₃OH, 88.6 vol% He, S.V.= $1.68 \times 10^5 \text{ hr}^{-1}$

4.3.4 Diffusion Control of Reaction

Figure 9 shows the Arrhenius plots for a silver catalyst after having undergone 3 reaction cycles (max temp=1023K, 1K/min). This plot is based on methanol conversion and not on the actual rates of reaction. The activation energies should, therefore, be representative of the apparent activation energies as determination of the frequency factor requires the intrinsic reaction rate to be known. Determination of the intrinsic reaction rate is made impossible by the very high conversions obtained. The extremely small activation energies (-1.95, 2.76, 6.91kJ/mol) indicate that the reaction, as performed under these conditions, is diffusion limited. Variation of the activation energy signifies a change of mechanism or the presence of diffusion inhibition. Two inflection points are seen in Figure 9. These points separate the Arrhenius curve into a number of linear segments which are indicated by vertical lines. This point will be touched upon in more detail later.

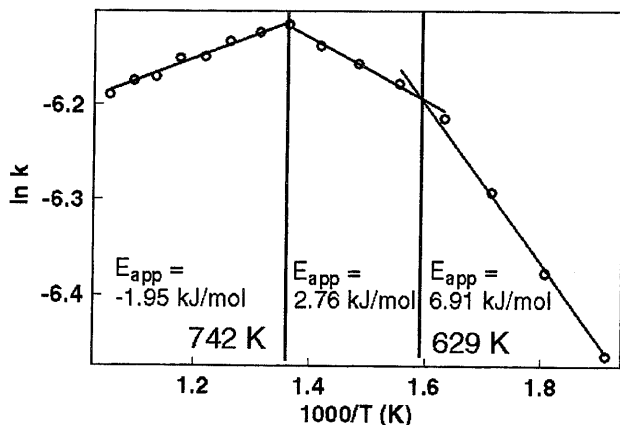


Figure 9. Arrhenius plot for methanol oxidation over an aged Ag catalyst: 0.3 g aged Ag (0.2-0.4mm), 3.5 vol% O_2 , 8.8 vol% CH_3OH , 87.7 vol% He, $S.V.=3.63 \times 10^5 \text{ hr}^{-1}$

4.3.5 Contributions from Homogeneous, Gas-Phase Reactions

The literature is contradicting regarding the participation of homogeneous, gas-phase reactions in the methanol oxidation reaction.^{8,9} A number of authors observed significant contribution from gas-phase reactions.^{10,11} These authors proposed a radical-chain mechanism in which the radical formation is initiated at the silver surface and the chain reaction occurs in the gas phase. This would also explain why the industrial reaction conditions (2 MeOH:1 O_2 , 873K) lie near the flame-point of the gas mixture in question. In contrast, Lefferts et. al⁶ found no contribution from gas phase reactions. The occurrence of gas-phase reactions was tested by varying the dead volume in the reactor. A quartz plug was inserted downstream of the catalyst bed to reduce the dead volume. Insertion of the plug results in an 8% decrease in methanol conversion. The results are shown in Figure 10. The empty reactor exhibits no catalytic activity. The conversion of methanol to CH_2O and H_2 are both approximately 10% higher for the reactor without the quartz plugs (higher dead volume) compared to that with plugs.

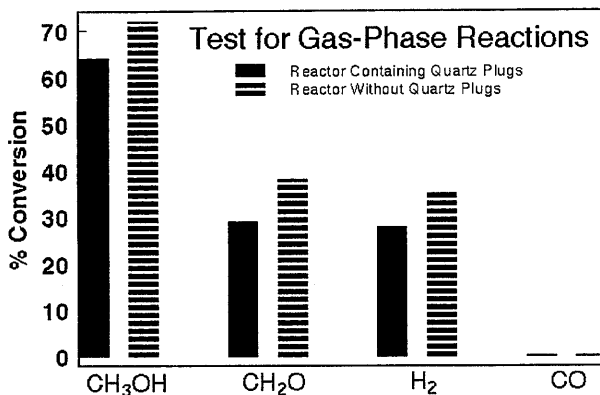


Figure 9. Evidence for the presence of gas-phase, homogeneous reaction in the methanol oxidation reaction at 600K. A quartz plug, downstream of the reactor bed was removed in order to increase the dead volume. 0.5k/min, 0.06g Ag+0.06g quartz, 4.3 vol% O₂, 7.1 vol% CH₃OH,

This observation provides strong evidence gas-phase reactions contribute to formaldehyde production. A possible explanation for the increased formaldehyde conversion could be that the plugs reduce the gas-phase dead volume reducing the likelihood that the thermally unstable formaldehyde decomposes homogeneously in the gas phase. This would be evidenced by an increase in the gas-phase decomposition products H₂ and CO which are the known products resulting from the thermal decomposition of formaldehyde¹². Figure 10 shows that this is obviously not the case as the CO yield does not increase for the reactor without plugs. The increase in H₂ formed for the reactor with increased dead volume shows that the direct dehydrogenation of methanol to formaldehyde may also occur in the gas phase. The absence of CO shows that this H₂ does not arise from CH₃OH or CH₂O decomposition. The catalyst appears, therefore, to function as a radical initiator. The radical species formed may then desorb and react further in the gas phase. The exact mechanism which takes place is

unknown and is likely to be a combination of both heterogeneously and homogeneously catalyzed steps.

These observations cannot be attributed to flow-stream changes induced by insertion of the plugs. This can be determined by analyzing the flow dynamics of the reactor used. Laminar flow in the catalyst bed cannot be disrupted by flow obstructions located downstream of the catalyst bed. The Reynold's number is a dimensionless number which allows an estimation of the conditions under which flow is laminar or turbulent. The Reynold's number (Re) for flow in a cylindrical tube can be calculated by using Equation 1.

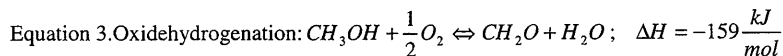
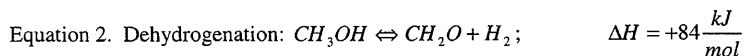
$$\text{Equation 1. } Re = \frac{\rho D v}{\mu}$$

Where ρ = density of the gas, D = reactor diameter, v = linear gas velocity and μ = viscosity of the gas mixture

The Reynold's number represents the ratio of the inertial forces to the viscous forces of the medium in question. The gas stream may be roughly estimated to have the fluid properties of air. The following values were used in the calculation of the Reynold's number: $\rho=1.225 \text{ kg/m}^3$, $\mu=1.79\text{e-}5 \text{ Pa s}$, $D=8\text{mm}$, $v=0.045\text{m/s}$. A Reynold's number of 25 was calculated. This value is far below the estimated value of $10,000^{13}$ necessary for turbulent flow which would lead to backmixing. The observed decrease in methanol conversion and increase in formaldehyde yield upon reduction of the dead volume cannot, therefore, be discounted on the argument of variations in fluid flow. It is unfortunately impossible to quantify the gas phase contributions using the present apparatus. It would be convenient to correlate systematic variations of the volume with corresponding changes in catalytic activity. There exists, unfortunately, a large thermal gradient over the length of the reactor oven which makes this impossible (Refer to Experimental in Chapter II). The participation of homogenous reactions in the partial oxidation of methanol to formaldehyde is a poorly-understood phenomenon which awaits further study with methods suited to the determination of gas-phase radical formation.

4.3.6 Evidence for the Temperature-Dependent Shift of the Reaction Mechanism

Both the direct dehydrogenation (Equation 2) and oxi-dehydrogenation (Equation 3) of methanol result in formaldehyde.



Thermodynamics dictates that the more endothermic reaction will dominate at higher temperatures. One way to determine the temperature dependence of these reaction mechanisms is to monitor the amount of H_2 and H_2O produced as a function of reaction temperature. It is, unfortunately, impossible to quantitatively measure the water concentration with the experimental apparatus used here. Measuring the $\text{H}_2/\text{CH}_2\text{O}$ ratio provides an estimate of the temperatures at which one mechanism prevails. The $\text{H}_2/\text{CH}_2\text{O}$ ratio for reaction over an aged silver catalyst decreases with increasing temperature as shown in Figure 11.

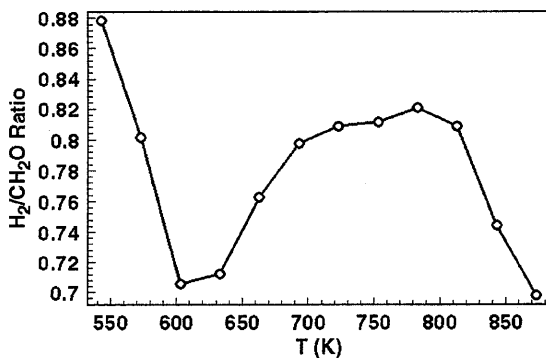
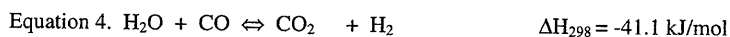


Figure 11. Ratio of moles H_2 to moles CH_2O produced. 0.5k/min, 0.06g Ag+0.06g quartz, 4.3 vol% O_2 , 7.1 vol% CH_3OH , 88.6 vol% He, S.V.= $1.68 \times 10^5 \text{ hr}^{-1}$

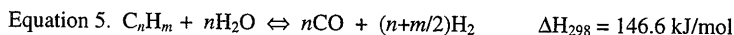
This does not, at first glance, seem to support the hypothesis that the dehydrogenation path increasingly dominates over the oxi-dehydrogenation path with increasing temperature. It is worth noting, however, that the accuracy of this ratio is questionable as hydrogen exhibits a poor sensitivity with a TCD detector, but the qualitative trend is obvious. The fact that hydrogen is produced with nearly a 1:1 stoichiometry with formaldehyde at temperatures as low as 550K indicates that the dehydrogenation mechanism may also be active at this relatively low temperature.

The direct dehydrogenation of methanol to formaldehyde is, however, not the only possible source of hydrogen. The water-gas shift reaction (Equation 4) and the steam reforming reactions (Equation 5) may also produce hydrogen according to the following equations.

Water-Gas Shift (WGS)



Steam Reforming (STR)



The likelihood of the STR reaction occurring at low temperatures ($T < 550 \text{ K}$) is improbable as the formation of CO is not observed and is thermodynamically unlikely at low temperatures ($K_{\text{eq},673\text{K}} = 6.18 \times 10^{-7} \text{ bar}$). Participation of the WGS reaction is thermodynamically plausible at low temperature ($K_{\text{eq},673} = 11.92 \text{ bar}$) but requires the presence of CO in the feed. CO was not observed for temperatures below 800K (See Figure 1). The nearly 1:1 ratio of $\text{H}_2\text{:CH}_2\text{O}$ observed at 573K cannot, therefore, be attributed to these reactions. The decrease in the $\text{H}_2\text{/CH}_2\text{O}$ ratio in Figure 11 at 623K is evidence for the strongly oxidative nature of the O_a species formed at this temperature which favors oxi-dehydrogenation to CH_2O and H_2O . The agreement between this temperature and the thermal desorption of the O_a species

^{1,2,3,14,15,16,17,18} is excellent and supports the assignment of this desorption peak to a surface-bound oxygen species which is formed directly from the gas phase. The unequivocal attribution of the decrease in the H_2/CH_2O ratio above 773K to an increase in the role played by the direct dehydrogenation or to increased consumption of H_2 by the WGS reaction is impossible as the contribution of both is likely under these conditions. The increased selectivity to CH_2O over CO_2 is shown in Figure 1 and supports the hypothesis that the direct dehydrogenation of methanol to formaldehyde increases at higher temperatures. This trend cannot be explained by the STR reaction which dominates at high temperatures. It is therefore suggested that both the direct dehydrogenation as well as the oxi-dehydrogenation of methanol to formaldehyde are possible over the entire temperature range studied here. The direct-dehydrogenation pathway dominates, however, at higher temperatures resulting in a higher selectivity to formaldehyde over CO_2 for similar methanol conversions. The fact that gas-phase reactions contribute to the overall mechanism makes it impossible to determine the exact role played by the various oxygen species located on and in the silver catalyst. It appears, however, that reaction with the various silver-bound oxygen species ultimately leads to either the formation of direct dehydrogenation or oxi-dehydrogenation products.

4.3.7 Reaction-Induced Changes in Catalyst Morphology

SEM images of the fresh sample as well as those subsequent to treatment at 573K, 773K and 948K are shown in Figures 12-15. Pretreatment conditions are identical to those used during catalytic reaction. These images prove that reaction results in major morphological changes. Figure 12 shows the SEM of the original silver foil. The long streaks are caused by the polishing of the surface prior to analysis. A sample which was pretreated at 573K in the reaction mixture is shown in Figure 13. The surface appears to be more inhomogeneous. Large, circular islands between 50 and 200 nm are formed. Treatment at 773K leads to the surface shown in Figure 14. The surface appears smoother and the islands formed after treatment at 573K are no longer present. Holes appear at the grain boundaries between silver crystals. Figure 15 shows the morphology of the surface after treatment at 948K. The surface exhibits many small crystalline domains similar to those seen in Figure 13 for the sample treated at 573K. The holes formed for the sample treated at 948K are no longer restricted to

the crystallite boundaries. They now cover large portions of the previously smooth silver surface

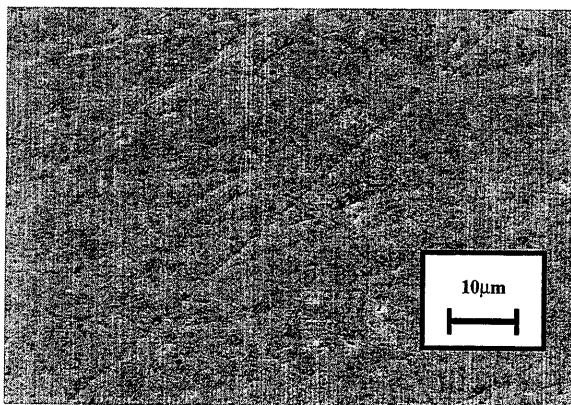


Figure 12. Scanning electron micrograph of the fresh silver foil.

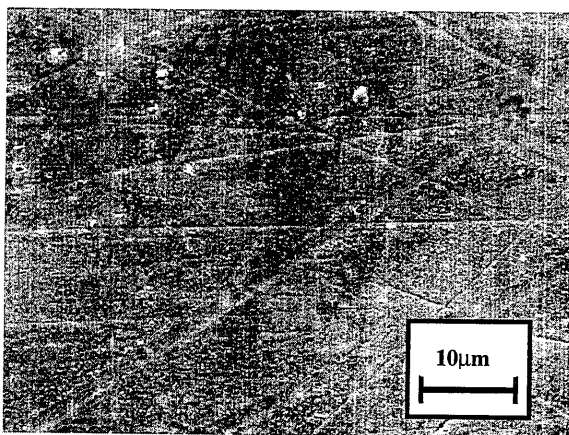


Figure 13. Scanning electron micrograph of the polycrystalline foil after having undergone the reaction cycle (423-573-423K), 3.5 vol% O₂, 8.8 vol% CH₃OH, 87.7 vol% He

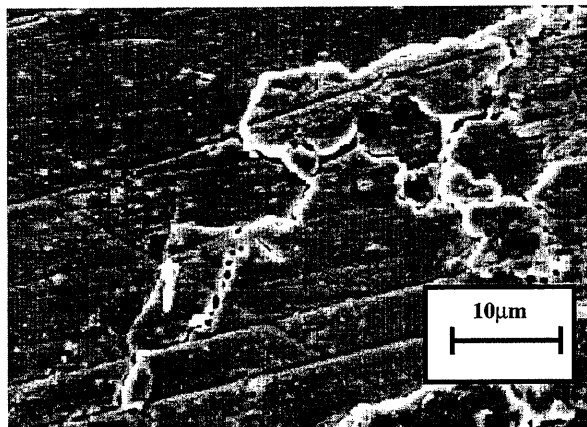


Figure 14. Scanning electron micrograph of the polycrystalline foil after having undergone the reaction cycle (423-773-423K), 3.5 vol% O_2 , 8.8 vol% CH_3OH , 87.7 vol% He

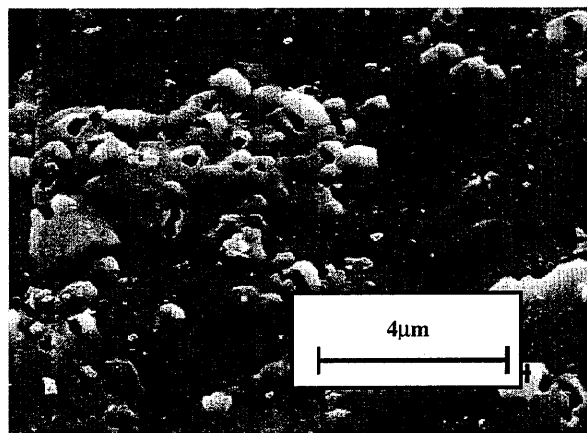


Figure 15. Scanning electron micrograph of the polycrystalline foil after having undergone the reaction cycle (423-948-423K), 3.5 vol% O_2 , 8.8 vol% CH_3OH , 87.7 vol% He

4.4 Discussion

It has been cited in the literature that bulk-lattice oxygen acts as the source of active oxygen for the selective partial-oxidation of hydrocarbons over a variety of catalysts (Mars-van Krevelen mechanism)¹⁹. The fact remains, however, that catalysis is a surface process occurring at the gas-surface interface. It was shown in Chapter IV that O_γ is essentially O_β in that instance when the oxygen segregates into the uppermost atomic layers of low-indexed-terminating silver surfaces where it may then participate in reaction. It is incorporated into the silver lattice via interstitialcy diffusion. It is this bonding of oxygen in the silver lattice which results in the unique ability to preferentially form de-hydrogenation products. The formation of atomically adsorbed O_a followed by bulk dissolution (O_β) and eventual surface segregation of oxygen are prerequisites for its formation. The direct incorporation of O_γ in (111) terraces from the gas phase is unlikely due to the extremely low sticking coefficient of oxygen on this surface ($\theta < 10^{-7}$). The silver metal serves as an electron-rich substrate upon which the catalytically-active oxygen species may be formed. In chapter 3, it was shown that O_γ shows an unsaturated thermal desorption peak centered at approximately 1000K (Chapter 3, Figures 2a-c). The peak is unsaturated because it is impossible to remove all oxygen from silver. This point was mentioned previously. One of the underlying principles of thermal desorption spectroscopy assumes that increasing the temperature leads to a concomitant exponential increase in the desorption rate. This assumption requires that no solid-state changes occur in the material under study which might affect the rate of desorption. This is clearly not the case with silver. Silver has a relatively high vapor pressure in vacuum. The rate of evaporation, r_e , of silver is related to the vapor pressure, p , through the Equation 6.

$$\text{Equation 6.} \quad r_e = p \left(\frac{1}{2\pi MRT} \right)^{\frac{1}{2}}$$

The vapor pressure of silver is 2×10^{-6} mbar at 920K²⁰ which results in the evaporation of about 2 monolayers/s! Heating well above the Tamann temperature ($T_i = 0.5T_{\text{melt}} = 753\text{K}$) leads, therefore, to significant mass transfer from the bulk to the surface followed by subsequent

sublimation and recondensation³. Closely packed terminating surface structures are, therefore, formed at the surface, essentially annealing it shut. Surface anisotropy therefore decreases significantly at elevated temperatures. This makes the complete removal of oxygen from silver impossible. One is forced to go to higher temperatures in order to maintain high diffusion kinetics which tends to slow the decreased concentration of bulk oxygen which is the driving force for desorption. The reconstruction of the surface to close-packed (111) terminating crystal structures results in diffusion inhibition.

Figure 3 shows that the fresh catalyst is active for methanol oxidation until approximately 623K. Comparison with the temperature-cycle run for this region (Figure 4) shows that there is no change in the intrinsic activity of the catalyst after reaction under these conditions hinting that no morphological change of the catalyst is necessary for activation. The reaction hysteresis observed for this cycle is an artifact resulting from the exothermicity of the net partial-oxidation reaction. The SEM image, (Figure 13), taken subsequent to this reaction cycle supports this hypothesis and shows no substantial change in the catalyst surface morphology. The enhancement of the boundaries between the polycrystalline domains seen in this image relative to the fresh sample is caused by the decomposition of Ag_2O ($T_{\text{dec}}=585\text{K}$) which is always present as a contaminant on sample surfaces which have been exposed for longer times to air¹³. Oxide formation is enhanced at defect sites resulting in their poorer SEM imaging. Previous studies^{2,615,16} have shown that the catalytically active O_α forms readily at these temperatures *via* direct dissociation of molecular oxygen on the surface. The formation of O_α *via* the gas phase shows a strong structure dependence. A number of authors have proposed that defect sites on the silver surface are exceptionally active for the formation of highly active, surface-bound atomic oxygen^{2,14,21}. Figure 1 shows a high yield and Figure 2 a high selectivity to CO_2 thus providing excellent evidence that O_α is the active species in this temperature regime. The absence of holes in Figure IV.13, resulting from the reaction of dissolved H_2 and O_2 to water^{2,3,22,23}, indicates that the reaction observed for temperatures below 573K takes place entirely on the surface. The only holes observed are those which were originally present in the fresh sample (See Figure 12). The catalytically active O_α species is, therefore, formed directly from gas-phase oxygen under these conditions. It forms

preferentially on sites of increasing surface-roughness. The sticking coefficient increases as shown: $(111) \sim 10^{-7} < (100) 10^{-4}, < (110) 10^{-3} < \text{Defects}$ ^{12,13,14,15,16,25}.

To our knowledge, this is the first report of such a reaction hysteresis for the partial oxidation of methanol in the literature. There are a number of possible explanations why the effect was observed in this study and nowhere else. Carbon is often reported as a contaminant for studies performed with electrolytic silver ^{1,2,3,14,15,16}. It is possible that previous groups have first treated the sample at elevated temperatures in flowing oxygen in order to burn off carbon impurities. This would lead to a restructuring of the catalyst and an elimination of the reaction hysteresis. Lefferts et al ^{2,6} treated their sample in dilute HNO_3 in order to remove impurities. Work in our laboratory has shown that treatment of Ag in NO containing environments leads to the formation of large amounts of AgNO_3 and Ag_2O . Subsequent decomposition of these samples (thermal or by dissolving in H_2O) reveals a spongy material which has undergone extensive reconstruction. This could explain why the deactivation effect was not observed in this study. Finally, any groups which used the same catalyst more than once at temperatures in excess of 875K would have not been able to observe this phenomenon.

The reaction hysteresis observed for the temperature cycle (423-773-423K) (Figures 5 and 6) results from the deactivation of the catalyst under these conditions. A comparison of the conversions seen for the ascending branch of Figure 4 with the ascending branches for Figure 5 shows the irreversibility of the deactivation occurring during cycle 2. This is evidence that the reaction hysteresis is not due to a temperature bistability of the system, but rather to a change in the intrinsic activity of the catalyst itself. Close inspection of the SEM micrographs (Figure 14) reveals the origin of this deactivation. Figure 14 shows the surface following this reaction cycle (423-773-423K). The reaction of O_p with dissolved H_2 to H_2O is evidenced by the holes formed. The fact that the holes are located almost entirely at the grain boundaries is evidence for the fact that reaction with bulk oxygen diffusing along grain boundaries takes place in this temperature range. It is also possible that significant mass transport from the crystal grain-boundaries to bulk defects formed during reaction (not visible in SEM) results in the hole formation at the boundaries. The energetically-unfavorable location of silver atoms at

grain boundaries makes them an excellent source for silver migration ultimately leading to defect healing²⁴. Bulk interstitial defects act, in this case, as sinks for the mass transfer of silver away from grain-boundaries. It is impossible to determine which of these solid-state reaction mechanisms dominates. Both phenomena find their origins in hole formation *via* subsurface water formation. The reaction with O_p is therefore activated under these conditions. Further evidence for this has recently been shown using *in-situ* environmental scanning electron microscopy^{20,21}. The formerly polycrystalline surface shows smooth contours indicative of pronounced sintering. The occurrence of this sintering corresponds well to the Tamann temperature of silver which is 754K ($T_m=1,234K$). Above this temperature the kinetics of bulk diffusion of silver atoms are sufficiently fast to result in significant mass transport of silver within the time frame of a typical run. Healing of the defect-rich, polycrystalline surface seen in Figure 12 *via* sintering explains the pronounced deactivation and reaction hysteresis of the catalyst seen for the temperature cycle (423-773-423K) (Figures 5 and 6). It is likely that the actual surface temperature is likely a great deal higher than the measured temperature. As was mentioned before, the decreased H_2 yield at elevated temperatures is likely due to its consumption by reaction with oxygen. This is a highly exothermic reaction with a reaction enthalpy of $-243kJ/mol$. This energy production is compensated, in part, by the $+84kJ/mol$ endothermicity of the direct dehydrogenation reaction. The overall oxi-dehydrogenation exothermicity is, therefore, $-159kJ/mol$. The temperature rise due to this reaction may be estimated using the following equations.

$$\text{Equation 3. } CH_3OH + \frac{1}{2}O_2 \rightleftharpoons CH_2O + H_2O \quad \Delta H_{rxn} = -159kJ/mol$$

$$\text{Equation 7. } \Delta T = \frac{m_{CH_3OH} \times \Delta H_{rxn}}{m_{he} \times C_{p,He}} \quad \text{where } C_{p,He} = \frac{0.0513kJ}{molHe \cdot K}, \text{ and } \Delta H_{rxn} = -159kJ/mol$$

It is assumed that all the heat of reaction is removed by convection in the He stream. This is quite accurate as the He constitutes 87.7 vol % of the total feed and has, by far, the highest heat capacity of any gases present. At 70% CH_3OH conversion (See Figure 1), this estimation results in a temperature rise of approximately 300K. This is obviously, a rough assumption but clearly shows, that the heat of reaction may considerably affect the local temperature at the

catalyst surface. Therefore, for reaction at 923K, the actual surface temperature may be as high as 1223K which is 100K above the melting temperature of silver. This local heating of the silver surface would enhance the grain-boundary sintering effect and would explain the melted appearance of the surface after reaction at 948K (Figure 15)

The assignment of the deactivation observed between 673 and 973K in Figure 3 to the inhibition of grain-boundary oxygen diffusion from the silver bulk also stems from the excellent agreement of the TDS desorption temperature for the oxygen species assigned to O_p with the deactivation temperature. This is the TDS peak shown in Figures 2a-c in Chapter 3 centered at approximately 773K. It was pointed out in Chapter 3 that the asymmetry of this peak hints that it is comprised of a number of desorption signals arising from the diffusion and desorption of several bulk-species evolving in the order of increasing diffusion resistance. Grain boundaries offer the lowest resistance to bulk diffusion. The temperature regime in which catalytic deactivation occurs (650-850K) coincides with this thermal desorption of O_p , indicating that the deactivation is likely due to oxygen diffusion inhibition of O_p along grain boundaries *via* sintering.

It has also been suggested that strongly-bound surface oxygen species form preferentially at defects^{25,26}. These authors suggest that strongly-bound oxygen is the active species in this temperature regime. It was previously mentioned that the integral desorption amount for the O_p peak for dosing at 100mbar O_2 in Figure 2c in Chapter 3 corresponds to about 7×10^{-7} mol O_2 /g. Estimating the surface area at $0.001 \text{ m}^2/\text{g}$ (calculate area of a sphere, divide by weight) and assuming a (111) surface structure with an atomic diameter of 2.35 angstroms yields a value of 2.3×10^{16} Ag atoms/ m^2 . Assuming a 100% oxygen coverage, one arrives at a value of about 30 monolayers of oxygen. This represents an absolute worse case scenario as the surface is not completely (111) oriented and, in reality, exhibits a very low sticking coefficient for oxygen ($<10^{-7}$). Formation of this many monolayers of oxygen at this temperature is impossible and the highest oxygen coverage for silver (111) is actually known to be well below 100%^{12,13,14,15,16}. It is therefore impossible to assign the desorbing species to a surface-bound oxygen species. The assignment of this peak to bulk-dissolved oxygen has also been

made by a number of other authors^{1,3,27}. A mechanism in which this bulk oxygen actively participates in reaction was, however, never proposed. The fact that a constant feed of O_2 is required for reaction necessarily implies that all active oxygen species are eventually consumed in the course of reaction. The bulk-dissolved oxygen formed under these conditions therefore undergoes equimolar counterdiffusion where the concentration in the bulk is determined by the balance between rate of O_2 dissolution in Ag and rate of segregation followed either by O_2 desorption or reaction at the surface.

The elimination of the reaction hysteresis is shown in Figures 7 and Figure 8 (cycle 3). This observation corresponds well with further structural changes of the silver surface. The SEM image shown in Figure 15 shows that the hole formation is no longer confined only to grain boundaries, but rather appears to cover large patches of the formerly smooth surface. This likely represents the transition from a system where grain-boundary diffusion and interstitial diffusion through high-indexed planes is the dominant diffusion mechanism to one in which volume diffusion is possible (interstitially diffusion). The transition is made possible by the drastic morphological reorientation of the silver surface and bulk after treatment in an oxygen containing atmosphere. It results in the proliferation of holes over the entire surface. The catalytic restructuring could only be reversed by heating an aged catalyst (exhibiting no reaction hysteresis) to 973K in vacuum for 20 minutes and subsequently testing it again in the flow reactor. Runs made with this sample show a reappearance of the deactivation ($573K < T < 873K$) and a pronounced reaction hysteresis (not shown). This results from the previously-mentioned sublimation and recondensation of silver which results in annealing of the metal surface and bulk with subsequent defect healing. The facets, grain boundaries and holes formed during reaction are therefore destroyed. The reappearance of the reaction hysteresis after vacuum treatment provides excellent confirmation of the promoting effect of reaction-induced restructuring.

Tests made with catalysts after having undergone high temperature ($T > 923K$) reaction do not show reaction hysteresis. Diffusion effects are therefore not directly observable from temperature-conversion plots obtained from tests made with these samples. Subtle changes of the reaction rate are often easier to identify after producing an Arrhenius plot (Figure 9). The

Arrhenius plot has three distinct regions of activity which correlate well with the areas of deactivation seen for the fresh silver sample (see Figure 3). Figure 3 shows that diffusion limitations also exist for samples which have undergone thermal pretreatment in the reaction

atmosphere although to a much lesser extent than in fresh samples. Lefferts et al.⁶ proposed that film-layer diffusion is present under the conditions used here. This explains the exceptionally small apparent activation energies measured in all three temperature regions. The first region corresponds to reaction of methanol with the surface-bound O_a species formed directly from the gas phase. It extends until the first inflection point seen in the temperature-conversion plot for reaction over a fresh silver sample (Figure 3). The excellent correlation of the TDS O_b desorption signal (Figures 2a-c, Chapter 3), the second inflection point in the Arrhenius plot (Figure 9) and the decrease in selectivity to CO_2 (Figure 2) indicates that this inflection point is likely the temperature at which bulk diffusion is activated and reaction with O_b becomes possible. Because the oxygen conversion is 100%, the CH_3OH conversion is determined by the equilibrium between the rate of oxi-dehydrogenation, direct dehydrogenation and total oxidation reaction paths (Equations 2 and 3). This is shown schematically in Figure 16.

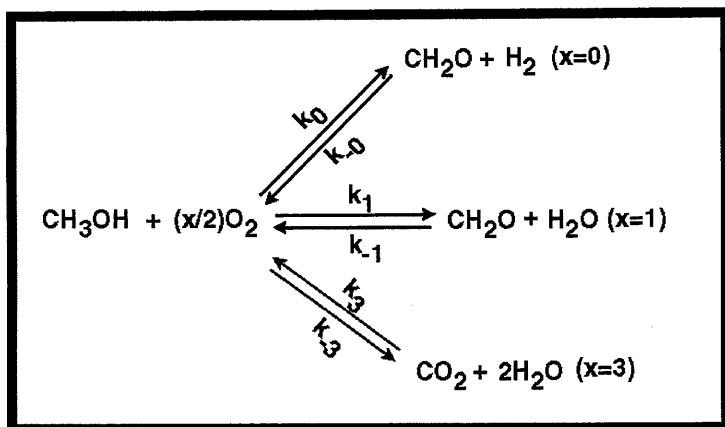


Figure 16. Proposed reactions in series and parallel for methanol oxidation over electrolytic silver.

Balancing the rate laws yields Equation 8.

Equation 8.

$$\begin{aligned}
 \frac{d[\text{CH}_3\text{OH}]}{dt} = & k_0[\text{CH}_3\text{OH}]^{a_0}[\text{O}_2]^{b_0} - k_{-0}[\text{CH}_2\text{O}]^{a_{-0}}[\text{H}_2]^{b_{-0}} + k_1[\text{CH}_3\text{OH}]^{a_1}[\text{O}_2]^{b_1} \\
 & - k_{-1}[\text{CH}_2\text{O}]^{a_{-1}}[\text{H}_2]^{b_{-1}} + k_3[\text{CH}_3\text{OH}]^{a_3}[\text{O}_2]^{b_3} - k_{-3}[\text{CH}_2\text{O}]^{a_{-3}}[\text{H}_2]^{b_{-3}}
 \end{aligned}$$

Some simplifying assumptions make the interpretation much easier. First, it is assumed that the three reactions are irreversible. Furthermore, it is assumed that the reaction order with respect to O_2 is zero and that with respect to CH_3OH is one.²⁸ The accuracy of these assumptions is questionable. In particular, product poisoning is assumed not to occur. The simplified equation leads to Equation 9.

Equation 9.
$$\frac{d[CH_3OH]}{dt} = (k_0 + k_1 + k_3)[CH_3OH]$$

It is clear, therefore, that the rate of consumption of methanol is proportional to the reaction path with the largest rate constant. The various active oxygen species (O_a , O_p , O_f) catalyze different reaction paths at different temperatures. Any change in the temperature dependence of the rate of consumption of methanol (E_{app}) is, therefore, an indication of the shift of reaction between the different paths. Both k_0 and k_1 are proportional to the rate of formation and consumption of O_a (the formation of surface atomic oxygen is likely the faster step). Similarly, the constant k_3 is proportional to the rate of O_f formation and reaction. The formation of O_f requires the segregation of O_p to the (111) surface. Bulk-diffusion is likely the rate-limiting step in its formation. It is critical to note that the strong bonding of O_f implies that a number of turnovers may occur on this species before it is actually consumed in reaction. It is impossible to quantify the turnover frequency due to the high conversions and inability to measure the number of active sites *in-situ*. The inflection seen in Figure 9 represents, therefore, a shift from preferential oxidehydrogenation to direct dehydrogenation *via* reaction with O_f produced *via* the O_p segregation to (111) facets. The third region showing extremely low or negative activation energies is attributed to sintering of the reaction-promoting defects formed during reaction at temperatures higher than 773K. The thermal reordering leading to defect healing occurs at a faster rate than hole production in this temperature regime. The Arrhenius plots, therefore, do not provide any direct kinetic data. The reaction simply occurs too quickly. The plots do show, however, the strong temperature dependence of the various rate-limiting steps of reaction. They support the hypothesis that diffusion of bulk oxygen to the surface is a critical step in the reaction mechanism.

Understanding the link between bulk-structural changes and surface reordering is critical to understanding the methanol oxidation reaction mechanism as a whole. It is known that high temperature treatment of silver in oxygen leads to crystallization of the silver bulk exhibiting, primarily, a (331) terminating surface structure (facets)¹. Formation of this structure results in

an optimum fit for oxygen diffusion along channels formed perpendicular to the (110) face found in the (331) surface. A view of the (331) face is shown in Figure 17.

Facet formation is, however, not observed under catalytic conditions. This is due to the previously mentioned hole formation resulting from dissolution of product hydrogen and subsequent reaction with O_p to form water. This is also likely due, in part, to the aforementioned surface melting resulting from the large exothermicity of reaction. Both hydrogen (a major reaction product) and oxygen have high diffusivities in silver ($D_{H_2}=2.82 \cdot 10^{-3} \text{ cm}^2/\text{s}$; $D_{O_2}=8.19 \cdot 10^{-2} \text{ cm}^2/\text{s}$ ²⁹). Holes function as sites of higher activity (high O_2 sticking coefficient and low diffusion resistance) which eventually results in the increased formation of more holes. The thermal rearrangement of the silver is constantly disrupted by the reaction-induced defect

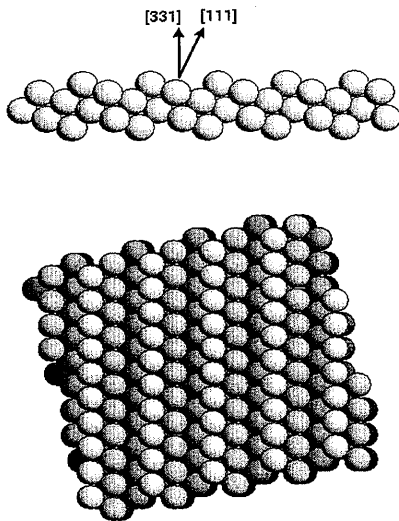
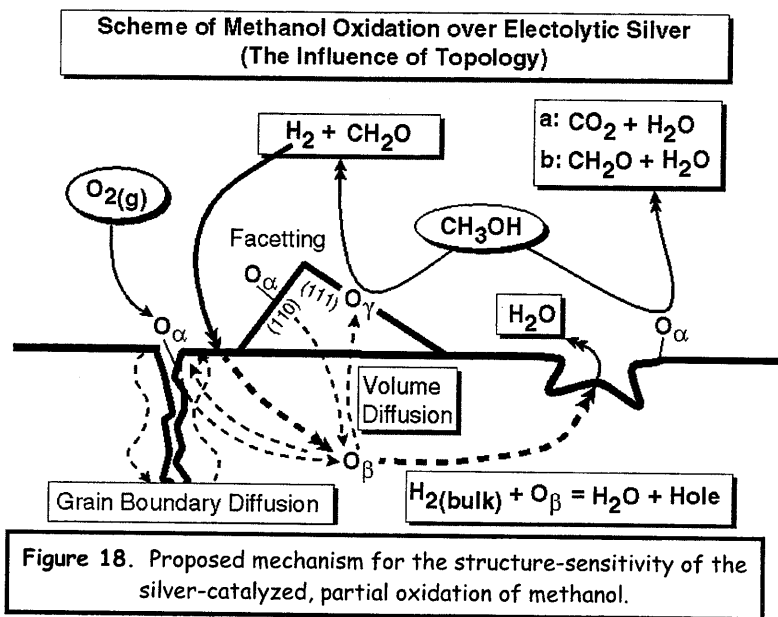


Figure 17. View of the (331) terminating silver surface.

production and surface melting. Reaction of silver under methanol oxidation conditions represents an extremely dynamic situation.

Facet formation, on the other hand, is observed under conditions where the system is allowed to form equilibrium structures resulting in an overall decrease in the surface free energy. Hole production and surface melting as a result of reaction prevents the silver from attaining these equilibrium structures. This situation is very different from that in which the silver is completely faceted. Such a situation represents the local thermodynamic energy minimum. Reaction at moderate reaction temperatures ($623\text{K} < T < 923\text{K}$), occurs primarily with oxygen diffusing along grain boundaries. The fact that hole formation is not restricted to grain boundaries at high temperatures ($T > 923\text{K}$) is clear evidence that volume diffusion

(interstitialcy) of oxygen is also a major reaction pathway. This behavior correlates well with the results shown in the last chapter which show that oxygen may diffuse *via* octahedral hole jumping at lower temperatures ($T < 900\text{K}$) or *via* interstitialcy diffusion at elevated temperatures ($T > 900\text{K}$).



A possible reaction scheme is shown in Figure 18 and summarizes the proposed methanol oxidation mechanism. Gaseous oxygen is dissociatively adsorbed on silver forming O_{α} . This occurs preferentially on defect sites and crystalline faces of low coordination. O_{α} diffuses into the bulk forming O_{β} . O_{α} may react at the surface with methanol forming CH_2O and H_2O via oxidehydrogenation or may form the complete combustion products CO_2 and H_2O . O_{β} may diffuse back forming O_{α} again or may diffuse to a densely-packed (111) surface. With increasing temperature, the diffusion of O_{β} atoms to the silver surface becomes more and more labile. At temperatures above 923K, the formation of (111) planes is enhanced and the diffusion of oxygen through these planes occurs via an interstitialcy mechanism. Oxygen

atoms are incorporated into the uppermost atomic layers forming O_γ^{30} which catalyzes the dehydrogenation of methanol to formaldehyde and hydrogen. Hydrogen formed *via* this reaction may dissolve into the silver bulk and react with O_β to water. The formation of subsurface water combined with the heat of reaction ultimately results in hole formation and surface melting with subsequent desorption of water and the destruction of the faceted surface. This process is competes with annealing of the silver surface via sintering. All of the processes occur simultaneously resulting in a system which is capable of attaining a dynamic equilibrium which is optimal for catalysis.

4.5. Conclusions

Treatment of electrolytic silver at elevated temperatures in a reaction mixture consisting of $MeOH/O_2=2.5$ results in a restructuring of the catalyst surface and bulk. Reaction with the highly-oxidative, surface-bound, atomic-oxygen species O_α dominates at temperatures lower than 623K. Reaction under these conditions does not result in a change in the catalyst morphology. Severe deactivation of the fresh catalyst in the region $573K < T < 873K$ occurs as a result of the annealing of grain boundaries present in the fresh polycrystalline sample. This sintering hinders the formation of active-surface oxygen *via* grain-boundary diffusion which is the prevailing mechanism in this temperature regime for fresh silver samples. Treatment of the catalyst at temperatures exceeding 873K results in a marked morphological change of the catalyst surface structure. Formation of O_γ *via* volume diffusion is possible under these conditions. This represents, essentially, a system where volume diffusion replaces grain-boundary diffusion as the dominant process for oxygen activation. Hole formation resulting from dehydroxylation of dissolved oxygen and hydrogen and surface melting results in enhanced defect formation at these higher temperatures. The O_γ oxygen species formed as a result of this high-temperature bulk diffusion process exhibits a less oxidative nature than the surface-bound O_α . The direct dehydrogenation of methanol to formaldehyde is, therefore, enhanced at higher temperatures and the complete oxidation suppressed. It is shown that morphological changes occur in the presence of reaction which do not result from pure thermal reordering. The resulting catalyst morphology provide an optimum for the formation

of O_γ via formation of and eventual segregation of O_β to the faceted surface where it may form O_γ in (111) terraces. This model is a deviation from the classical idea of a heterogeneously catalyzed surface reaction occurring on a morphologically undefined solid surface. The partial oxidation of methanol to formaldehyde over silver shows an intimate connection between catalyst morphology and catalytic activity which strongly influences the steady-state formation of a bulk intermediate which is necessary for the promotion of the desired reaction at the gas-metal interface.

References

1. Herein D., Nagy A., Shubert H., Weinberg G., Kitzelmann E., Schlögl R., *Z. Phys. Chem* **107**, S. 67 (1996).
2. Schubert H., Tegtmeier U., Herein D., Bao X., Muhler M., Schlögl R., *Cat Lett.*, **33**, 305 (1995).
3. Bao X., Lempfuhr G., Weinberg G., Schlögl R., Ertl G., *J. Chem. Soc. Faraday Trans.*, **88**(6), 865 (1992).
4. Rues G., Disteldorf W., Grundler O., Hilt A., "Formaldehyde", Verlag Chemie, Weinheim, **A11**, 619, (1988).
5. Lefferts L., van Ommen J.G. and Ross J., *Appl Cat.* **23**, 385 (1986).
6. Lefferts L., van Ommen J.G., Ross, *J. Appl Cat.* **31**, 291 (1987).
7. Bukhtizarov V.I., Prosvirin I.P., Kvon R.I., *Surf. Sci.* **320**, L47 (1994).
8. Robb D. and Harriot P., *J. Catal* **35**, 176 (1974)
9. Bhattacharyya, S., Nag N., and Ganguly N., *J. Catal.* **23**, 158 (1971)
10. Brigoryan R.R., Garbyan T.A. and Nalbandyan A.B., *Arm. Khim. Zhurn.* **34**, 832 (1981).
11. Garibyan T.A., Grigoryan R.R., Ya Margolis L and Nalbandyan A.B., *Kinetika i Kataliz*, **17**, 229 (1976).
12. Sperber H., *Chemie-Ing.-Technology* **41**, 962 (1969).
13. Perry R. and Green Editors D., "Perry's Handbook of Chemical Engineering", 7th ed. (1997).
14. Grant R. and Lambert R., *Surf. Sci.* **146**, 256 (1984).
15. Bowker M., *Surf. Sci.* **155**, L276 (1985).
16. Rovida G., Pratesi F., Maglietta M. and Ferroni E., *Surf. Sci.* **43**, 230 (1974).
17. Prince K., Paolucci G., and Bradshaw A., *Surf. Sci.* **175**, 101 (1986).
18. Backx C., de Groot C. and P. Biloen, *J. Catal.* **72**, 364 (1981).
19. Mars P. and van Krevelen D., *Chem. Eng. Sci. Special Suppl.* **3**, 41 (1954).
20. Espe W., in "Werkstoffkunde der Hochvakuum-Technik", VEB Deutscher Verlag der Wissenschaften, Berlin, (1959).
21. Frank E. and Hamers R., *J. Catal.* **172**, 406 (1997).
22. Millar G., Nelson M. and Uwins P., *Catal. Lett.* **43**, 97 (1997).

-
23. Uwins P., Millar G and, Nelson M., *Microscopy Research and Technique*, **36**, 382 (1997).
 24. Kittel Ch., "Introduction to Solid-State Physics", R. Oldenbourg Verlag GmbH, München, ISBN 3-486-20240-5 (1988).
 25. Lefferts L., van Ommen J. and Ross J., *Appl. Catal.* **34**, 329 (1987).
 26. Lefferts L., van Ommen J. and Ross J., "Proc 9th ICC, Congress in Calgary: Chem. Inst. Of Canada, Ottawa" **4**, 1672 (1988).
 27. van Santen R. and de Groot C., *J. Catal.*, **98**, 530 (1986).
 28. Ullman, in "Ullman's Encyclopedia of Industrial Chemistry", 5th Edition, **A11**, 619 (1988)
 29. Eichenauer W. and Pebeler A., *Z. Metallkde.* **48**, 373 (1957).
 30. Bao X., Muhler M., Schedel-Niedrig Th. and Schlögl R., *Phys. Rev. B*, **54** 2249 (1996).

The Oxidative Coupling of Methane as a Test Reaction to Clarify the Role of Sub-Surface Oxygen in Silver-Catalyzed Partial Oxidation Reactions

Abstract

The silver-catalyzed, oxidative coupling of methane to C_2 hydrocarbons (OCM) is shown to be an extremely structure-sensitive reaction. This structure-sensitivity is used here to confirm the proposed hypothesis that the catalytically active O_γ oxygen species, intercalated in the uppermost silver layers, is the active and selective species for high-temperature, silver-catalyzed dehydrogenation reactions. Reaction-induced changes in the silver morphology lead to changes in the nature and extent of formation of the bulk and terminating crystal structures. This, in-turn, impacts the oxygen diffusivity necessary to the formation of active O_γ which subsequently explains the structure sensitivity of reaction. It is found that the activation energy for methane coupling over silver of 138kJ/mol is nearly identical to the value of 140kJ/mol for oxygen diffusion in silver at this temperature. This provides a quantitative connection between the diffusion kinetics of bulk-dissolved oxygen, and the reaction kinetics of the oxidative coupling of methane to C_2 hydrocarbons. Silver-catalyzed, dehydrogenation reactions are, therefore, limited by the formation of O_γ via interstitialcy diffusion of the bulk-dissolved oxygen species through (111) facet terraces of silver. Sintering of the catalyst occurs during reaction and leads to a marked deactivation of the catalyst with time on stream. Sintering is effectively prevented by mixing equal amounts (by weight) of SiO_2 and Ag. The elimination of catalyst sintering reveals improvements in catalyst activity and selectivity for the formation of C_2 reaction products resulting from surface facetting. Catalysis over fresh silver catalysts shows an initial preferential oxidation of CH_4 to complete oxidation products. Reaction-induced facetting of the silver results in a restructuring of the catalyst from one which initially catalyzes the complete oxidation of methane to CO_x and water to a catalyst which preferentially catalyzes the formation of coupling products.

5.1 Introduction

Silver is used industrially as a catalyst for the partial oxidation of methanol to formaldehyde^{1,2,3} and for the epoxidation of ethylene to ethylene epoxide^{4,5,6}. It is generally accepted that the particularly high activity and selectivity of silver for these reactions is due to

its ability to activate molecular oxygen in a variety of ways leading to the creation of different types of silver-bound oxygen species. A wealth of literature exists on the silver-oxygen interaction^{7,8,9,10,11,12}. Much of this literature is, unfortunately, contradicting and a great deal of ambiguity still exists as to the exact nature of the various oxygen species formed. Silver is known to undergo morphological restructuring as a result of high temperature treatment in various gas atmospheres^{9,13,14,15,16}. The impact of morphology on catalytic reaction is a field in which surface-science techniques have provided valuable information. The large differences between the UHV conditions under which these surface-science studies are made and the actual conditions of catalysis lead to the well known „pressure-gap,, problem. This, unfortunately, lends a degree of ambiguity to the interpretation of this data which one would, idealistically, like to avoid. In either case, the wealth of surface science literature dedicated to understanding silver catalysts clearly shows that obtaining a solid understanding of the relationship between structure and activity is essential to grasping the subtle mechanistic details of catalytic reactions.

The Model: The existence of three different, catalytically active, oxygen species is proposed here. They have been previously characterized with a variety of spectroscopic techniques^{17,18,19,20,21}. These species differentiate themselves in both their electronic properties as well as their location in the silver. All three species are shown schematically in Figure 1. The first is referred to as O_{α} . This is chemisorbed atomic oxygen which is believed to catalyze the oxi-dehydrogenation of methanol to formaldehyde as well as the complete oxidation to CO_2 and water²². It is a highly-reactive oxygen species exhibiting a strongly nucleophilic character. It has a thermal-desorption temperature of approximately 573 K and shows an XPS binding energy of 530 eV. The second species is referred to as O_{β} and is assigned to bulk-dissolved oxygen. It shows a broad-asymmetric thermal desorption peak at approximately 773K, whose desorption maximum shows a strong dependence on oxygen dosing pressure and temperature^{9,11,17}. It is also characterized by an XPS signal showing a broad peak centered at 530.3 eV. The third species is referred to as O_{γ} . O_{γ} is characterized by an unsaturated, thermal-desorption signal beginning at approximately 973 K and an XPS binding energy of 529 eV^{9,11,17}. It is assigned to intercalated oxygen which diffuses *via* interstitially diffusion into the uppermost layers of the reconstructed silver surface. Previous work⁹ has shown that oxygen diffusion in silver is highly anisotropic. Interstitial diffusion

was shown to occur primarily in the [110] direction through canals formed in the (110) plane of the silver crystallites. Diffusion through the (111) planes is activated only at elevated temperatures ($T > 923\text{K}$). This high-temperature diffusion occurs *via* the interstitial diffusion of oxygen through the closely packed (111) facet terraces. Diffusion of oxygen by silver substitution results in significant mass transport of silver which manifests itself in the formation of surface facets.

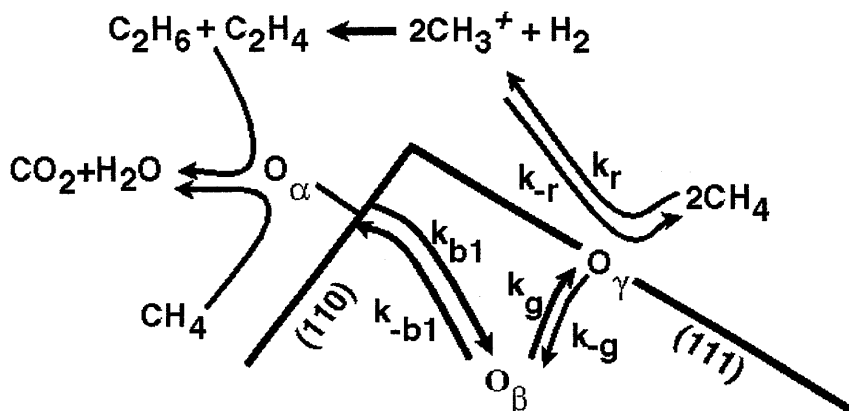


Figure 1. The proposed reaction mechanism for the oxidative coupling of methane to C_2 hydrocarbons over electrolytic silver.

This work was carried out in an attempt to test the hypothesis that O_γ is the catalytically active and selective dehydrogenation species for silver-catalyzed, high-temperature, oxidative dehydrogenation reactions. The oxidative coupling of methane to C_2 hydrocarbons was chosen as an appropriate test reaction. A major motivating force in deciding to study the OCM reaction stems from the fact that a detailed study of the dependence of reaction kinetics of the industrially-relevant formaldehyde synthesis reaction is hampered by exceptionally reactant high conversions.²⁷⁻³⁰ Reaction of methanol and oxygen over silver almost always results in complete oxygen consumption. The relatively slow reaction rates typical for the OCM reaction allow for a much more thorough investigation than is possible when studying the partial oxidation of methanol to formaldehyde. In addition, both the OCM reaction and

the formaldehyde synthesis reaction take place in similar temperature regimes ($T > 873$ K) and are believed to be catalyzed by O_γ ^{18-23,31}. Both reactions require the dehydrogenation of a C-H bond as a key step in the formation of the desired product and have a single carbon atom forming the organic substrate. Reaction of oxygen with methane provides information about the ability of the system to directly dehydrogenate an R-H bond as opposed to completely oxidizing the organic substrate. The OCM reaction is therefore, an ideally suited test reaction for studying the high-temperature behavior of silver-catalyzed, partial-oxidation reactions in general.

The proposed reaction mechanism is shown in Figure 1. The role of O_α , O_β and O_γ is essentially the same as was proposed in Chapter 4 for the methanol oxidation. O_α should react with O_α to form CO_2 and H_2O . Reaction of methane over O_γ should, however, result in the dehydrogenation of methane to a methyl radical. This mechanistic step has been proposed by a number of authors for reaction over a variety of catalysts and is believed to be the reaction-limiting step.^{23, 24, 25} The gas-phase recombination of radicals occurs quickly with respect to the dehydrogenation step.²⁶ The suggestion that the formation of O_γ is necessary for reaction implies that the reaction of methane is limited by the rate of diffusion O_β to the (111) facets where it is incorporated into the silver lattice forming O_γ . The fact that the oxygen conversions obtained for the OCM reaction (20-30% O_2) are so much lower than for the methanol oxidation (100% O_2) implies that the activation energy barrier for the former (~140 kJ/mol O_2) is much higher than the latter (no E_{app} measured under relevant conditions). Using this model, it should be possible to probe the extent of silver surface reconstruction and O_γ formation using the OCM reaction.

The participation of bulk oxygen in reaction has been proposed by a number of authors using a variety of different catalysts^{27,28,29}. These studies typically proposed a Mars van Krevelen-type mechanism where the lattice oxygen of a stoichiometric oxide participates in reaction.³⁰ It will be shown later that stoichiometric silver oxide is not present under typical OCM reaction conditions. Silver acts as an electron-rich substrate which may activate various types of oxygen species which each play a different role in reaction.

5.2. Experimental

The reactions were carried out in a small, quartz-tube reactor (10mm O.D., 8mm I.D.). A K-Type thermocouple was attached to the tube wall directly adjacent to the catalyst bed. The high activity of the thermocouple made it's location directly in the catalyst bed impossible. Quartz rods were inserted above and below the catalyst bed in order to minimize contributions from gas-phase reactions. Electrolytic silver was generously provided by BASF AG. Qualitative EDX analysis showed the presence of small amounts of Na, Cl, Si and C contaminants. The catalyst particles were 0.2-0.4mm in diameter. Runs made by mixing SiO₂ with the silver sample contained equivalent weights of Ag and SiO₂. SiO₂ was purchased from Aldrich (99.999%) and consists primarily of the cristobalite phase. Blank runs showed this material to be catalytically inactive. Helium (5.0) was purified with an Oxisorb filter and was used as a carrier gas for all runs. Oxygen (5.0) and methane (3.5) were purchased from Linde and were used without further purification. Space velocities varied from 10,480 hr⁻¹ for the Ag sample mixed with SiO₂ to 16,113 hr⁻¹ for the pure Ag sample (equal amounts of Ag uses). The linear-gas velocity was kept constant at 0.045m/s. The reaction used here was only operated under integral conditions. The reaction rates shown are, therefore, overall rates of reaction and are attributed to intrinsic rates of reaction. It is impossible to assign these values on a per surface area basis as catalyst facetting and sintering leads to large changes in the active surface area during the reaction. Reaction rates and conversions are, therefore, normalized to the catalyst weight. The following definitions are used throughout:

- Rate of O₂ consumption= $((\text{Mol React}_{\text{in}} - \text{Mol React}_{\text{out}}) / (\text{Mol React}_{\text{in}}) \times (\text{O}_2 \text{ Flow}))$
- %C₂ Product selectivity= $(2x(\text{Mol Prod}) / (\text{Mol CH}_{4\text{in}}) - (\text{Mol CH}_{4\text{out}})) \times 100\%$
- %CO_x Product selectivity= $((\text{Mol Prod}) / (\text{Mol CH}_{4\text{in}}) - (\text{Mol CH}_{4\text{out}})) \times 100\%$

TDS measurements were made in an UHV chamber with an average background pressure of 3×10^{-8} mbar (background gas is primarily H₂O). Monitoring of desorption products was made with a Hiden (Hal2) quadrupole mass spectrometer coupled to a Next workstation. A sampling rate of 1s was standard. A home-made convection oven was used for heating. The thermocouple (Type K) was placed immediately below the sample and was in direct contact with the quartz holding tube. Linear heating rates from room temperature to 1000 K were

possible with this setup. A heating rate of 1 K/s was used for all TDS runs. A special pretreatment procedure was used in order to minimize the amount of carbon present in the sample. This consisted of treating the sample in flowing O₂ (17ml/min) at 973 K, transferring to the UHV through air and subsequently performing numerous oxidation-reduction cycles. This had to be done for approximately one week before a sufficiently clean sample was obtained.

5.3. Results and Discussion

5.3.1 Comparison of the OCM Reaction Kinetics and the Oxygen Diffusion Kinetics in Silver

Before discussing the kinetic parameters obtained, it is critical to show that the testing conditions are sufficiently ideal to produce reliable data where the effects of channeling, mass and heat transport limitations do not lead to the production of erroneous data.

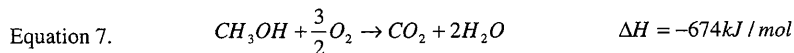
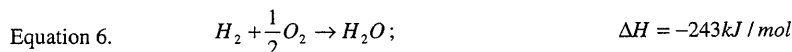
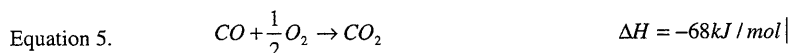
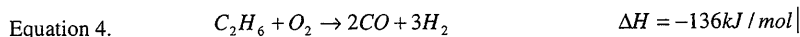
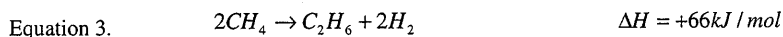
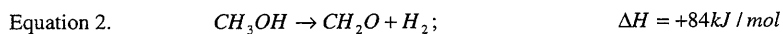
Plug flow and absence of radial temperature gradients: Evidence for the plug-flow nature of flow and absence of radial temperature gradients may be determined as follows. Dautzenberg³¹ determined the necessary criteria for plug flow. This is shown in Equation 1.

Equation 1.
$$\frac{L}{d_p} > (92.0) N_{Re_p}^{-0.23} \ln \frac{1}{1-x} ; N_{Re} = \frac{\rho D v}{\mu}$$

L is the necessary reactor bed length, d_p is the catalyst particle diameter, N_{Re} is the Reynold's number, ρ is the gas density, v is the linear flow velocity, μ is the gas viscosity and x is the conversion. Typical values of N_{Re} obtained for the reactions used fall in the range of 25-75.

Particle sizes are between 0.2 and 0.4 mm for the OCM reaction leading to $\frac{L}{d_p}$ ratios between 25 and 60. Insertion of the calculated N_{Re} with a maximum methane conversion of 5% (worst case scenario) into equation 6 results in a value of 16 which is significantly smaller than the calculated $\frac{L}{d_p}$ values of 25-60 (depending on d_p). Axial variations in temperature are, therefore, negligible for this setup.

The presence of local temperature gradients: The presence of large temperature gradients near the catalyst surface are possible with the reactor setup used here. It was mentioned in the introduction that one of the reasons for using the OCM reaction instead of the industrially-relevant, methanol oxidation reaction is that the low conversions obtained for the OCM reaction result in less local heating. In principle, both the direct dehydrogenation of methanol to formaldehyde and the coupling of methane to ethane or ethylene are endothermic reactions (See Equations 2 and 3).



The degree of local heating may be estimated mathematically as follows. First, a number of simplifying assumptions have been made. Heat is assumed to arise only from the heat of reaction. Convective heat transfer from the oven to the catalyst bed is neglected. Secondly, the convective removal of heat is assumed to occur entirely *via* transport in the Helium stream. This is an accurate assumption as helium exhibits the highest thermal conductivity and is present concentration in excess of all products and reactants (See experimental). The heat balance obtained appears in Equation 8.

$$\text{Equation 8. } Q - F_{A0} \sum \Theta_i C_{pi} (T - T_{i0}) - F_{A0} X [\Delta H_R] = 0$$

Q is the convective heat removal from the reactor, Θ_i is the stoichiometric factor for the component i with heat capacity, C_{pi} , being fed to the reactor with the molar flow rate F_{A0} . Exact values of C_{pi} depend, of course, on the exact product-reactant compositions. C_p is also

approximated using that of helium. The actual value of C_p is likely to be smaller, so assuming the value for helium should result in a slight underestimation of the temperature rise due to the heat of reaction. The He concentration assumed here (90%) is a typical gas-phase concentration for a number of literature references concerning formaldehyde synthesis.^{32,33,34,35}

Excess heat is produced in the OCM reaction *via* the subsequent reaction in series of a certain percentage of the desired partial oxidation product to CO_2 and H_2O . Evidence for the reaction in series of methane to C_2 hydrocarbons and then CO_2 over silver is seen in Figure 2. The reactant/product profile is shown as a function of the space velocity. The maximum in CO_2 conversion clearly lies further down in the reactor bed indicating that the coupling and oxidation reactions take place in series and not in parallel. This is agreement with a number of investigations of methane coupling in the literature. Ekstrom et al.³⁶ studied methane coupling over a Sm_2O_3 catalyst and Nelson et al.³⁷ investigated Li/MgO . It was determined that reaction at temperatures greater than 1010K results in preferential CO_x formation from C_2 products. It may be concluded therefore, that the CO_x products formed over silver are the result of the oxidation of C_2 products over oxygen-containing silver sites. The selectivity to CO_x products was not observed to change upon increasing the dead volume of the reactor. This is shown in Figure 3. Increasing the dead volume only results in an overall increase in reaction rate. This is a result of the increased volume for the gas-phase recombination of methyl radicals to C_2 products^{38,39}.

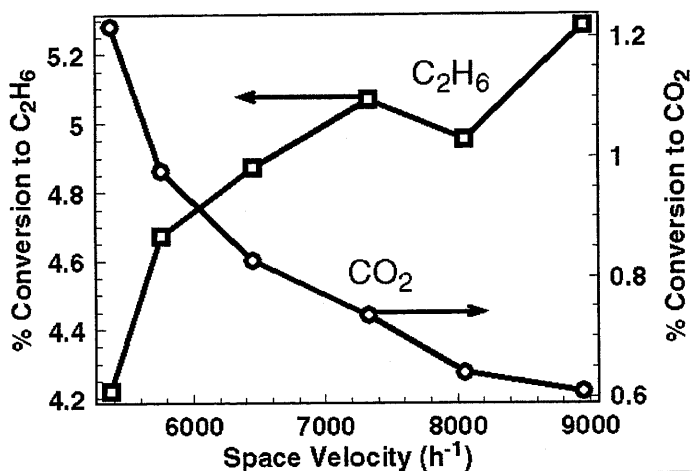


Figure 2. The % Conversion to CO_2 and C_2H_6 as a function of the space velocity at 1023K. Proof for the formation of CO_2 as a reaction in series of C_2H_6 with oxygen.

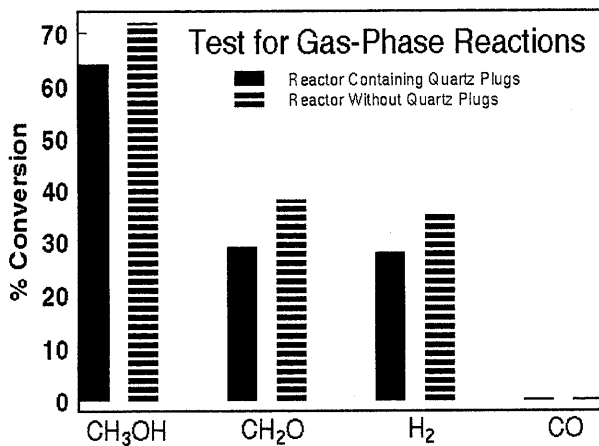


Figure 3. Test for the presence of gas-phase reaction at 1023K. Quartz plug located downstream of the reactor was removed in order increase the dead volume for reaction.

Reaction in series or parallel: Figure 4 shows the % conversion of CH_4 to C_2H_4 and C_2H_6 as a function of the space velocity. The nearly identical variation of conversion to both products as a function of space velocity suggests that both products are formed in parallel from CH_4 . Reaction to C_2H_4 via the formation of CH_2 radicals has been shown to be most unlikely⁴⁰. The kinetics of the reaction of C_2H_6 to C_2H_4 are simply too fast to result in a substantial difference in the form of the concentration profiles of C_2H_4 and C_2H_6 in the reactor bed. This would be quite a reasonable assumption as the C-H bond strength of C_2H_6 (422kJ/mol) is less than in CH_4 (439kJ/mol) and should lead to a preferential reaction of C_2H_6 .

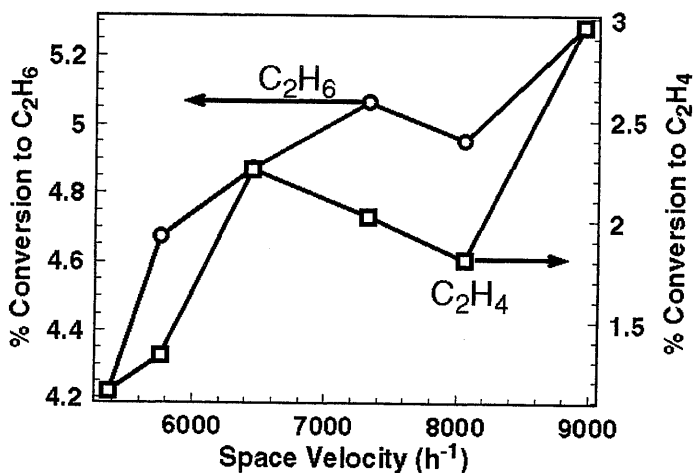


Figure 4. The % Conversion to C_2H_4 and C_2H_6 as a function of the space velocity at 1023K. Evidence for parallel reactions or fast reaction-in-series kinetics.

Using the appropriate steady-state stoichiometric coefficients (OCM selectivity: 80% C_2H_6 , 20% CO_2 , 30% O_2 conversion/Formaldehyde Synthesis selectivity: 70% CH_2O , 30% CO_2), one obtains temperature rises of 88 K for the coupling reaction and 944 K for the methanol oxidation. This simple calculation shows that local heating effects are present in the case of methanol oxidation over silver. The lack of such effects for the OCM reaction obviously eliminates the ambiguity arising from the inability to directly measure the temperature at the

catalyst surface. It is worth noting that the exceptionally high temperature rise of 944K calculated here has been observed experimentally by Flytzani-Stephanopoulos et al.⁴¹ using an pyrometer for NH_3 , C_3H_8 and CO oxidation reactions over Pt catalysts. These authors measured surface temperatures between 800 and 1500K while the gas-phase temperature was 300K. This shows the magnitude of uncertainty encountered when using a thermocouple separated from the reactor by quartz, a relatively poor thermal conductor; $(15\text{-}20)\times 10^{-4}$ ($\text{cal}\cdot\text{cm}/\text{cm}^2\cdot\text{s}\cdot\text{deg C}$).

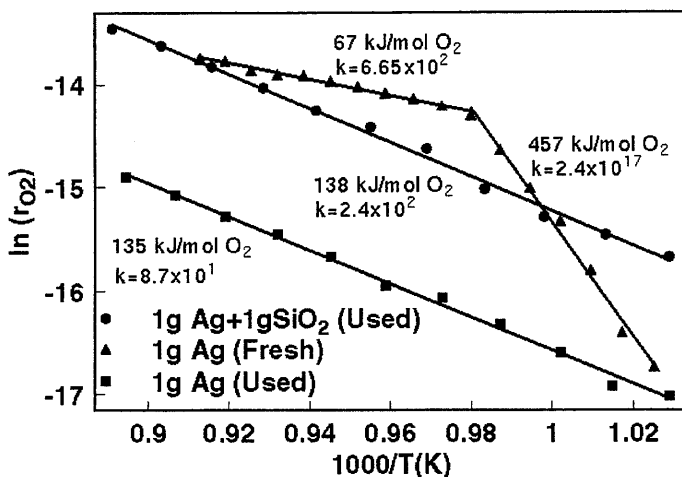


Figure 5. A comparison of the Arrhenius temperature dependence of both fresh and used silver catalysts with and without mixing in SiO_2 .

The Arrhenius-temperature dependence of reaction: The Arrhenius temperature dependence of the reaction rate [mol O_2 converted/ $(\text{m}^2 \text{Ag min})$] is shown in Figure 5. Intrinsic changes of the catalyst result in the appearance of inflection points in the Arrhenius plots. Reaction over the fresh catalyst mixed with SiO_2 shows an initially extremely high activation energy of 457 kJ/mol. This value correlates with the calculated gas-phase C-H bond energy of CH_4 which is 439 kJ/mol⁴². This portion of the curve obviously corresponds to the non-catalyzed, homogeneous reaction of CH_4 with O_2 in the gas phase. There is an inflection point in the curve at 1023 K, above which a very small activation energy of 67 kJ/mol is measured. This indicates the onset of the heterogeneously catalyzed reaction of

CH_4 with O_2 over a catalyst which is undergoing a solid-state transformation. This explains the exceptionally low value of 67 kJ/mol. The shift from a homogenous, gas-phase reaction to a heterogeneously-catalyzed reaction is further supported by the decreased pre-exponential factor. The initial value is representative of the high, gas-phase collision frequency of molecules in the gas phase ($2.4 \times 10^{17} \text{ s}^{-1}$) and the second to a rather low pre-exponential factor for a heterogeneously catalyzed reaction ($6.7 \times 10^2 \text{ s}^{-1}$).

The irreversibility of reaction: The irreversibility of the catalyst transformation was tested by aging the catalysts with and without mixing with SiO_2 , cooling and repeating the identical run. The absence of inflection points for these runs confirms the assumption that no further changes in the intrinsic catalyst activity occur during reaction. Furthermore, the nearly identical activation energies of 135 and 138 kJ/mol indicate that the same reaction mechanisms are active for both the pure Ag as well as that mixed with SiO_2 . The pre-exponential factor for the sample containing SiO_2 ($2.4 \times 10^2 \text{ mol O}_2/\text{g s}^{-1}$) is, however, nearly three times greater than that of the sample without SiO_2 ($8.7 \times 10^1 \text{ s}^{-1} \text{ mol O}_2/\text{g s}^{-1}$). An increased pre-exponential factor indicates that more active sites are present on the sample which was thinned with SiO_2 . This is partly a result of the fact that the catalyst thinned with SiO_2 is less sintered than the pure Ag sample. It is also a consequence of the increased amount of O_γ formed in the (111) terraces of the faceted surface seeded with SiO_2 . Quantitative determination of the increase in faceted area is impossible on the basis of SEM data. Chemisorption methods also proved to be too insensitive (O_2 sticking coefficient on silver is too low). A method for the quantitative determination of the extent of (111) and (110) facet formation would be of obvious assistance. This is unfortunately not possible.

The correlation of reaction rate with bulk-oxygen diffusion: One of the key points of this work was to determine if a correlation exists between the oxygen diffusion kinetics in electrolytic silver and the reaction kinetics for the OCM reaction. The proposed model was shown schematically in Figure 1. It is suggested that molecular oxygen is activated at the silver surface where it forms atomically adsorbed oxygen (O_α). On the one hand, O_α may react with CH_4 or any reactant which is reductive in nature (H_2 , C_2 Products, etc) to form H_2O and CO_x . O_α may also diffuse into the silver bulk forming O_β . This occurs preferentially *via* adsorption on and diffusion through the (110) terminating side of the crystal facet. At elevated temperatures, the interstitial diffusion of oxygen through the silver lattice is

activated. Diffusion through (111) terminating facets then becomes possible. Figure 6 shows the result of a fit to the TDS data for a 100mbar dose of O_2 over silver at 973K shown in the Arrhenius form.

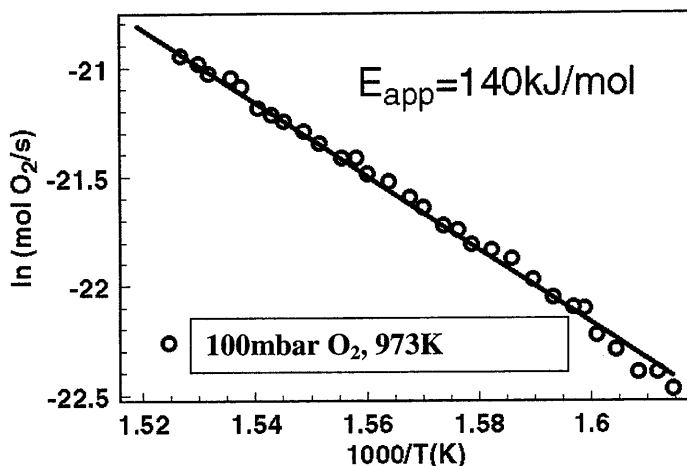


Figure 6. Arrhenius plot of a temperature-programmed desorption spectra using the front line method. 1g Ag, 100mbar O_2 , 973K, 5 min dose, 1K/s heating rate

This is the „front-line,, method of analysing gaseous species which desorb from a solid. It is assumed that the concentration-dependent activation energy does not vary in the temperature region analysed. This is supported by the fact that a straight line Arrhenius relationship is obtained. The results show an activation energy of 140kJ/mol. The correlation between the activation energy of reaction seen in Figure 5 (138kJ/mol) and that of oxygen diffusion in silver (140kJ/mol) in Figure 6 provides strong evidence for the supposition that the formation and diffusion of a bulk-dissolved oxygen species (O_b) is the rate-limiting step of reaction.

Estimating the depth of O_b penetration into silver during steady-state reaction: The proposed diffusion-reaction mechanism is, in many ways, similar to the accepted mechanism of reaction in and on a porous catalyst particle. The primary difference lies in the fact that silver is only permeable to oxygen. The reaction, therefore, only takes place on the silver

surface and not in the catalyst pores as is often the case with supported catalysts. The formation of O_γ from bulk O_β is, however, necessary for reaction. The situation of the OCM reaction over silver was shown schematically in Figure 1. The equimolar counterdiffusion (ECD) of oxygen to and from the silver bulk can be solved by performing a mass balance over a hollow sphere. It is assumed that only the outer portion of the silver particle participates in the formation of O_γ . The depth of the silver particle participating in reaction may therefore be estimated as follows.

The diffusion equation for diffusion in a sphere is shown in equation 14.

$$\text{Equation 9.} \quad \frac{\partial C}{\partial t} = D \left(\frac{\partial^2 C}{\partial r^2} + \frac{2}{r} \frac{\partial C}{\partial r} \right)$$

Equation 9 may be simplified by assuming steady-state diffusion conditions. The presence of steady-state diffusion is confirmed by the steady state conditions under which the kinetic data was attained. The simplified equation is shown in Equation 10.

$$\text{Equation 10.} \quad \frac{d}{dr} \left(r^2 \frac{dC}{dr} \right) = 0$$

Equation 10 may be solved analytically by double integration. The time for diffusion is doubled to account for diffusion to the bulk with subsequent segregation to the surface yielding Equation 11.

$$\text{Equation 11.} \quad Q_t = 8\pi D t \frac{ab}{a-b} (C_2 - C_1)$$

The outer diameter, b , of the silver particles used is 0.4mm. The diffusion coefficient of oxygen in silver at 1073 K may be calculated from Equation 12, which was determined by Outlaw et al. for silver foil at temperatures greater than 900 K.⁴³

$$\text{Equation 12.} \quad D_{Ag(poly)} = 2.96 \times 10^{-3} \exp \left(\frac{-11050}{RT} \right); \text{ cm}^2/\text{s}$$

This yields a value of $1.66 \times 10^{-5} \frac{\text{cm}^2}{\text{s}}$. The following boundary conditions are used.

Equation 13. $C_{O_2} = 0$ at $r = a$

Equation 14. $C_{O_2} = S_{O_2} P^{\frac{1}{2}}$ at $r = b$

The solubility of oxygen was calculated from the oxygen uptake performed using temperature programmed oxygen desorption (data not shown). A value of $1.4 \times 10^{-7} \frac{\text{molO}_2}{\text{g} \cdot \text{Ag}}$ was obtained for doses made at the partial pressure of oxygen present at steady state (6.2% O₂ in feed, 7% O₂ conversion) of 60mbar. Insertion of these values into equation 11 yields an oxygen penetration depth of 0.35 μm . It is estimated, therefore, that the uppermost 0.35 μm of the silver surface participate in the formation of O_p. The silver metal functions essentially as an electron rich substrate capable of activating molecular oxygen into the desired state. The actual catalysis takes place over the oxygen species formed.

5.3.2 Results obtained under unsteady-state conditions

The activity and selectivity of reaction over silver are found to vary drastically during the first days of reaction. This arises from the fact that the relatively slow solid-stated kinetics of the silver restructuring limits the approach to equilibrium. The observed changes in selectivity to oxidation products or C₂ products as well as variations in reaction rate provide an excellent indicator for the degree of facetting and subsequent O_γ formation.

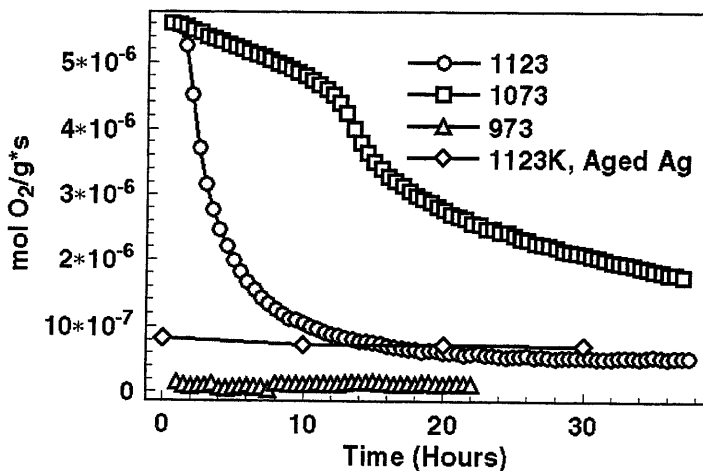
5.3.2.1 Isothermal Run without SiO₂

Figure 7a. Rate of O₂ reaction as a function of time and temperature for reaction over a fresh silver catalyst. 1g Fresh Ag, 0.2-0.4mm diameter, 8.4ml/min O₂, 50 ml/min CH₄, 77 ml/min He, S.V.=6,113 hr⁻¹, v_i=0.045 m/s

Changes in reaction rates: Figure 7a shows the rate of oxygen reaction as a function of time on stream for a number of isothermal runs made over a catalyst bed containing 1g of fresh, (0.2-0.4mm) electrolytic silver samples. The reactor was stepped from room temperature to the set-point temperature and held there, isothermally. The silver bed was allowed to equilibrate for 20 minutes at the desired

temperature before taking the first point. The rate of oxygen reaction shown in Figure 7a decreases quickly as a function of time for measurements made at both 1073 K and 1123 K. No conversion was observed at 973 K which appears to be too low a temperature for catalyst activation. The observed temperature dependence of the time necessary to reach steady state results from the slow, solid-state transformation of the silver during reaction. Reaction-induced changes in morphology are shown below. The form of the deactivation curves also shows a strong temperature dependence. The run made at 1073 K shows a strong inflection point at 25 hours on stream hinting that there are likely a number of transformations in the

silver catalyst occurring on different time scales. The run made at 1123 K shows a more rapid deactivation than that at 1073 K. This is simply a result of the enhanced sintering of silver at more elevated temperatures

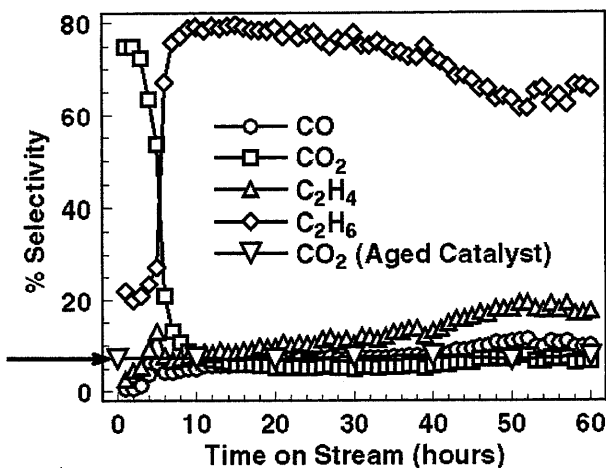


Figure 7b. Selectivity for reaction over a fresh silver catalyst. 1g Fresh Ag, 0.2-0.4mm diameter, 8.4ml/min O₂, 50 ml/min CH₄, 77 ml/min He, S.V.=6,113 hr⁻¹, v_i=0.045 m/s, 1073K

Changes in Product Selectivity: Figure 7b shows the % selectivity to selected products corresponding to the run shown in Figure 7a made at 1123 K. The time-dependent variation in selectivity for the run made at 1123 K (See Figure 7a for the corresponding rate of oxygen reaction) shows initially 75% selectivity to CO₂. The CO₂ selectivity drops off rapidly with time on stream and the selectivity to C₂H₆ increases from 20% to 70%. Figure 7b shows that for longer reaction times ($t > 20$ hrs), the selectivity to C₂H₄ gradually increases to 20% and the selectivity to C₂H₆ decreases to 65%. This corresponds with a slight decrease in CH₄ conversion which is not shown. No deactivation was observed for times on stream greater than 50 hours, indicating equilibration of the silver transformations responsible for the observed changes in catalytic activity. The plateau in selectivity obtained for times on stream greater than 40 hours correlates well with the plateau in O₂ reaction rate shown in Figure 7a. The gradual facetting of the silver surface and subsequent formation of O₂ over the course of time explains, qualitatively, the observed changes in selectivity. As was mentioned before, an

increase in selectivity to dehydrogenation products indicates an increase in the amount of O_γ present. O_γ is, however, only formed in the (111) terraces. The increased selectivity to C_2 products with time on stream provides, therefore, qualitative evidence for the role of facet and O_γ formation in the direct dehydrogenation of methane.

The attribution of this selectivity change to variations in the catalyst morphology and the formation of O_γ was proven by cooling the sample under the reaction mixture to 1023 K and then repeating the identical experiment. The dashed line in Figure 7a shows the rate of O_2 consumption obtained after cooling this catalyst and then repeating the identical procedure used to obtain the other curves in Figures 7a-b. A steady-state rate is reached for the used sample within the 20 minute equilibration time prior to taking the first point. This clearly shows that the aged catalyst does not undergo any further structural transformations. The downward pointed triangles connect by a solid line in Figure 7b (marked with an arrow) shows the selectivity to CO_2 for the used catalyst. The absence of the initial high selectivity to CO_2 , as shown in Figure 7b for reaction over the fresh catalyst, clearly indicates that an intrinsic change in the catalyst activity has occurred which leads to a decrease in the overall activity and a significantly improved selectivity to C_2 products. This behavior also rules out the possibility that the initial CO_2 production results from the formation of hot spots in the catalyst bed. The fact that the used catalyst has sintered implies that it has a substantially higher packing density than the fresh silver. This hot spot formation should, therefore, be enhanced for the sintered catalyst. The fact that this is not the case agrees excellently with the supposition that O_γ , the catalytically active species at this temperature¹⁷⁻²², has formed in the (111) terraces of surface facets formed during reaction and is responsible for the decreased selectivity to CO_2 . Surface defects and open crystalline planes present on the fresh silver exhibit high sticking coefficients and are known to form O_α ⁶⁻¹². Fresh samples tend, therefore, to show exceptional activity and selectivity for the formation of complete oxidation products. Gradual annealing of these surface defects and their subsequent replacement by (111) terraces in which O_γ is incorporated explains the selectivity behavior seen in Figure 7b.

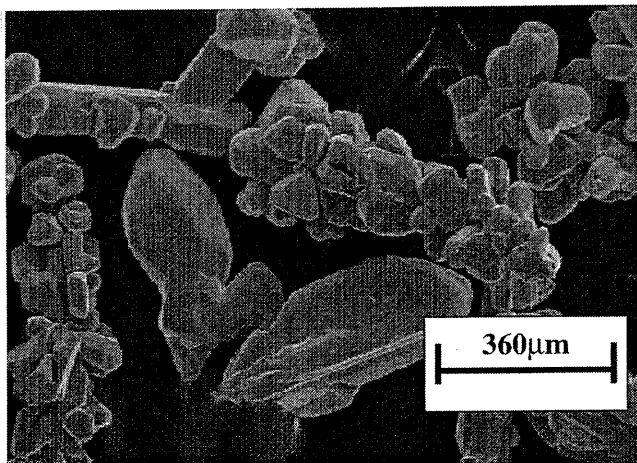


Figure 8a. Scanning electron micrograph of the fresh electrolytic silver catalyst.

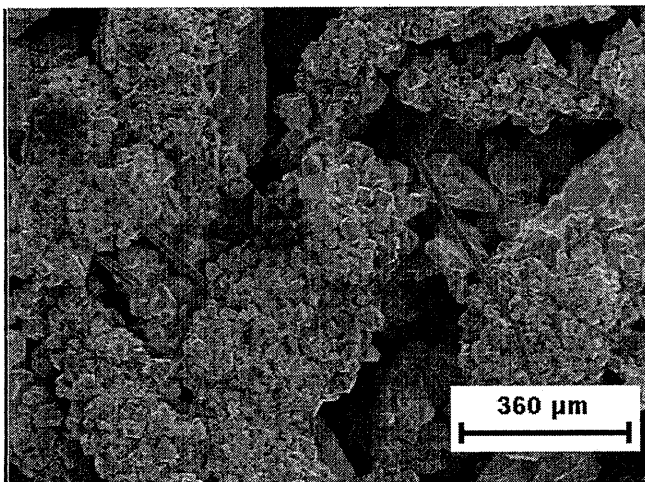
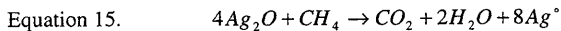


Figure 8b. Scanning electron micrograph of a used electrolytic sample showing the pronounced sintering of the silver crystallites.
0.2-0.4mm diameter, 8.4ml/min O_2 , 50 ml/min CH_4 ,
77 ml/min He, S.V.=6,113 hr^{-1} , $v_t=0.045$ m/s

As shown above, catalyst activity and selectivity act as qualitative gauges for reaction-induced changes in catalyst morphology. The curve forms shown in Figure 7a provide, therefore, important information about the types of solid-state transformations occurring during reaction. Figure 8a shows an SEM micrograph of a fresh silver catalyst. The SEM micrograph in Figure 8b shows that the used catalyst has undergone pronounced sintering. The sample has also recrystallized, forming small microcrystallites (See Chapter 3). The small silver crystallites have melted together forming larger silver aggregates. This observation, combined with the drastic decrease in catalytic activity suggests that sintering is the dominant solid-state transformation for reaction over pure silver samples. This is no surprise as the reaction temperatures used here ($T > 973$ K) are significantly higher than the Tamann temperature of silver ($T_f = 750$ K). The Tamann temperature is the temperature at which the kinetics of solid-state transformations of solids are sufficiently high to result in marked mass transport within a relatively short time frame of interest. Investigation of the catalyst sample subsequent to reaction showed it to be annealed into a single silver frit. It is very interesting to note, however, that the deactivation does not follow the deactivation profile typical of sintering kinetics. Sintering effects typically follow a power-law dependence whose exact exponential value depends on the type of sintering mechanism present⁴⁴. A simple power-law relationship could not be fitted to the deactivation curves shown in Figure 7a. The deactivation in conversion for the 1123 K run shown in Figure 7a could only be fitted using an inverse exponential relationship. This observation, combined with the fact that the form of the deactivation in conversion for the 1073 K run is significantly different above and below the point of inflection at 25 hours on stream implies that the observed behavior cannot simply be attributed to sintering of the catalyst particles. There appears to be more than one morphological change taking place under these conditions.

The absence of Ag_2O : The attribution of the initially high selectivity to CO_2 for reaction over fresh silver cannot be attributed to the reaction of methane with silver oxide which could hypothetically be present for a fresh sample stored in air. Two facts support this. The first is that the reaction temperatures used here are well above the thermal-decomposition temperature of bulk Ag_2O ($T_{\text{dec}} = 585$ K). Secondly, stoichiometric reaction of CH_4 with Ag_2O to CO_2 for 10 hours on stream under the conditions used and with the stoichiometry in Equation 15 would require slightly more than 1 kilogram of Ag_2O .



The fact that gas-phase oxygen is consumed during reaction indicates that the purely stoichiometric reaction of Ag_2O with CH_4 is definitely not occurring. The large amount of Ag_2O which would be necessary for reaction shows, however, that the reaction of CH_4 with Ag_2O cannot explain the observed initial selectivity to CO_2 .

The deactivation resulting from sintering significantly complicates the interpretation of the data with regard to other, less dominant, solid-state processes. Improved selectivity to C_2 products may very well result from the formation of O_v by faceting and subsequent formation of (111) terraces (See Figure 1c, Chapter 3). Determination of the effect of these processes on catalyst activity is, however, masked by the dominant effect of catalyst sintering. This problem was circumvented by mixing the sample with an equal amount (by weight) of catalytically-inactive SiO_2 .

5.3.2 Isothermal Run with SiO_2 -Diluted Ag Catalyst

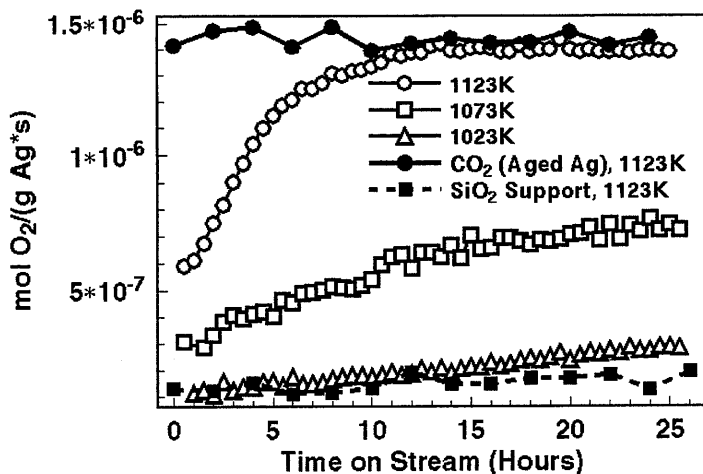


Figure 9a. Rate of O_2 reaction as a function of time and temperature for reaction over a fresh silver catalyst mixed with SiO_2 . 1g Fresh Ag, 0.2-0.4mm diameter, 1g SiO_2 , 200 μm diameter, 8.4ml/min O_2 , 50 ml/min CH_4 , 77 ml/min He, S.V.= 16,113 hr^{-1} , $v_t=0.045$ m/s

Changes in catalyst activity: Equivalent amounts (1g Ag:1g SiO₂) of silver and SiO₂ were mixed and placed in the reactor. The rate of O₂ reaction obtained with this catalyst mixture is shown in Figure 9a. The O₂ reaction rate follows a completely different trend than that shown in Figure 7a for the sample without SiO₂. The initially high O₂ reaction rate observed at 1123K for the pure Ag sample without SiO₂ shown in Figure 7a $\left(5.7 \times 10^{-6} \frac{\text{molO}_2}{\text{g} \cdot \text{s}}\right)$ is not observed for the run made with the catalyst bed mixed with SiO₂ in Figure 7a $\left(6.7 \times 10^{-7} \frac{\text{molO}_2}{\text{g} \cdot \text{s}}\right)$. In addition, reaction over the catalyst mixed with SiO₂ shows a gradual activation with increasing time on stream as opposed to the deactivation observed for the case of pure Ag shown in Figure 7a. Mixing with SiO₂ has obviously hindered catalyst sintering, allowing the observation of other changes in activity arising from more subtle changes in morphology. The activation shows an initial rapid increase in the first 7 hours followed by a more gradual increase for times greater than 20 hours. The presence of more than one activation profile again suggests, as in the case of pure Ag, that a number of solid-state transformations are responsible for activation of the SiO₂-thinned bed. The approach of the O₂ reaction to steady-state is also observed to vary as a function of temperature again arising from the temperature dependence of the silver diffusion coefficient which determines the rate at which the catalyst reconstruction takes place. Quantitative evidence for this is provided in the next section. The solid-state kinetics resulting in the increased activity obviously occur on the time scale of hours with steady-state being reached after 15 hours on stream for the run made at 1123 K (Figure 9a). An increase in the formation of the catalytically active O₂ with time on stream as a result of surface facetting would explain the gradual increase in catalytic activity. A contradiction appears to exist, however, in the difference in initial activities for the pure Ag sample (Figure 7a) and the SiO₂-thinned sample (Figure 9a). The reason for the initially low-activity for the thinned sample is only revealed after studying the surface morphology with SEM.

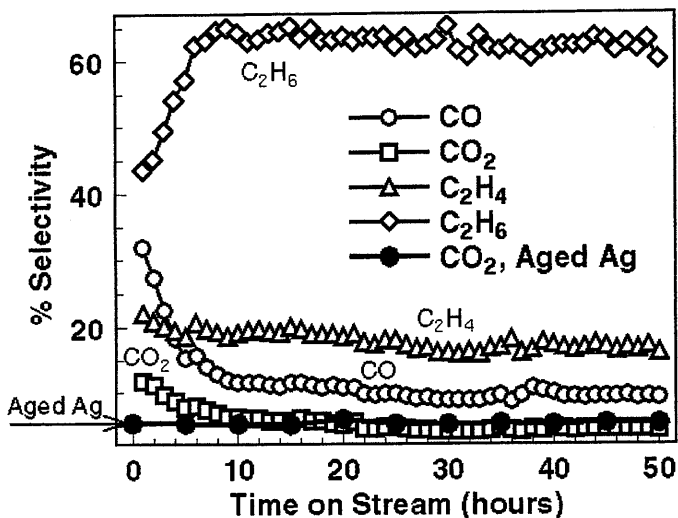


Figure 9b. Selectivity for reaction over a fresh silver catalyst mixed with SiO₂. 1g Fresh Ag, 0.2-0.4mm diameter, 1g SiO₂, 200μm diameter, 8.4ml/min O₂, 50 ml/min CH₄, 77 ml/min He, S.V.= 16,113 hr⁻¹, v_i=0.045 m/s, 1073K

Changes in selectivity: The time-dependence of selectivity for the sample mixed with SiO₂ seen in Figure 9b is also very different than that observed for the pure Ag sample (Figure 7b). The sample initially shows an elevated selectivity to CO. This decreases rapidly within the first 10 hours on stream to 15%. This value is similar to that observed for the run made using pure Ag (Figure 7b). The reason for the initially high conversion to CO as opposed to CO₂ is not clear. In either case, the initial 30% conversion to CO for the SiO₂ diluted sample is significantly less than the 75% conversion to CO₂ seen for the non-diluted sample in Figure 7b. The steady-state selectivities for all products are approximately the same for runs made with (Figure 9b) and without (Figure 7b) SiO₂ thinning. This suggests that the final state of the silver catalyst responsible for the observed selectivities is identical for both runs made with and without thinning by SiO₂. The difference in steady-state activities (Figures 7a and 9b) lies, therefore, in the aforementioned sintering of the catalyst.

The reversibility of the solid-state transformation subsequent to cooling was tested by cooling the reactor to 1023K under the reactant stream and then repeating the identical run. The filled squares in Figure 9a shows the O_2 consumption obtained over this sample after subsequent cooling and re-heating to 1123K. Steady-state O_2 consumption is obtained within the 20 minute equilibration time prior to taking the first point. This behavior is identical to that observed for reaction over pure Ag (see Figure 7a). In addition, the filled circles in Figure 9b shows that the initially high CO selectivity does not appear for reaction over the used sample. Again, the used catalyst appears to have undergone a transformation which has changed it from a catalyst which prefers complete oxidation (albeit to a much lesser extent than the case of pure Ag) to one exhibiting an excellent selectivity to C_2 products. The morphological changes leading to this change in behavior are shown below.

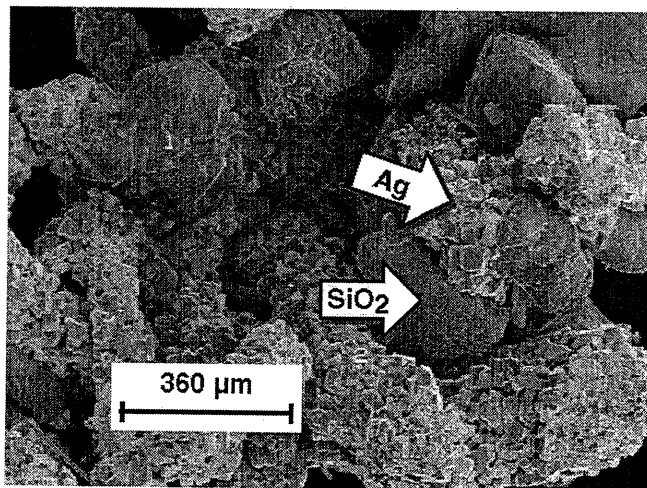


Figure 10. Scanning electron micrograph of the silver catalyst mixed with SiO_2 following reaction. 1g Fresh Ag, 0.2-0.4mm diameter, 1g SiO_2 , 200 μm diameter, 8.4ml/min O_2 , 50 ml/min CH_4 , 77 ml/min He, S.V.= 16,113 hr^{-1} , $v_l=0.045$ m/s

SEM evidence for catalyst sintering: The minimization (but not complete removal) of catalyst sintering by mixing with SiO_2 is confirmed by the micrograph shown in Figure 10 (compare to the fresh catalyst in Figure 5a). Small silver crystallites (10-30 μm) have formed

agglomerates which are separated by grains of SiO_2 . The recrystallization of the silver catalyst in an oxygen-containing atmosphere was dealt with in Chapter 3. The effects of lesser solid-state transformations on catalysis for the non-diluted sample were not visible in Figures 7a and 7b because they are therefore superimposed on a background of deactivation which is the dominant process for the non-diluted situation.

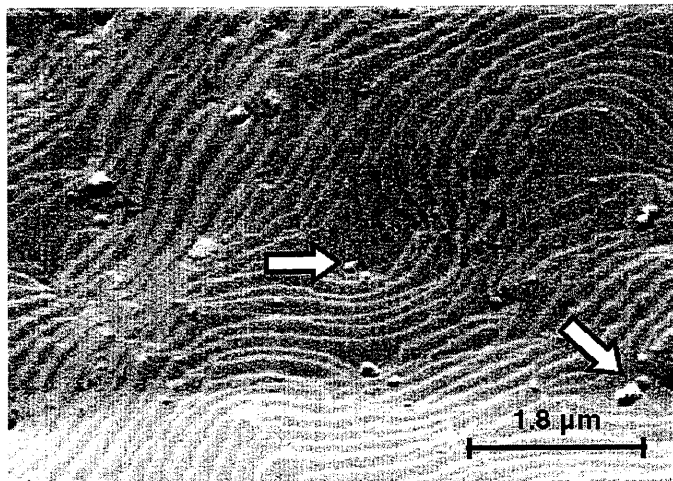


Figure 11. Scanning electron micrograph of the surface of a silver catalyst mixed with SiO_2 after 20 minutes on line. 1g SiO_2 , 200 μm diameter, 8.4ml/min O_2 , 50 ml/min CH_4 , 77 ml/min He, S.V.= 16,113 hr^{-1} , $v_f=0.045$ m/s

The effect of surface-pinning by SiO_2 : The activity for the 1023 K run in Figure 9a appears to increase linearly. This is contrast to the reaction made over a pure Ag bed in Figure 7a at 1023 K which exhibits no activity. Two reasons for the observed activity increase for the SiO_2 thinned sample are likely. The first explanation is that reduction of the sintering effect by SiO_2 dilution allows the observation of the activation by faceting. This does not, however, explain the completely different selectivity trends observed in Figures 7b and 9b. The second reason for the increased activity lies in the morphological changes caused by the presence of the SiO_2 in the reaction bed. Figure 11 shows an SEM micrograph of the surface of the silver catalyst which was mixed with SiO_2 subsequent to 20 minutes reaction on stream.

The surface is observed to be strongly faceted. The terrace-step structure has been shown to be caused primarily by the pinning of the silver surface during reaction⁴⁵. Surface pinning of single-crystalline silver surfaces was studied by Ozcomert et al⁴⁵. The pinning arises from the blocking of the flux of silver atoms diffusing across the silver surface during reconstruction. The formation of pinning sites suggests that the dominant mechanism for silver restructuring under these conditions is surface diffusion and not evaporation and recondensation due to super-saturation in the gas phase. The „seeding„ of the surface facets with SiO₂ provides further evidence for the importance of the surface reconstruction on reaction. In addition, the equilibration time has been significantly reduced from 50 hours for the pure Ag sample (Figure 7a) to 25 hours for the sample mixed with SiO₂ (Figure 9a). This suggests faster facet formation for the case where silver is mixed with SiO₂. This also explains the lower initial activity of the SiO₂ thinned catalyst (Figures 9a) relative to the pure silver catalyst (Figure 7a). The rapid formation of facets at the surface result in a lower conversion, but higher selectivity to C₂ products (lower CO_x conversion in Figure 9b compared with Figure 7b). It is impossible to absolutely rule out the presence of local heating effects in this case. It could be that the lowered activity is due to lessened local heating effects as a result of SiO₂ thinning. The initially high O₂ reaction rate in Figure 9a and the preferential formation of complete oxidation products seen in Figure 9b result in a more exothermic reaction over the fresh catalyst which may lead to local heating effects for reaction over the fresh catalyst for times on stream less than 10 hours. This is different from the steady-state situation shown in section 5.3.1 where local heating effects may be safely neglected. Use of N₂ instead of He (5x lower thermal conductivity) as a carrier gas instead of He resulted in the same conversion and selectivity. This suggests that local temperature gradients should not play a significant effect. The reason for the lower initial activity for the SiO₂-thinned catalyst is, therefore, most likely a result of the SiO₂-induced facetting.

Evidence for surface-diffusion controlled facet growth: Investigation of the time-dependence of the activation profiles yields information about the mechanism of facetting. The increase in activity for the run at 1073K follows a power law of the following form.

Equation 16.
$$\frac{d[O_2]}{dt} = K \times t^{0.24}$$

The 0.24 power law dependence agrees excellently with the value of 0.25 for the silver facetting kinetics predicted by Mullins et al.⁴⁶ for surface-diffusion controlled facetting. This is, therefore, a quantitative tie between facet growth and catalyst activity for the OCM reaction in this temperature region. This finding is also in agreement with the previously made proposition that the dominant mechanism for facetting under these conditions was surface diffusion of silver and not sublimation and recondensation.

The contribution of sublimation to facet growth: The activation of the catalyst occurs very rapidly at 1123K (Figure 9a). This curve could only be fit using a natural exponential function, indicating that surface-diffusion limited facetting is no longer likely to be the dominant process. It is possible that sublimation and recondensation of the silver may play a significant role at this temperature. Mullins²⁴ showed, however that facetting which occurs by gas-phase transport follows a power-law relationship with an exponent of 1/3. There appears, therefore, to be a discrepancy between the observed time-dependence of activity and the predicted facetting kinetics. The possible explanation of gas-phase transport may be estimated by considering the rate of vaporization of silver from the surface. The vapor pressure of silver at 1073K is approximately 4×10^{-6} mbar⁴⁷. The flux of metal from one plane to another *via* gas-phase transport may be defined using Fick's first law as shown in Equation 17. Here, the gas-phase flux of silver, J_{Ag} , is proportional to the concentration gradient of silver, $\vec{\nabla} C$, in the gas phase.

Equation 17.
$$J_{Ag} = -D_{Ag} \vec{\nabla} C$$

The rate of facet growth can be approximated by estimating the concentration gradient of gas-phase silver parallel to the surface with Equation 18.

Equation 18:
$$\vec{\nabla} C = \frac{P_{Ag}}{R \times T \times l}$$

The average measured facet width for a 20 minute run is approximately 200nm. The facet height was determined by varying the SEM electron flux for the facet imaging by 45°. The facet height, X_{act} , may therefore be estimated from the shadowing effect using equation 4.

Equation 19.
$$\frac{X_{act}}{X_{obs}} = \frac{\theta_{act}}{\theta_{obs}}$$

Where θ_{act} is the angle of the vector normal to the surface used for obtaining the SEM micrograph from which the step height, X_{act} is measured. X_{obs} is the observed step height for an electron image taken at a different angle θ_{obs} . An average value of 150nm for the facet length and 300nm for the facet height was obtained for this run. Typical facet lengths, l , were between 1.5 and 2 μm . It is worth noting that the facet sizes obtained vary quite widely. The values used in these calculations represent values averaged over 50 different measured facets. These dimensions results in an average facet volume of $9 \times 10^{-20} \text{m}^3$ which would require $1.02 \times 10^{-13} \text{mol Ag}$ using a density of 10.5g/mol. A metal deposition rate of $8.5 \times 10^{-17} \text{mol/s}$ or $0.9 \frac{\mu\text{m}}{\text{hr}}$ would therefore be necessary to result in the formation of a rectangular facet of these

dimensions. This would result in a diffusive flux of $1.42 \times 10^{-4} \frac{\text{molAg}}{\text{s} \times \text{m}^2 \times \text{g}}$, This value agrees with the calculated rate of $1 \frac{\mu\text{m}}{\text{hr}}$ calculated using equation 20 for the rate of evaporation of silver, r_e , as a function of temperature.

Equation 20.
$$r_e = p \left(\frac{1}{2\pi MRT} \right)^{\frac{1}{2}}$$

The vapor pressure of silver is approximately $6 \times 10^{-6} \text{mbar}$ at 1073 K²⁵. M is the atomic mass of 108 and R is the ideal-gas constant. The agreement between the flux resulting from the silver evaporation rate and the growth of the silver facets shows that it is possible that the observed increase in reaction rate arises from the gas-phase transport of silver despite the lack of a 1/3 power law time dependence. The reason for the deviation from a 1/3 power law most

likely rests in the fact that both surface diffusion as well as sublimation play a role at elevated temperatures leading to enhanced mass transfer and rapid formation of silver facets.

The SiO_2 used during reaction was observed to change color from white to dark gray after reaction. Qualitative EDX analysis shows the presence of trace amounts of carbon and silver on the surface. The sublimation of silver obviously occurs to some extent during reaction and recondenses on the SiO_2 particles. It is absolutely essential to determine how active this material is as it may contribute to the increased activity seen in Figure 9a. The sample was first broken apart by hand and then subsequently treated for 10 minutes in an ultra-sonic bath containing distilled water. This allowed the easy separation of the SiO_2 and silver. The used SiO_2 was then placed in the reactor and the activity tested. The results show that the activity is the same as that obtained for an empty reactor (data not shown). The contribution of Ag deposited on SiO_2 is, therefore, negligible.

These results show that the rate of reaction depends on the extent of facetting. The rate of facetting, in turn, shows a strong temperature dependence which results from the dominant mechanism of mass transport of silver at that temperature. The qualitative variation of catalyst activity and selectivity provides a strong argument in favor of the suggested model (See Figure 1). The quantitative agreement of the observed activation profile and that predicted on the basis of facet growth kinetics further supports the proposed model. Further quantitative evidence in support of this model may be found in the comparison of the reaction kinetics and the oxygen diffusion kinetics in silver.

5.5. Conclusions

In this work it is suggested that the formation of subsurface oxygen is necessary for activation of electrolytic silver in the OCM reaction. A number of authors have shown that the incorporation of subsurface oxygen plays a critical role in the ethylene epoxidation by modifying the silver surface electronically^{4,6,7}. The major deviation of the model proposed in this work from the ethylene epoxide model is that subsurface oxygen is believed to play a dynamic role in the OCM reaction where it is continuously created by bulk dissolution from the gas phase and destroyed *via* surface segregation and reaction. This is not a classical Mars van Krevelen mechanism³⁰ as the participation of lattice oxygen in a stoichiometric oxide is

not assumed. The dependence of the diffusion mechanism and rate of diffusion on the crystallographic orientation of the silver crystallites explains the strong structure sensitivity of the OCM reaction over silver. Changes in the surface and bulk morphology are intrinsically connected and play key roles in the overall reaction mechanism. Catalyst activation kinetics correlate with facet growth kinetics. In addition, a quantitative correlation exists between the activation energy of reaction (138 kJ/mol) and the activation energy of oxygen diffusion in silver (140 kJ/mol). This provides a strong argument in favor of the supposition that the formation of active oxygen (O_p) via the continuous surface segregation of bulk-dissolved oxygen (O_b) is a necessary prerequisite to the formation of a silver catalyst which is active for direct dehydrogenation reactions.

References

1. Ullman, „Ullman’s Encyclopedia of Industrial Chemistry,,, 5th edition, Vol. 11, 619 (1988).
2. Sperber H., *Chemie-Ing.-Technology* **41**, 962 (1969).
3. Reuss G., Disteldorf W., Grundler O. and Hilt A., „Formaldehyde,,, Verlag Chemie, Weinheim, Vol. A11, 619 (1988).
4. van Santen R.A. and. DeGroot C.P.M.J., *J. Catal.* **98**, 530 (1986).
5. Voge H.H. and. Adams C.R., *Adv. Catal.* **17**, 151 (1967).
6. Bukhtiyarov V.I., Boronin A.I. and. Savchenko V.I., *Surf. Sci. Lett.* **232**, L205, (1990).
7. Boronin A.I., Bukhtiyarov V.I., Vishnevskii A.L., Boreskov G.K and Savchenko V.I., *Surf. Sci.* **201**, 195 (1988).
8. Grant R.B. and Lambert R.M., *J. Catal.* **92**, 364, (1985).
9. Herein D., Nagy A., Schubert H., Weinberg G., Kitzelman E. and Schlögl R., *Z. Phys. Chem Bd.* **197**, 67 (1996).
10. Lefferts L., van Ommen J.G. and Ross J.R.H., *Appl. Cat.* **23**, 385 (1986).
11. Schubert H., Tegtmeier U., Herein D., Bao X., Muhler M. and Schlögl R., *Catal. Lett.* **33**, 305 (1995).
12. Prince K.C., Paolucci G. and Bradshaw A.M., *Surf. Sci.* **175**, 101 (1986).
13. Frank E.R. and Hamers R.J., *J. Catal.* **172**, 406 (1997).
14. Uwins P.J.R., Millar G.J. and Nelson M.L., *Microscopy Research and Technique*, **36**, 382 (1997).
15. Millar G.J., Nelson M.L. and. Uwins P.J.R., *Catal. Lett.* **43**, 97 (1997).
16. Rao C.N.R., Aiyer H.K.N., Arunarkavalli T and Kularni G.U., *Catal. Lett.* **23**, 37 (1994).
17. Bao X., Muhler M., Schedel-Niedrig Th. and Schlögl R., *Phys. Rev. B*, **54**, 2249 (1996).
18. Herein D., Werner H., Schedel-Niedrig Th., Neisius Th., Nagy A., Bernd S. and Schlögl R., *Proc. 3rd World Congress on Oxidation Catalysis*, Eds.. Oyama S.T et al., Sept 21 (1997).
19. Bao X. and Deng J., *J. Catal.* **99**, 391 (1986).
20. Bao X., Lempfuhl G., Weinberg G., Schlögl R. and Ertl G., *J. Chem. Soc. Faraday Trans.* **88(6)**, 865 (1992).
21. Bao X., Pettinger B., Ertl G. and Schlögl R., *Ber. Bunsenges. Phys. Chem.* **97**, pg 97 (1993).
22. Rehren C., Muhler M., Bao X., Schlögl R and Ertl G., *Z. Phys. Chem.* **174**, 11 (1991).
23. Nelson P.F., Lukey C.A., Cant N.W., *J. Phys. Chem.* **92**, 6176 (1988).

-
24. Mims C.A., Hall R.B., Rose D., Martin G.R., *Catal. Lett.* **2**, 361 (1989).
 25. Zhang H.S., Wang J.X., Driscoll D.J., Lunsford J.H., *J. Catal.* **112**, 366 (1988).
 26. Campbell K.D., Morales E., Lunsford J.H., *J. Am. Chem. Soc.* **109**, 7900 (1987).
 27. Wang J.X. and Lunsford J.H., *J. Phys. Chem.* **90** 5883 (1986).
 28. Peil K., Goodwin J. and Marcelin G. in *Natural Gas Conversion, Studies in Surface Science and Catalysis* (Eds: A. Holmen, K..J. Jens and S. Kolbee), Elsevier, Amsterdam **61** 73 (1991).
 29. Zhang H.S., Wang J.X., Driscoll D. and Lunsford J. *J. Catal.* **112** 366 (1988).
 30. Mars P. and van Krevelen D.W., *Chem.Eng.Sci.Special Suppl.*, **3**, 41 (1954).
 31. F. Dautzenberg, „Ten Guideline for Catalyst Testing,,, American Chemical Society 105 (1989) ISBN 0097-6156/89
 32. Leffers L., van Ommen J.G., Ross J.R.H., *Appl. Cat.*, **23** 385 (1986).
 33. Lefferts L., van Ommen J.G., Rosss J.R.H., *Appl. Cat.*, **23**, 385 (1986).
 34. Lefferts L., van Ommen J.G., Rosss J.R.H., *Appl. Cat.*, **34**, 329 (1987).
 35. Nagy A., Mestl G., Rühle T., Weinberg G., Schlögl R., Accpeted in *J. Catal*
 36. Ekstron A., Lapszewicz, Campbell I., *Appl. Catal.* **56** L29 (1989).
 37. Nelson P.F., Cant N.W., *J. Phys. Chem.* **94**, 3756 (1990).
 38. Nelson P.F., Lukey A., Cant N.W., *J. Phys. Chem.* **92**, 6176 (1988).
 39. Mims C.A., Hall R.B., Rose K.D., Martin G.R., *Catal. Lett.* **2**, 361 (1989).
 40. Hutchings G.J., Scurrall M.S. in *Methane Conversion by Oxidative Processes*, (Ed: E.E. Wolf), van Nostrand Reinhold, N.Y., 201-258 (1992).
 41. Flytzani-Stephanopoulos M., Wong S., and Schmidt L.D., *J. Catal* **49**, 51 (1977).
 42. Lunsford J. in „The Handbook of Heterogeneous Catalysis,, **Vol 4**, 1843-1856 VCH Weinheim, ISBN 3-527-29212-8 (1997).
 43. Outlaw, R.A., Wu, D., Davidson, M.R., Hoflund, G.B., *J. Vac. Sci. Tech. A* **10(4)** (1992).
 44. Kuczynski G., „Sintering and Catalysis,,, **10**, Materials Science Research, N.Y. Plenum Press (1975).
 45. Ozcomert J.S., Pai W.W., Bartelt N.C. and Reutt-Robey J.E., *Surf. Sci.* **293**, 193 (1993).
 46. Mullins, W.W., *Phil. Mag.*, **6**, 1313 (1961).
 47. Espe W., in *Werkstoffkunde der Hochvakuum-Technik*, VEB Deutscher Verlag der Wissenschaften, Berlin, 195947 Ullman, „Ullman’s Encyclopedia of Industrial Chemistry,,, 5th edition, **A11**, 619 (1988).

Summary

Silver is used industrially as a catalyst for both the epoxidation of ethylene to ethylene epoxide as well as the oxi-dehydrogenation of methanol to formaldehyde. The remarkable activity of silver for these reactions lies its ability to activate molecular oxygen into a number of different, catalytically active, forms.

Atomic oxygen is formed above 160K *via* dissociative chemisorption of gas-phase, molecular oxygen. This atomic-surface oxygen is referred to as O_α and is a strong nucleophile which tends to form complete oxidation products. It is formed preferentially on high-Miller indices terminating silver crystal surfaces exhibiting high sticking coefficients for dissociative adsorption of molecular oxygen. This species desorbs from the silver surface at approximately 523K in vacuum. An equilibrium between adsorption, desorption and bulk diffusion of O_α into and out of the silver bulk occurs above 573K when a gas-phase partial pressure of oxygen is maintained. Oxygen preferentially occupies octahedral holes in the silver lattice below 923K. This bulk-dissolved oxygen is termed O_β . The dominant diffusion mechanism is grain-boundary diffusion or octahedral hole jumping for temperatures below 923K. The hole jumping mechanism is strongly anisotropic and results in preferential channeling of oxygen in the [110] direction in the silver crystallites.

Above 923K, the interstitialcy diffusion of oxygen in the silver bulk becomes activated and results in the incorporation of oxygen into the silver lattice. Under steady-state reaction conditions at temperatures in excess of 923K, both oxygen in interstitial and lattice positions is present. Oxygen undergoes equimolar counter-diffusion where it dissolves into the bulk and segregate to the surface under steady-state reaction conditions. At the same time, the silver surface undergoes massive restructuring. This restructuring arises from the thermodynamic drive of the silver surface to obtain a minimum surface energy configuration. This process results in the formation of surface facets. These are believed to consist of (111) terraces and (110)-terminating steps. The (111) terraces exhibit extremely low sticking coefficients for oxygen adsorption ($\theta < 10^{-6}$) and subsequently do not form significant amounts of O_α . The (110) steps exhibit a high sticking coefficient for oxygen ($\theta \sim 10^{-3}$) and provide channels for the above-mentioned diffusion of oxygen along the [110] direction into the silver bulk. This oxygen may either diffuse back to the (110) surface or may diffuse to the (111)

terraces *via* interstitialcy diffusion. This lattice oxygen may react with gas-phase organic species in that moment when it has segregated into the uppermost silver layer. This species is referred to as O_γ and is responsible for the direct dehydrogenation of organic molecules. Both the direction and kinetics of oxygen diffusion through silver are strong functions of the silver morphology as bulk oxygen will always seek out the path of least resistance. It is the coincidence of the morphological restructuring of the silver into a thermodynamically favorable (111) terminating structure with the activation of the interstitialcy diffusion mechanism at temperatures greater than 923K which culminate in the diffusion of oxygen in a direction other than [110] and ultimately in the formation of O_γ .

Studies on the methanol oxidation reaction show an excellent correlation between the various diffusion mechanisms and the catalytic activity. The dominant diffusion mechanism may be estimated from the location of holes which act as morphological fingerprint which sub-surface oxygen leaves after reacting with bulk-dissolved hydrogen resulting from the dehydrogenation of methanol to formaldehyde. The absence of holes for reaction temperatures lower than 573K indicates that the reaction takes place entirely at the silver surface. The presence of holes at silver grain boundaries for temperatures between 623K and 823K shows that grain-boundary diffusion of oxygen acts as the primary diffusion path for the formation of O_β . Reaction temperatures above 923K results in the proliferation of holes across the silver surface, indicating the participation of oxygen which is transported by volume diffusion. The morphological restructuring of silver results in grain boundary sintering above 623K which results in the deactivation of fresh silver catalysts at temperatures between 573K and 873K. This deactivation is removed after reacting the catalyst at temperatures greater than 923K.

The measured activation energy of diffusion for the oxidative coupling of methane (OCM) to C_2 hydrocarbons of 138 kJ/mol corresponds excellently with the measured activation energy of oxygen diffusion in the silver bulk of 140 kJ/mol. This provides a quantitative correlation between the kinetics of bulk-oxygen diffusion and the rate of catalytic reaction. This is, therefore, quantitative evidence for the proposed mechanism of O_β and O_γ formation. The activity and selectivity of the OCM reaction also act as excellent qualitative indicators for the formation of O_γ which is correlated with the formation of (111) facet terraces. Oxidative coupling of methane over fresh silver initially results in the formation of complete oxidation

products. This is due to the preferential formation of O_α on the initially rough, polycrystalline surface which has a high sticking coefficient for oxygen adsorption. Gradual facetting and bulk texturing transform the catalyst into one which preferentially catalyzes the formation of C_2 coupling products. This provides excellent qualitative confirmation of the proposed model for high-temperature partial oxidation over silver.

Zilver wordt in de industrie toegepast als katalysator in zowel de epoxidatie van etheen naar etheenoxide als de oxidatieve dehydrogenering van methanol naar formaldehyde. De opmerkelijke activiteit van zilver in deze reacties hangt samen met het vermogen van zilver om moleculaire zuurstof om te zetten in een aantal verschillende reactieve species.

Chemisch gebonden atomaire zuurstof wordt op een zilveroppervlak gevormd door dissociatieve chemisorptie van moleculaire zuurstof uit de gasfase. Dit chemisch gebonden oppervlaktezuurstofatoom, aangeduid als O_a , is sterk nucleofiel en reageert doorgaans a-selectief met koolwaterstoffen. O_a wordt preferentieel gevormd aan zilveroppervlakken met hoge Miller-indices en hoge sticking coefficients voor dissociatieve adsorptie van moleculaire zuurstof. Desorptie van deze species vanaf zilveroppervlakken *in vacuo* vindt plaats bij ongeveer 523 K. Bij temperaturen boven de 573 K kan zich een evenwicht instellen door adsorptie, desorptie en diffusie van zuurstofspecies tussen het oppervlak en het inwendige van het zilver zolang een zuurstofatmosfeer aanwezig is. Bij temperaturen lager dan 923 K bezet zuurstof bij voorkeur octaëdrische holten in het zilverrooster. Deze opgeloste zuurstofspecies wordt aangeduid als O_p . Diffusie van zuurstof in de vaste stof vindt voornamelijk plaats langs korrelgrenzen, en in de individuele kristallieten door octahedral hole jumping. Het hole jumping mechanisme is sterk anisotroop en leidt binnen individuele kristallieten tot preferentiële migratie van zuurstof in de [110] richting ("diffusiekanalen").

Boven 923 K wordt interstitiële diffusie van zuurstof in zilver mogelijk en wordt zuurstof ook op interstitiële posities in het kristalrooster ingebouwd. Bij het bedrijven van een katalytische reactie boven de 923 K is zuurstof onder steady-state condities zowel aanwezig op roosterposities als op interstitiële posities, en vindt uitwisseling van zuurstof tussen inwendige en oppervlak plaats. Tegelijk treedt reconstructie op van het zilveroppervlak, dat streeft naar een configuratie met minimale energie. Als gevolg van dit proces worden oppervlaktefacetten gevormd, waarvan aangenomen wordt dat ze bestaan uit (111)-terraces en (110)-terminerende steps. Sticking coefficients voor zuurstofadsorptie op de (111)-terraces zijn extreem laag ($\theta < 10^{-6}$) en O_a wordt er niet significant gevormd. De (110)-steps daarentegen hebben een hoge sticking coefficient voor zuurstof ($\theta < 10^{-3}$) en fungeren bovendien als ingang van de bovengenoemde diffusiekanalen langs de [110]-richting naar het inwendige van het zilver. Via interstitiële diffusie kan een deel van de zuurstofatomen uiteindelijk via het inwendige naar het oppervlak van de (111)-terraces migreren en segregeren. De aldus gevormde zuurstofspecies, aangeduid als O_p , kunnen reageren met moleculen uit de gasfase en zijn in staat directe oxidatieve dehydrogenering van organische moleculen te bewerkstelligen. Zowel de richtingsvoorkeur als de

kinetiek van zuurstofdiffusie door zilver is sterk afhankelijk van de morfologie van het zilver. Het is de samenloop van de morfologische reconstructie van het zilver onder vorming van een thermodynamisch stabiele (111)-getermineerde structuur en het optreden van interstiële diffusie bij temperaturen boven de 923 K die leidt tot diffusie van zuurstof in andere richtingen dan [110] en uitmondt in de vorming van O_γ .

Studies aan de zilveragekatalyseerde oxidatie van methanol laten zien dat een uitstekende correlatie bestaat tussen het optreden van de verschillende diffusiemechanismen en de katalytische activiteit. Een indicatie van het diffusiemechanisme dat onder een bepaalde omstandigheid dominant is kan men verkrijgen door voorkomen en positie te bepalen van holten, die als het ware een vingerafdruk vormen achtergelaten door subsurface zuurstof na reactie met in het inwendige opgelost waterstof, op diens beurt gevormd door dehydrogenering van methanol naar formaldehyde. De afwezigheid van zulke holten na katalyse bij temperaturen lager dan 573 K wijst erop dat de reacties zich alleen aan het zilveroppervlak afspelen. De aanwezigheid van holten op de korrelgrenzen van het zilver na katalyse bij temperaturen tussen 623 K en 823 K wijst erop dat korrelgrensdifusie het voornaamste mechanisme is voor de vorming van O_β . Bij reactietemperaturen boven de 923 K ontwikkelen zich holten in het gehele inwendige, hetgeen wijst op participatie van zuurstof aangevoerd door het gehele kristalvolume. Morfologische reconstructie van het zilver resulteert in sintering van korrelgrenzen bij temperaturen hoger dan 623 K, hetgeen leidt tot deactivering van verse zilverkatalysatoren die doorgaans wordt waargenomen bij temperaturen tussen 573 K en 873 K. Bij temperaturen hoger dan 923 K wordt deze deactivering weer opgeheven.

De gemeten waarde van 138 kJ/mol voor de activeringsenergie van de oxidatieve koppelingsreactie van methaan (OCM) naar ethaan en etheen stemt nauwkeurig overeen met de gemeten waarde van 140 kJ/mol voor de activeringsenergie van zuurstofdiffusie in het inwendige van het zilverrooster. Deze kwantitatieve correlatie tussen de kinetiek van diffusie van opgeloste zuurstof en de reactiesnelheid is tevens een kwantitatieve aanwijzing voor de geldigheid van het voorgestelde mechanisme voor de vorming van O_β en O_γ species. De activiteit en selectiviteit in de OCM reactie geven ook goede kwantitatieve indicaties voor de vorming van O_γ die gecorreleerd is met de vorming van (111) facet terraces. Oxidatie van methaan over verse zilverkatalysatoren leidt in eerste instantie tot volledige verbranding. De a-selectieve reactie is toe te schrijven aan preferentiële vorming van O_a op de aanvankelijk ruwe kristalvlakken van het polykristallijne materiaal. De geleidelijke vorming van facetten en van textuur in het inwendige van de kristallieten maakt de katalysator uiteindelijk selectief

Samenvatting

voor de vorming van C_2 koppelingsproducten. Deze observaties bevestigen kwalitatief op overtuigende wijze het voorgestelde model voor zilvergekatalyseerde partiële oxidatiereacties bij oxidatiereacties.

Acknowledgements

Deciding to do my PhD at the Fritz-Haber Institute was one of the wisest decisions of my life and one which I will frankly always look back upon with fond memories. Performing one's thesis work is probably the last time that most of us will ever have the freedom to pursue our scientific fancy without having to make it add up in terms of dollars and cents. Knowledge is, unfortunately, a commodity not looked upon with great favor by stock brokers and boards of trustees. In this case I have to thank Prof. Robert Schlögl for giving me the flexibility to pursue many of my own ideas (however fanciful they were). His dedicated work to making Fritz a better place to do top-notch science is something which deserves great merit.

I had the good fortune to have two advisors during the course of my thesis work. Harald Werner proved not only to be a great source of help in times of need, but also proved to be a great source of good humor and advice. Advisor number 2, Gerhard Mestl, arrived about 1.5 years into my PhD work. Too bad, because we probably could have ditched science and gerged around Germany with music that would have redefined the meaning of noise. Due to bad timing, however, he was forced into the position of having to be my boss. Despite my constant disruption, his door was always open and his answer was always loaded with enthusiasm. You are a great inspiration and a dear friend to me. Never stop looking for that famed guitar amp that goes to 11 !!!

There's a long list of people with whom I worked who I could write chapters about. Here are a few which deserve particular attention. Emilio Sanchez Cortezon.....my fellow diplomat. Your humor saved me from the damning silence of German seriousness. Best of luck with your dice-rolling techniques (Chemometrie ???) in chemistry. Martin Dieterle...I owe you lots of Bountys. Thanks for not killing me for never returning your CD player on time. Jörg I'll never forgive you for not taking me to your art history seminar. Thomas Rühle is the world's greatest drummer. A man whose greatness is only revealed when you can scrape through his thick hide of pessimistic humor. Many thanks to Herr Brust and Herr Kessel for building everything under the sun for me, for educating me in the niceties of machine technique and electronics and for providing me with a reliable source of sugar for my morning coffee. Gisela Lorentz's SEM work was absolutely critical to getting this PhD done. The woman is not only incredibly sophisticated and polite, but also has an aesthetic feel which

Acknowledgements

enables her to often find the morphological keys to solving our catalyst problems. Many thanks to Ute Wild, for her patience and calm composure when I managed to almost destroy the XPS and for trusting me to operate it. Your kindness and attention to detail were inspirational. Ute Röper for sharing her great music collection and always bringing the beauty of her smile and optimism plus an amazing attention to detail in our lives at Fritz. Dimitri Zemlianov... "Don't worry, be happy" What else is there to say? Probably one of the best scientists I've ever had the luck to cross paths with. A rare man who combines scientific expertise with the ability to sit down, drink a beer and have a normal conversation. Mischa Bonn for being a great friend and a constant source of inspiration. Some day we're going to get rich on science and sip 20 year old St. Emillion on our porch in Provence and laugh about these times. Stay cool and keep on loving life. Marcello Rigutto for translating my Stellingen and Samenvatting. Good luck with uncle Shell! Others who helped: Edith Kitzelman, Daniel Herein, Joseph Find, Andrea Möbius, Dr. Niemantsverdriet, Prof. Lercher, Andreas Nowak, Prof. J.P. Gilson, Prof. Bob Thompson, Prof. William Moser, Prof. Bettina Kraushaar Czarnetzki, Prof. Fabio Ribiero, Dimitri Zemlyanov, Wolf Guenter, Bettina Behms, Fritz Zemlin.

I cannot of course complete this section without including Prof. Rutger van Santen. I hope you realize how much your kind consideration has meant to me and what an enormous impact it will have on my future. Thank you so much for your help.

This list would by no means be complete without thanking the woman I love for tolerating my mild fits, lack of scheduling and incessant babbling about the lab. Yvonne Hylla embodies that other world I can escape to when I leave Fritz at the end of the day.

Last but not least I have to thank the two people who made this all possible for me: my parents. Thank you for never giving up on me and for always pushing me to be the best I could be and for helping me to realize my dreams, even if it meant seeing each other only once a year. Your selflessness and unconditional love are human qualities which I can only hope one day to attain. You are both absolutely precious to me.

Curriculum Vitae

Name: Anton J. Nagy

Birthdate and Place: March 1st 1970, Oak Lawn, IL, USA

High School: 1984-1988, Marist H.S., Chicago, IL

University: 1988-1992, Illinois Institute of Technology
Chicago, IL, USA
Bachelor's of Science, Chemical Engineering

1993-1994, Worcester Polytechnical Institute,
Worcester, Mass, USA
Master's of Science, Chemical Engineering

1996-Present, Fritz-Haber Institute, der Max
Planck Gesellschaft, Berlin, Germany
Thesis work. PhD to be received at the Technical
University Eindhoven, Eindhoven, Netherlands